Cell Adhesion and Growth on Self-Assembled Monolayers of Alkanethiols

Thesis submitted in accordance with the requirements of the University of St. Andrews for the Degree in Doctor of Philosophy on the 2nd May 2006

By:
Wendy E M Crocker

I, Wendy Elizabeth Murray Crocker, hereby certify that this thesis, which is approximately 39,000 words in length, has been written by me, that it is the record of work carried out by me and that it has not been submitted in any previous application for a higher degree.

Date 30 APR 2006 . Signature of Candidate . . .

I was admitted as a research student in October 2000 and as a candidate for the degree of PhD in October 2000; the higher study for which this is a record was carried out in the University of St Andrews between 2000 and 2005

Date 30 APR 2006 . Signature of Candidate . .

I hereby certify that the candidate has fulfilled the conditions of the Resolution and Regulations appropriate for the degree of PhD in the University of St. Andrews and that the candidate is qualified to submit this thesis in application for that degree.

Date . . 2/5/06 . . . . . Signature of Supervisor . .

In submitting this thesis to the University of St. Andrews I understand that I am giving permission for it to be made available for use in accordance with the regulations of the University Library for the time being in force, subject to any copyright vested in the work not being affected thereby. I also understand that the title and abstract will be published, and that a copy of the work may be made and supplied to any *bona fide* library or research worker.

Date 30 APR 2006 . . . Signature of Candidate

Abstract

It is known that cells can respond to both the chemistry and topography of their surroundings in culture. Several studies have used self-assembled monolayers of alkanethiols on gold to control surface chemistry so that the effect of chemistry on cell growth may be studied. While there is evidence that alkanethiol self-assembled monolayers have many different structures, and it has been seen that cells can respond to changes in topography at a nanometre level, only one study has suggested that there may be a relationship between alkanethiol structure and cell growth.

This study addresses the relationship between the structure of monolayers of alkanethiols on gold and the growth of cells on that surface. This has been done by first analysing the structures formed by alkanethiols on gold with Fourier transform polarisation modulation infrared reflection adsorption spectroscopy (FT-PMIRRAS) and then by growing BHK and SF268 cells on the studied surfaces.

The cell adhesion was characterised by using a fluorescent compound (BCECF) to assess differential adhesion. A non-toxic metabolic indicator solution (alamarBlue) was used to determine the amount of cell growth over time. The results showed changes in cell adhesion and growth on different types of alkanethiol monolayers; unfortunately most of these differences were not significant. Limited conclusions could be drawn from this work. There is a change in cell growth with structure but further work is needed to determine exactly what the surface structures causing variation are.

Acknowledgements

In the course of this work I am lucky to have received help, advice and support from many people. I would like to thank my supervisor Professor Neville Richardson for enabling me to undertake this work and for all his help in keeping it going when it was going nowhere. For his attempts to keep the equipment running and for being there when it all went wrong-yet again I thank Dr Steve Francis. I would also like to thank the EPSRC and Integrin Advanced Biosystems for funding this project. In particular I would like to thank Dr J. Douglas McKenzie, Dr Charlie Bavington and all the staff at Integrin Advanced Biosystems for their indulgence, assistance and support in the cell growth work. I would also like to thank all the members of the surface science team of St. Andrews University for their help and cooperation. I am also very grateful Dr Alan Aitken at St. Andrews University for his help in making the unobtainable. In addition I thank Dr Bengt Kasemo and Dr Robert Corn and their research groups for hosting me at their universities while I was questing for answers to the unanswerable question-why won't this work. For help when I was unsure if I would ever submit a thesis I thank Professor J. Derek Woollins and his wife Dr Alex Slawin. Finally I would like to thank all my friends and family, mainly for putting up with me during the course of this PhD.

Contents

Abbreviations

X%AUTY%MUA	self-assembled monolayer on Au made from a solution of X% molar composition 11-aminoundecanethiol and Y% molar composition 11-mercaptoundecanoic acid
ADT	10-aminodecanethiol
ADT.HCl	10-aminodecanethiol hydrochloride
Ag	silver
Ar	argon
Asym	asymmetric
Au	gold
AUT.HCl	11-aminoundecanethiol hydrochloride
BCECF	2',7'-bis-(2-carboxyethyl)-5-(and-6)-carboxyfluorescein
BCECF-AM	2',7'-bis-(2-carboxyethyl)-5-(and-6)-carboxyfluorescein acetoxymethyl
BHK	baby hamster kidney
BrdU	5-bromo-2'-deoxyuridine
Br-dUTP	bromolated deoxyuridine triphosphate
BTT	1-butanethiol
BTDT	1,4- butanedithiol
CG	cystyl glycine
CH_3	methyl group
COOH	carboxylic acid group
Cys	cysteine
DCT	1-decanethiol

DDT	1-dodecanethiol
Ditbsu	dithiobis(succinimidyl undecanoate)
Ditbsu R1 solution	dithiobis(succinimidyl undecanoate) reacted with ammonia
DMF	N,N – dimethylformamide
DNA	deoxyribonucleic acid
DTT	dithiothreitol
EDC	1-ethyl-3 [3(dimethylamino)propyl] carbodiimide hydrochloride
ELISA	enzyme-linked immunosorbent assay
ETT	ethanethiol
ETDT	1,2-ethanedithiol
FTIR	Fourier transform infra-red
H-bond	hydrogen bond
HPT	1-heptanethiol
HXT	1-hexanethiol
HXDT	1,6- hexanedithiol
HDT	1-hexadecanethiol
IR	infra-red
MAA	2-mercaptoacetic acid
MAbs	monoclonal antibodies
MBA	4-mercaptobutyric acid
MCT	mercury cadmium telluride
MEA	2-mercaptoethylamine
Meth	2-mercaptoethanol

MHDA	16-mercaptohexadecanoic acid
MOA	8-mercaptooctanoic acid
MPA	3-mercaptopropionic acid
MTS	5-(3-carboxymethoxyphenyl)-2-(4,5-dimethylthiazolyl)-3-(4-sulpho- phenyl) tetrazolium salt
MTT	3-[4,5-dimethylthiazol-2-yl]-2,5-diphenyltetrasodium bromide
MUA	11-mercaptoundecanoic acid
MUA R	All11-mercaptoundecanoic acid monolayers reacted with NHS/EDC then ammonia solution
MUA R1	11-mercaptoundecanoic acid monolayer reacted with NHS/EDC then ammonia solution
MUA R2	11-mercaptoundecanoic acid monolayer (Reacted with NHS/EDC then ammonia solution) twice
MUA R3	11-mercaptoundecanoic acid monolayer (Reacted with NHS/EDC then ammonia solution) thrice
N_2	nitrogen gas
NaOH	sodium hydroxide
NH_2.HCL	amine hydrochloride group
NHS	N-hydroxysuccinimide
NHSS	N-hydroxysulfosuccinimide
OEG	oligoethyleneglycol
OH	hydroxy group
OTT	1-octanthiol
ODT	1-octadecanethiol
PBS	phosphate buffered saline

PMIRRAS	polarization modulation infra-red reflection absorption spectroscopy
PPT	1-propanethiol
PPDT	1,3- propanedithiol
PTT	1-pentanethiol
PTDT	1,5- pentanedithiol
RGDC	arginyl glycyl aspartyl cysteine
X%RGDCY%Cys	self-assembled monolayer on Au made from a solution of X% molar composition arginyl glycyl aspartyl cysteine and Y% molar composition cysteine
Rp	reflectance of P polarised light
Rs	reflectance of S polarised light
SAM	self-assembled monolyaer
SAMs	self-assembled monolayers
SBIP	strand break induced photolysis
SH	thiol group
Si	silicon
SPDP	N-succinimidyl 3-[2-pyridyldithio]-propionamido
STM	scanning tunnelling microscopy
Sym	symmetric
TdT	terminal deoxynucleotidyl transferase
Ti	titanium
TUNEL	terminal deoxynucleotidyltransferase-mediated dUTP nick end labeling
UDT	1-undecanethiol
UHV	ultra high vacuum

WST-1	2-(4-iodophenyl)-3-(4-nitrophenyl)-5-(2,4-disulfophenyl)-2; H; -tetrazolium salt
WST-8	2-(2-methoxy-4-nitrophenyl)-3-(4-nitrophenyl)-5-(2,4-disulfophenyl)-2H tetrazolium salt
XPS	X-ray photo electron spectroscopy
XTT	2,3-bis[2-methoxy-4-nitro-5-sulfophenyl]-2H-tetrazolium-5-carboxanilide

Chapter 1

Literature Review

1.1 Introduction

Growth of biological cells is controlled by their environment; it is controlled by the chemistry and topography of their surroundings and by signalling molecules sent from other cells. This knowledge has been used for many years to grow cells in culture outside their natural environment. These cell cultures have been invaluable as experimental subjects in the study of toxicity, viral infection and for testing the ability of compounds to cause or cure cancer [1]. Cell culture is also used for producing biologically active compounds for pharmaceuticals [2]. It has not been possible to culture all types of cells of interest; animal cells can be particularly difficult to culture. It is often necessary to grow animal cells on specialised surfaces which mimic their natural environment [3]. The aim of this project is to create surfaces for the growth of animal cells, and to analyse the relationship between the chemistry of the surface and the growth of different cell types.

1.2 Chemical Modification of Surfaces

A large variety of surfaces have been used as substrates for cell growth, from common, commercially available tissue culture plastic (a plastic coated with cell adhesion promoters such as collagen) [4], to more obscure surfaces such as part of a jellyfish [5]. The majority of surfaces used as cell growth substrates have been fabricated for the purpose by chemically and/ or topographically controlling the parameters of the surface. Many of these surfaces have known biological adhesion molecules [6, 7] (or the active parts of them [8]) incorporated or are designed to mimic them [9].

1.2.1 Polymers

Initially polymers were the preferred way of creating surfaces for cell growth; they are stable, can be created presenting many different chemical functionalities, and they can be easily moulded into any desired shape, which makes them well-suited to this purpose. The disadvantage of using polymeric materials is that their topography cannot be controlled on a microscopic level, and this can lead to variation in the amount of cell growth seen on surfaces created by the same technique. The homogeneity of the actual presenting surface is also difficult to confirm, which means that it is difficult to determine what characteristics of the surface are having a positive or negative effect on cell growth.

1.2.2 Self- Assembled Monolayers

A self-assembled monolayer (SAM) (Figure 1.1) is a layer only one molecule thick on a surface that has spontaneously formed itself into an ordered structure. Zisman first performed systematic studies of these monomolecular layers in 1946 [10] and the use of SAMs has grown considerably since then, particularly in the past two decades [11].

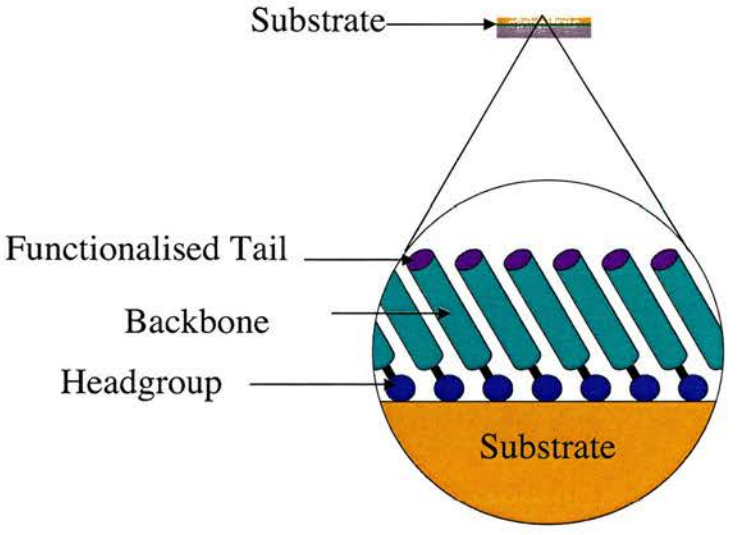

Figure 1.1 A schematic of self-assembled monolayer (SAM). The headgroup binds to the substrate and the backbone supports the functionalized tail. Modified from a figure by Dr A. McDowall

A SAM has three features to it: the head group which binds to the surface, a tail group which is presented to the ambient surroundings, and a backbone which separates the head group and the tail group. This is shown in the diagram (Figure

1.1). There are two types of particularly stable monolayers, which are used in cell culture: alkylsiloxane monolayers and alkanethiol monolayers.

1.2.2.1 Self-assembled Monolayers of Alkylsiloxanes

Alkylsiloxane monolayers are formed from trichlorosilane head groups that lose the chlorine atom as they bond irreversibly to a hydroxylated surface via an oxygen to silicon bond [12-14] (Figure 1.2).

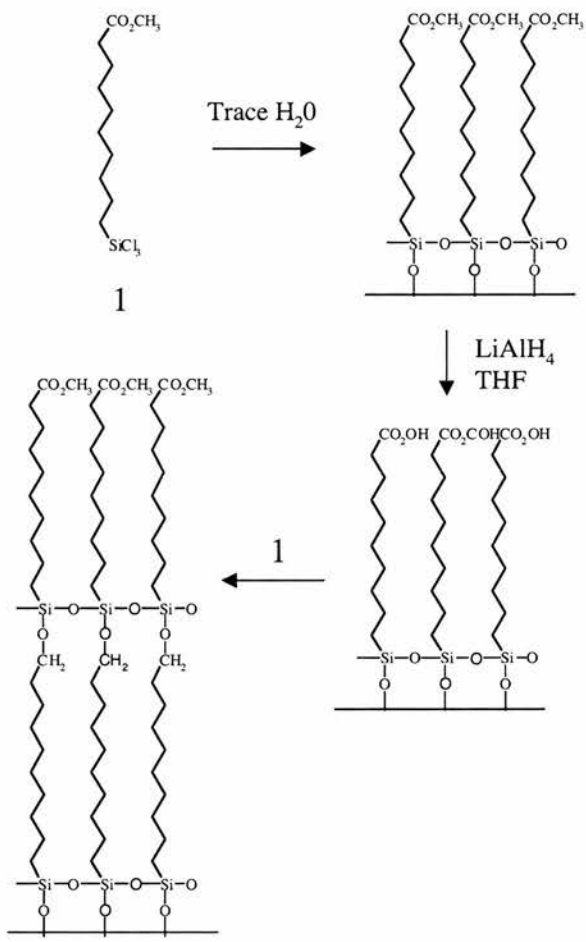

Figure 1.2 The process whereby a self-assembled monolayer of alkylsiloxane is formed from trichlorosilane. Based on a figure by Ulman (1996) [17]

Alkylsiloxanes make very stable monolayers, which have the advantage that they can be bound directly to glass for cell culture. The disadvantages are that not very many tail groups are available, the formation of the monolayer is non-trivial, reproducibility of the monolayer is not always possible and the monolayers produced are generally more disordered than those of alkanethiolates [12].

1.2.2.2 Self-assembled Monolayers of Alkanethiols

Monolayers made from alkanethiols assembled on gold (Au) are well ordered and stable in many conditions, including those required for cell culture. They are however, susceptible to degradation by UV radiation in the presence of oxygen [15], when exposed to atmospheric ozone, and when subjected to kiloelectron volt ion bombardment [16]. SAMs also desorb on heating above 70 °C on Au [15]. Monolayers of alkanethiols on silver (Ag) are more stable, however they are also cytotoxic due to the release of Ag^+ ions from the surface [15].

Monolayers of alkanethiolates have the advantage that they are very easy to form. The alkanethiol is dissolved in a solvent and slides coated with noble metals, or single crystals of the noble metals, are immersed in this solution [17] (Figure 1.3). The period of immersion used has ranged from seconds to hours, and the immersion time, among other factors, determines the level of ordering in the monolayer. It

should be noted that vapour deposition has also been used to produce alkanethiolate monolayers up to ten carbons long [18, 19].

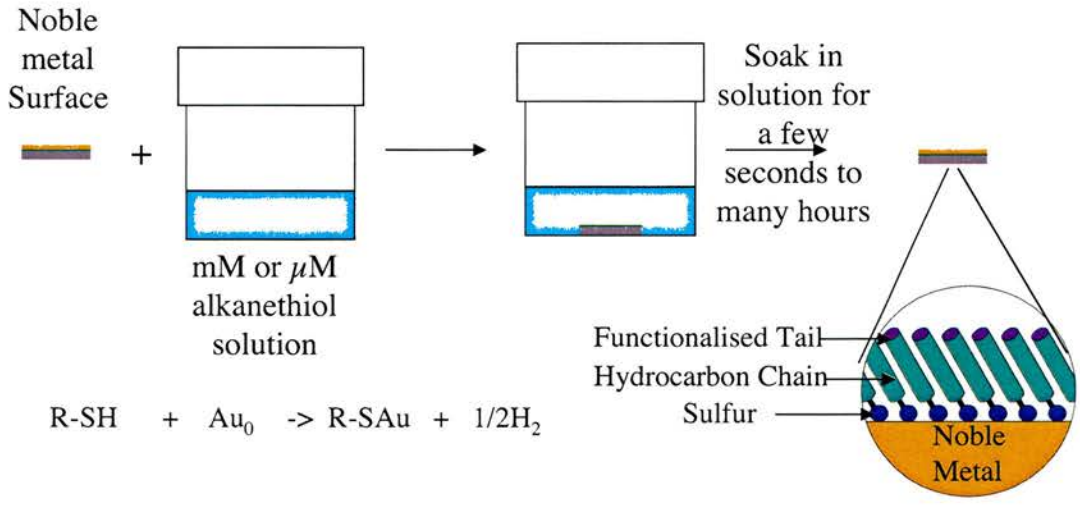

Figure 1.3 The formation of an alkanethiolate monolayer by soaking a noble metal surface in a mM or μM solution of alkanethiol for a few seconds to a few hours. An equation for this reaction is shown using gold as the noble metal.

1.2.2.2.1 Formation and Structure of Self-assembled Monolayers of Alkanethiols

The preferred noble metal substrate for thiol monolayer formation is Au; this is because it produces the most densely packed ordered monolayers. The Au used is usually coated by sputtering [20] or vapour deposition [21] onto slides of glass or silicon which have a thin layer of chromium [22] or titanium (Ti) [23]. Alternatively the gold can be deposited directly onto mica [24]. This usually produces an Au (111) surface, which has a cubic close packed structure based on the bulk lattice (fcc). The

surface has unit cell dimensions of $(a/\sqrt{2} * a/\sqrt{2})$, where a is the dimensions of the fcc cell (Figure 1.4). This is the lowest energy conformation. The Au substrate, while it is relatively inert, generally has a layer of contaminants on it. These are displaced by the more favourable sulfur- Au interaction [25-27].

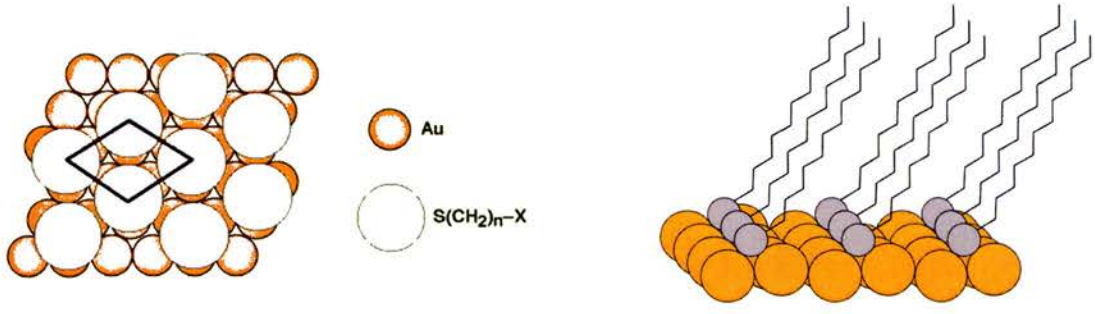

Figure 1.4 Left: The $(a/\sqrt{2} * a/\sqrt{2})$ unit cell of Au with the $(\sqrt{3} * \sqrt{3})$ alkanethiol unit cell adsorbed on it [11]. Right: The three dimensional nature of the $(\sqrt{3} * \sqrt{3})$ R30° structure that predominates for alkanethiols on gold [17].

The first interaction the alkanethiol has with the Au surface is physisorption. This is viewed by scanning tunnelling microscopy (STM) as a "striped phase" [28] (Figure 1.5). The force causing this structure is van der Waals' bonding, which is an interaction between the hydrocarbon chain backbones that increases with increasing length of the backbone [29, 30]. The thiol molecules then chemisorb to the surface forming a thiolate and losing the hydrogen as molecular hydrogen [18]. The chemisorbed molecules are observed in various structures as they order first the hydrocarbon backbones, then their tail groups, into the most thermodynamically favourable arrangement (Figure 1.5). The most commonly observed arrangement is a densely packed standing up phase.

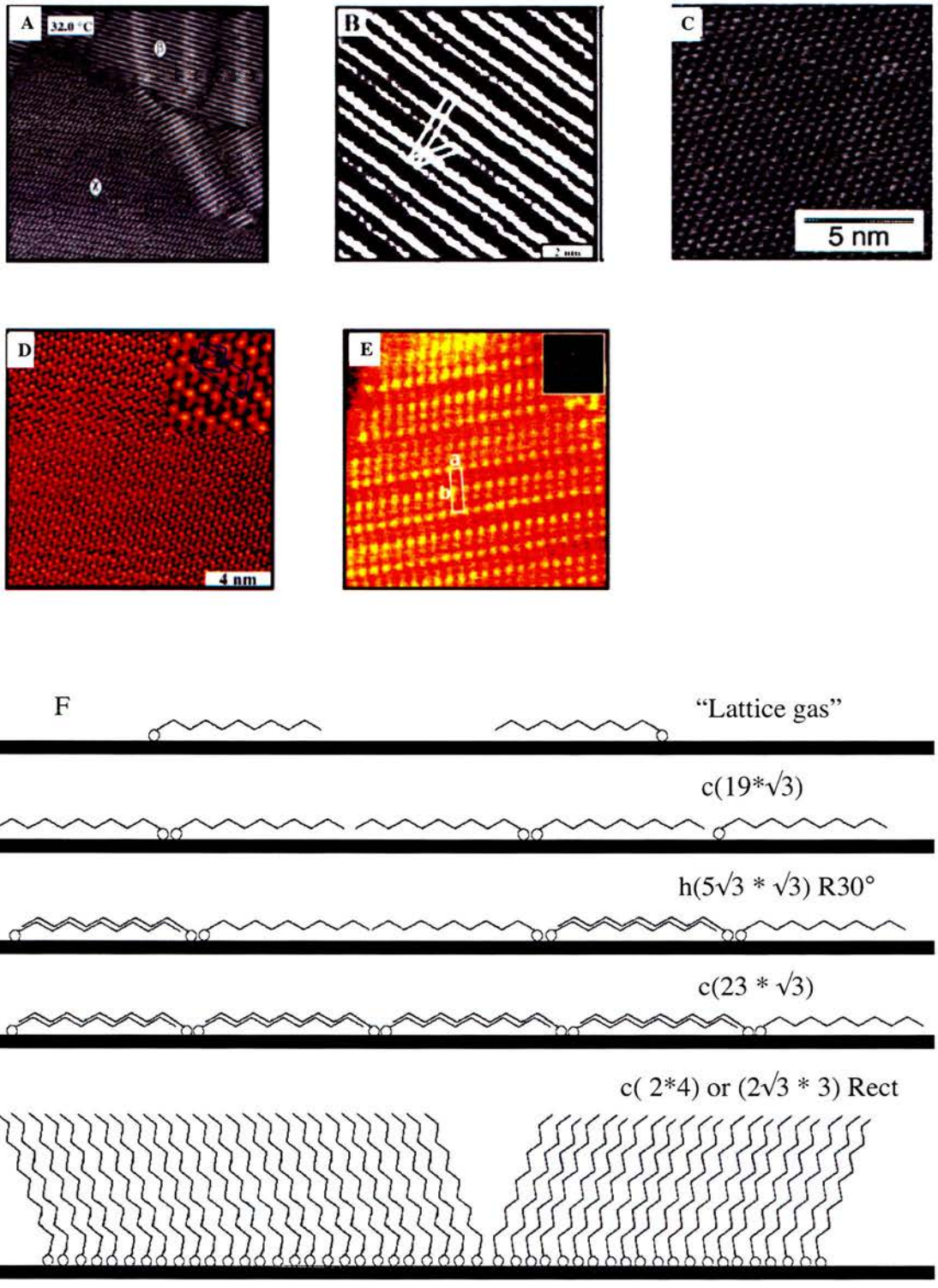

Figure 1.5 A. Structure ß c(23 * √3) and χ c(19*√3) [134] B. Structure h(5√3 * √3)R30° [19] C. Structure √3 * √3 R30° [135] D. Structure c(2*4) or (2√3 * 3) [136] E. Structure 6 * √3 Structure [39] F. Schematic of unit cells of different molecular arrangements of alkanethiols based on Schreiber *et al* [47]

The sulfur is conventionally believed to be absorbed in the three fold hollow sites of Au [31] in a cubic close packed arrangement [32]. The unit cell of the alkanethiolate monolayer was initially thought to be ($\sqrt{3} * \sqrt{3}$) R30° with the structure containing only one molecule. For this configuration the distance between sulfur atoms is 4.97 Å, and the calculated area per molecule is 21.4 $Å^2$. This appears to be true for long chain alkanethiolate SAMs [18]. However the unit cell appears to be distorted for vapour deposited shorter chain alkanethiols to ($n\sqrt{3} * \sqrt{3}$) R30° (Figure 1.5) where n varies from 1-6 [18].

Further investigation revealed another structure was common in long chain alkanethiolate monolayers; a ($2\sqrt{3} * 3$) Rect superlattice of 4 molecules (usually called a c (4*2) superlattice) [20, 32-39] (Figure 1.5). This unit is formed from changes in the tilt structure of the basic unit cell; in this structure the sulfur still occupies the three fold hollow sites [38, 39]. There is some evidence suggesting that not all alkanethiolates occupy this type of site [40]. It has been calculated that, for ethanethiol and above, the lowest energy position is at the twofold bridge sites [41-43]. A different superstructure of unit cell ($6 * \sqrt{3}$) has been found to form from the ($2\sqrt{3} * 3$) superstructure (Figure 1.5). This structure only forms completely after the monolayer has been left at room temperature for 6 months [39]! The formation of this phase involves the movement of some of the sulfur head groups onto the bridge sites, as well as to the on top sites. It is a densely packed phase which appears much

like the initial low-density striped phase, although the latter involves flat lying molecules.

1.2.2.2.2 Surfaces of Self-Assembled Monolayers of Alkanethiols

It should be apparent from the variety of structures that can be formed, and the variety of tail groups that are possible that many different surfaces can be produced. This means that there are many different structures and functionalities available using SAMs of alkanethiols, which can be tailored for cell growth including presenting biological signalling molecules [44].

The surfaces that have been chosen in this study are all made from SAMs of alkanethiols with an aliphatic hydrocarbon backbone. It is believed that alkanethiols containing an aromatic molecule in the backbone form better-ordered structures [45, 46]. However, the limited number of different functionalities available [45] with aromatic backbones and the wealth of data proving that well ordered structures are to be found from alkanethiols with aliphatic backbones [30, 47] led to only molecules with aliphatic backbones being used in this study.

1.2.2.2.2.1 Self-assembled Monolayers of Methyl-terminated Thiols

Methyl-terminated alkanethiols are the most commercially available variety of thiol. Probably as a consequence of this they have been one of the most extensively studied. They have been characterised by many different surface science techniques [47], so more is known about them than most thiol SAMs. The majority of the studies have been carried out on SAMs of thiols on Au.

1.2.2.2.2.1.1 Chain Length and Order

Monolayers of methyl-terminated SAMs have been found to be well ordered and free of defects with their hydrocarbon chains in an all *trans* conformation [48]. The degree of order of long chain aliphatic thiols (14 carbons or more) is very similar to that found in the bulk crystalline phase of packed alkane chains [49]. Alkanethiol SAMs with a chain length shorter than C14 have been found to be of varying degrees of order.

The data provided by Porter *et al* [49] suggests that the chains take on more liquid-like character from a carbon chain length of 12 (C12) and below. This is similar to the position of structural change found by Fenter *et al* [50], who discovered that C14 and below had a different tilt angle and direction from that seen in longer carbon chains. It was concluded from the latter study that there were 2 distinctly different

tilt structures that could be formed [50]. This was not confirmed by an atomic force microscopy (AFM) study which found that monolayers self-assembled from thiols with a chain length of C5 or more all had the same structure [51]. Another study that tested C3 to C18 found that the maximal degree of ordering was at C8 [52]. The fact that there is maximal packing at C8 for this experiment indicates that a different structure is present.

Different structures have been observed for C6 to C10 in different studies [18, 51, 53], this supports the idea that the structures in this area are changeable. What is uncertain is whether the structures are present simultaneously or whether they change over time or due to the conditions of formation. It is clear that the structures produced for C6 to C10 and perhaps C12 and C14 are different from those above and those below. This has been attributed to the different forces acting on the head group and the hydrocarbon chain.

The head group defines the preferred binding sites on Au and the hydrocarbon chains want to be parallel to each other to maximise the CH_2 to CH_2 interactions [50]. The orientation of the alkanethiols that provides the preferred head group orientation is not the orientation that allows for maximal interaction of the hydrocarbon chains and as such the structure is a compromise, favouring whichever of the interactions is stronger. The chain interactions reach a magnitude of force that make it feasible for the sulfur to move to another site at around C10 [50], this is called a phase transition.

The sulfur and the hydrocarbon chain can order in a variety of different ways around this chain length producing a many different structures known as phases. This conclusion is supported by the finding that there are different sulfur adsorption sites and that these change with chain length [54].

Some studies on very short chain SAMs (C4 or shorter) have found that there is no order in the monolayer [50, 51]. The investigators claim that there is unlikely to be much order in SAMs shorter than C5. More recent results indicate that this hypothesis, at least for certain assembly conditions, can be wrong. A recent study has found that the short chain thiol SAM (1-butanethiol (BTT (C4)) has an all *trans* chain and concludes that the structure is likely changing due to a phase transition. Further evidence of ordered short-chain thiols comes from STM images, which are available for C2 (1-ethanethiol (ETT)) [55, 56], C3 (1-propanethiol (PPT)) [57] and C4 (BTT) [34, 58].

1.2.2.2.2.1.2 Odd-Even Effect

The odd-even effect is a trend where there is consistent variation between SAMs containing an odd number of carbon atoms and SAMs containing an even number of carbon atoms. An example of this effect is seen for CH_2 peak positions in methyl-terminated SAMs. The peak positions change dependant on whether the molecule had an even or odd number of carbons in the chain was first seen for alkanoic acids SAMs adsorbed on aluminium [59], though it is also thought to be present in

alkanethiol SAMs on Au [60]. The cause of this phenomenon is the different orientations of the head group of the thiol altering the SAM structure differently depending on whether there are an even or odd number of carbons present [61].

The odd-even effect has also been directly observed by infrared (IR) spectroscopy of long chain methyl-terminated (C17 & C18) alkanethiol SAMs [62] and by Raman scattering of short chain C4 and C5 SAMs [48]. This orientational effect has been found to influence the reactivity of the head group [63]. Somewhat surprisingly even the reactivity of a methyl-terminated SAM differs depending on the odd-even orientation [64]. It is due to the differential reactivity of the methyl group that this phenomenon is of interest in this study. If the interaction of ions with the surface can differ, perhaps the interaction of proteins or cells with the surface can differ too.

1.2.2.2.2.2 Self-Assembled Monolayers of Dithiols

Many studies have been performed on dithiol SAMs on Au [47, 65]. The results from these studies provide conflicting evidence. One of the first ideas was that the thiol bends over so that both of the thiol groups are attached at the same time. The genesis of this idea is unclear [65], there is however some evidence to support this suggestion though it appears to be circumstantial. The theory is based on the idea that the CH_2 wagging modes increase in intensity for structures that do not have an all-*trans* conformation, and are not sigma conjugated [66]. In effect the CH_2

wagging is more distinct the more liquid-like the thiol is. This has been said to support the idea that the thiol is folded over [65, 67].

The second more plausible idea is that the molecules stand upright. This is supported by ellipsometry [68] and surface plasmon resonance [69], which suggests that the layer continues to grow because the pendant SH reacts with free SH to form a bilayer and so on. Electrochemical results also suggest that one of the thiols groups is pendant as there are the same number of molecules present on the surface for hexanedithiol and hexanethiol [70]. There are also XPS (X-ray photoelectron spectroscopy) results to suggest the presence of two different sulfur moieties on the surface after exposure to oxygen [71], which supports the idea that the sulfurs are in two different environments. Another study performed by XPS in which dithiol was adsorbed from ethanol solution in air found no sulfonate species [72]. Perhaps not enough oxygen naturally dissolves in the ethanol to produce a significant number of sulfonate groups. The upright structure is also supported by the ability of the pendant sulfur atom to react [68] and by the presence of an S-S stretching frequency of a dithiol multilayer in Raman spectra. It should be noted that the dithiol was adsorbed to a Au colloid, which could have an impact on the structure [73].

The situation becomes more confusing by the introduction of the idea that the solvent and the amount of oxidation possible controls whether or not a multilayer is formed. To eliminate the possibility of a multilayer in one study the ethanol solution was

purged with N_2 or Ar before use and this appeared to be effective in producing only a monolayer [70]. In another study using ethanol as a solvent in air this was thought to promote multilayer formation [69] and using ethanol as a solvent under argon was thought to prohibit a multilayer formation [69]. In a third study, it was thought that ethanol prohibited the formation of a multilayer in air as the oxidation of the pendant sulfur to a SO_3 moiety stopped further reaction [74]. A fourth study found that depositing the dithiol from ethanol in air gave no sulfonate peak [72]. A fifth study investigated dithiol in ethanol under an inert atmosphere and allowed reaction of the monolayer with oxygen to produce an SO_3 moiety but did not address the possibility of a multilayer [71]. So in effect it is uncertain whether a sulfonate is formed or not and whether this has any effect on whether a multilayer or a monolayer will be formed. It appears to be fairly conclusive that it is easier to get a monolayer formation by assembly under inert gas though it is probably due to the thiol being unable to oxidise rather than anything to do with the presence of a sulfonate, which is the incidental oxidation product if a multilayer is not formed. It is possible that the tail end of a multilayer could also oxidise to form a sulfonate, so the presence of a sulfonate does not preclude the existence of a multilayer.

A third structure has been proposed for dithiols on Au where the dithiol adsorbs to the Au with its carbon backbone parallel to the surface. STM studies provide the most evidence to support this theory as there are STM images of dithiol molecules lying flat on the surface [72]. This suggestion has also been supported by a study on

the hydroxy-substituted dithiol dithiothreitol (DTT). In this study there is no reaction of the SH groups which implies both SH groups are bound to the surface. A looped structure is unlikely for DTT due to the chain length of the dithiol so it is probable that it is lying prone on the surface [75]. It is however possible that this has something to do with the hydroxyl groups in the DTT rather than just the thiol groups.

It has been suggested that the flat orientation of the dithiol is only possible for low surface coverage when the dithiol is deposited from the gas phase [70]. In effect the deposition from solution causes an upright conformation. This is not supported by other studies where no evidence was found to suggest that deposition from ethanol can give any other results [72] either by deposition from solution or by thermal experiments. It is however interesting that both these studies find no ordered phase for dithiols on Au deposited from ethanolic solution, though the flat phase can be produced by heating [70, 72].

1.2.2.2.2.3 Self-assembled Monolayers of Amino Acids and Peptides

Thiol containing cysteine (Cys) and Cys containing peptides have been found to adhere to Au via the thiol group to form a monomolecular layer of thiolates on the surface [76, 77]. Cys adheres well to the surface in a highly ordered manner [78]. This has been investigated by many different techniques: XPS [77, 79], STM [78, 80,

81], Fourier transform infrared (FTIR) spectroscopy [76] and electrochemical methods [81]. It has been concluded from FTIR spectroscopy and XPS data that Cys can exist in either a zwitterionic state or a neutral state depending on the conditions from which it was assembled. In FTIR spectroscopy the zwitterionic state can be identified by the CO_2^- symmetric stretching bands appearing at around 1409 cm^{-1} and 1393 cm^{-1}, the NH_3^+ degenerate deformation at around 1610 cm^{-1} and the absence of the C=O stretch at around 1715 cm^{-1} [76]. In XPS the state of the Cys can be inferred from the core level regions showing peaks corresponding to both the neutral and ionic forms of the amine and the carboxylic acid [77].

RGDC (Figure 1.6) has previously been used for promoting cell adhesion by self-assembly on Au [82]. The actual structure of the molecule on Au has not been examined in any detail, however an RC peptide adsorbed on Au has been characterised by FTIR spectroscopy [83] and this provides an indication of which spectral peaks are expected from the RGDC peptide. The RGDC peptide is expected to adsorb on the surface as a monolayer. In this study, the mixed structure of RGDC and Cys will be investigated as it is hoped that spacing out the RGDC molecules so that they are accessible to cells will improve the amount of cellular adhesion to this monolayer.

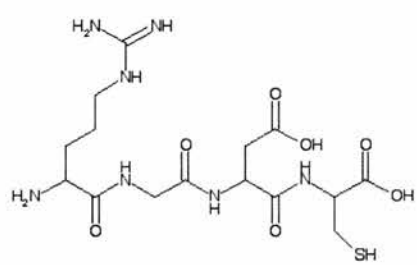

Figure 1.6 Structure of the RGDC Molecule

1.2.2.2.2.4 Amine- and Amine Hydrochloride-terminated Self-assembled Monolayers

The main work that has been done with amine-terminated SAMs has been to use them as an attachment site for proteins or other molecules of interest. This is of use for such applications as the immobilisation of proteins for AFM imaging or the preparation of microarrays of peptides or antibodies.

Not much work has been done on the structure of the amine-terminated SAMs and that which has been done is usually incidental to the main point of the study. In a recent comprehensive review amine-terminated SAMs were not even given a comment [47]. One of the reasons that so few amine-terminated SAMs have been synthesised and utilised is because they are very expensive to purchase and time consuming to synthesise.

There is also the problem when working with amine-terminated thiols that it is possible for the amine-terminated end to adsorb directly to the Au rather than the sulfur. This property has been suggested both in long chain (C11 AUT [84]) and short chain SAMs (C2 MEA [85]). In AUT, this was determined by the presence of SO moieties in the FTIR spectra at 1352 cm^{-1} and 1391 cm^{-1} which had formed due to the oxidation of the thiol because the amine had adsorbed to the surface [84]. This

is contradictory to the finding that amines do not spontaneously adsorb from ethanol [86].

The only reasonably priced, commercially available, amino-terminated unsubstituted alkanethiol is 2-mercaptoethylamine (MEA) otherwise known as cysteamine. The structure of this thiol assembled on Au has been investigated by STM [87] and XPS [85].

1.2.2.2.2.5 Carboxylic Acid-terminated Self-assembled Monolayers

The majority of studies performed on carboxylic acid-terminated monolayers have been performed using 3-mercaptopropionic acid (MPA) (C3), 11-mercaptoundecanoic acid (MUA) (C11) and MHDA 16-Mercaptohexadecanoic acid (MHDA) (C16) due to the fact that these are commercially available [88]. This does not give a particularly clear overall picture. Most of the studies that have explored a larger range of mercaptoalkanoic acids SAMs have been electrochemical and while this is useful it does not give a very complete picture of the structure of these thiols.

Due to the interesting and useful immobilisation and charge transfer properties of omega-mercaptoalkanoic acids their properties as SAMs on Au electrodes have been extensively studied. The pKa of the mercaptoalkanoic acids SAMs has been found to be independent of chain length [89]; however, the microenvironment is still

significant in that the carboxylic acid moieties in the SAMs are less acidic than those in solution [90]. It has also been found that the structure of the monolayer increases in density as the chain length increases [91].

The effect of hydrogen bonding (H-bonding) on the monolayer is unclear. In one case H-bonding was found to stabilise the monolayer (for an intermediate length alkanethiol [92]) which agreed with another study where ionic H-bonding was thought to be a source of stability [84]. These disagreed with another group who thought H-bonding to be the cause of disorder in the acid-terminated monolayer [93].

MHDA has been found by IR spectroscopy to be well ordered while containing some H-bonding character [62]. However, this was contradicted by Dannenberger *et al* who concluded that it was not possible to obtain an ordered monolayer from carboxylic acid-terminated thiols due to H-bonding of newly adsorbed thiolates [94]. Arnold *et al* concluded that the differences were due to differences in concentrations of MHDA in solution. The explanation for this was that the H-bonding of cyclic dimers (Figure 1.7), which disorder the surface, was only found at high carboxylic acid concentrations [93]. This leads to the conclusion that ordered COOH presenting monolayers composed of long chain thiols should be possible when using suitably low solution concentrations.

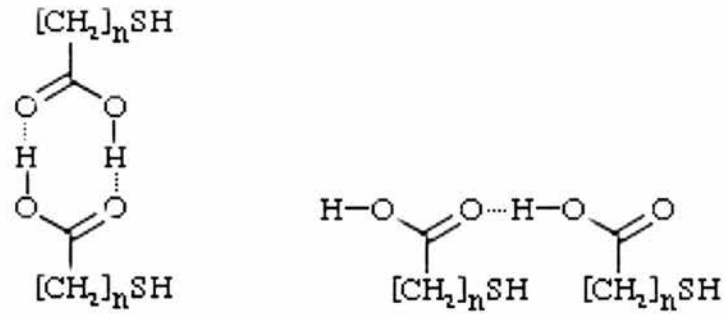

Cyclic H-bonding Acyclic H-bonding

Figure 1.7 Acyclic and cyclic hydrogen bonding of carboxylic acid-terminated thiols as described by Arnold *et al* [93]

The effect of H-bonding on MPA SAMs has been investigated by Ihs & Liedberg [76], and it was found that the peak at 1724 cm^{-1} indicated that the monolayers were H-bonded in what Arnold *et al* refer to a acyclic dimers (Figure 1.7) [93]. From this study it was concluded that a very stable monolayer of MPA is formed on Au.

Various STM studies of the MPA monolayer have also concluded that it forms ordered structures on the surface [70, 95-98] though they have found more than one type of structure present. Esplandiu *et al* concluded that the strange structure they found for MPA was probably due to H-bonding [70]. These studies give the impression that MPA has a dense ordered structure, which has different forms caused by differences in the adsorption process.

The ordered structures found for MPA (C3) SAMs suggests that 4-mercatobutyric acid (MBA (C4)) and 2-mercaptoacetic acid (MAA (C2)) monolayers may be ordered too, as there is not much difference in the chain length to give any more or

less van der Waals' interaction. One study on the structure of MAA found that the monolayer was incomplete and as such enabled the passage of small ions through the film [99]. This indicates that the carboxylic acid head groups do not help to stabilise the monolayer in this case. No evidence has been found for the structural ordering of MBA.

1.2.2.2.2.6 Mixed Self-assembled Monolayers

Mixed monolayers of alkanethiols are monolayers that present more than one tail group. One way to form mixed monolayers is by co-adsorption from a mixed solution of more than one alkanethiol [100-103]. A second method is by exchange; the assembled alkanethiolate monolayer is placed in a solution of a different alkanethiol [22, 104, 105], some of the adsorbed molecules displace and are replaced by those in solution.

The co-adsorption method has the problem that the ratio of thiols in solution rarely corresponds to the ratio of the thiols bound on the surface. It has been concluded that generally the longer thiol occupies a larger proportion of the surface when coadsorbed from an equimolar solution with a short thiol [106]. The tail group of the thiol also plays a determining role in the composition of the monolayer [107]. It can take some investigation to discover the quantities that are necessary in solution to form a specific ratio on the surface [103].

The displacement method is even more problematic in that exchange does not always take place. It is believed that only monolayers that are not very densely packed are capable of undergoing exchange [105], this is commonly thought to be those with short chain or those with carboxylic acid functionalities. While it is true that these monolayers are susceptible to exchange by longer monolayers, there is a growing body of evidence that suggests that these types of monolayers are not as disordered and or as badly packed as was first believed. This could be due in part to the phase separation of mixed monolayers [108, 109].

There has been some debate as to whether mixed monolayers form an evenly distributed or a phase separated structure, where the thiols assemble in patches of single component monolayers and do not mix [47]. It has been concluded that thiols of the same chain length, even those with different functionalities seem to form better mixed and more stable SAMs [51] compared to those formed from different chain lengths thiols. SAMs of thiols with different chain lengths tend to form phase separated structures [110].

1.2.2.2.2.6.1 Mixed Monolayers of 11-Mercaptoundecanoic Acid and 11-Aminoundecanethiol

The carboxylic acid-terminated thiol only accounts for 25% of the surface moieties when it accounts for 50% of the solution when adsorbed with a methyl-terminated thiol [107].

Carboxylic acid- and amine-terminated thiols are thought not to affect the packing structure of the hydrocarbon chains due to their size being similar to that of methyl groups [111]. This is supported by the fact that a mixed monolayer can be formed from a solution of carboxylic acid and amine terminated thiols to form a well-packed monolayer [90].

Both carboxylic acid- and amine-terminated thiols have been found to be well distributed among methyl-terminated molecules when coabsorbed from solution to form mixed SAMs [110, 111]. Carboxylic acid-terminated SAMs have been found to be more stable than amine-terminated SAMs [112]. The carboxylic acid will probably have a higher molar fraction when assembled from an equimolar solution with an amine of the same chain length as the most stable monolayer generally has the highest molar fraction on the surface [114]. However, is possible to alter the molar fraction of each thiol on the surface by changing the solvent used.

The only instance where a binary SAM of carboxylic acids and amine has been formed is with Cys and MEA [114]. It should be noted that the two SAMs were not coadsorbed but attached to specific regions. Therefore mixing did not occur.

1.2.2.2.2.6.2 Reacted Mixed Self-assembled Monolayers

An alternative method of producing mixed monolayers on the surface is to react the tail groups of the SAM surface after they have been assembled [115]. The stability of the monolayer means that several reactions are possible such as the deacetylation of a carbohydrate presenting monolayer [116]. The reactions discussed here have been selected as two of the most useful in the immobilization of biomolecules [117-120].

1.2.2.2.2.6.2.1 NHS Reacted Self-assembled Monolayers

The NHS reaction involves reaction of an *N*-hydroxy succinimide (NHS)/ 1-ethyl-3 [3(dimethylamino)propyl] carbodiimide hydrochloride (EDC) mixture with a carboxylic acid-terminated SAM to produce an NHS ester presenting surface , which is capable of reacting with amines to form amide presenting SAMs (Figure 1.8). It should be noted that this surface cannot be fully reacted to form an NHS monolayer that does not contain COOH moieties due to steric factors. After 3 cycles of the reaction 80% of the surface can be covered with an amide [121].

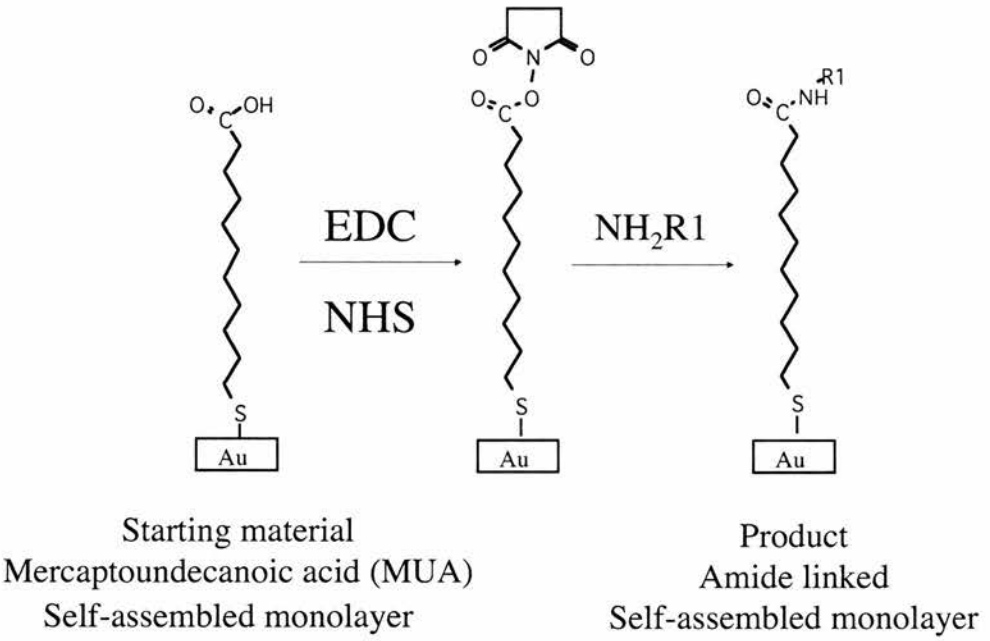

Starting material
Mercaptoundecanoic acid (MUA)
Self-assembled monolayer

Product
Amide linked
Self-assembled monolayer

Figure1.8 The NHS/EDC reaction carried out on a carboxylic acid-terminated SAM

The NHS intermediate is not necessary for the formation of an amide linkage. An amide bond can be formed by putting EDC and the amine to be linked in solution with the carboxylic-acid SAM [121]. This is not used in this study as the peptides to be linked are only feasibly usable (without huge cost) at a relatively low concentrations, and by reacting via the NHS intermediate the peptide molecules are given more time to react so lower concentrations can be used.

The NHS reaction performed in this study is modelled on that used by Frey and Corn [121]; the only difference is that NHS was used instead of the NHSS (*N*-hydroxysulfosuccinimide) used previously. This change was undertaken as the NHS

was significantly cheaper and NHSS is only useful because the monolayers take longer to hydrolyse [122]. As the monolayers are generally reacted immediately or removed from solution and put under vacuum with phosphorous pentoxide this was not deemed to be a significant problem. The type of analysis performed on the monolayers in this study was also the same as that done by Frey & Corn; it is therefore relevant to compare the results achieved by that study to those found in this one.

Another way in which NHS ester presenting SAMs can be formed is to buy the disulfide and assemble it directly onto the Au surface. As it is generally thought that disulfides form the same types monolayers [123-125] as thiols this surface should be no different from a fully reacted carboxylic acid surface. The succinimide presenting disulfide is available commercially and has been investigated previously [117, 126].

This reaction has one disadvantage when linking peptides; the NHS ester can react with an unprotected arginine residue. The reaction occurs between the arginyl guanidion group and the NHS [127].

1.2.2.2.2.6.2.2 SPDP Reacted Self-assembled Monolayers

SPDP is a bifunctional molecule, which has a succinimide group at one end that is reactive towards amines and a pyridylthiol group at the other, which is reactive

toward sulfhydryls [128]. This means that this molecule is particularly useful for biological crosslinking, and also makes it of use for surface immobilisation of biologically relevant molecules.

The SPDP can react with an amine-terminated monolayer. This causes the formation of an amide bond and produces a surface that is very reactive towards thiols (Figure 1.9). This reactive surface can then be used to immobilise cysteine residue containing peptides or proteins [120] via the formation of a pyridin-2-thione group [128].

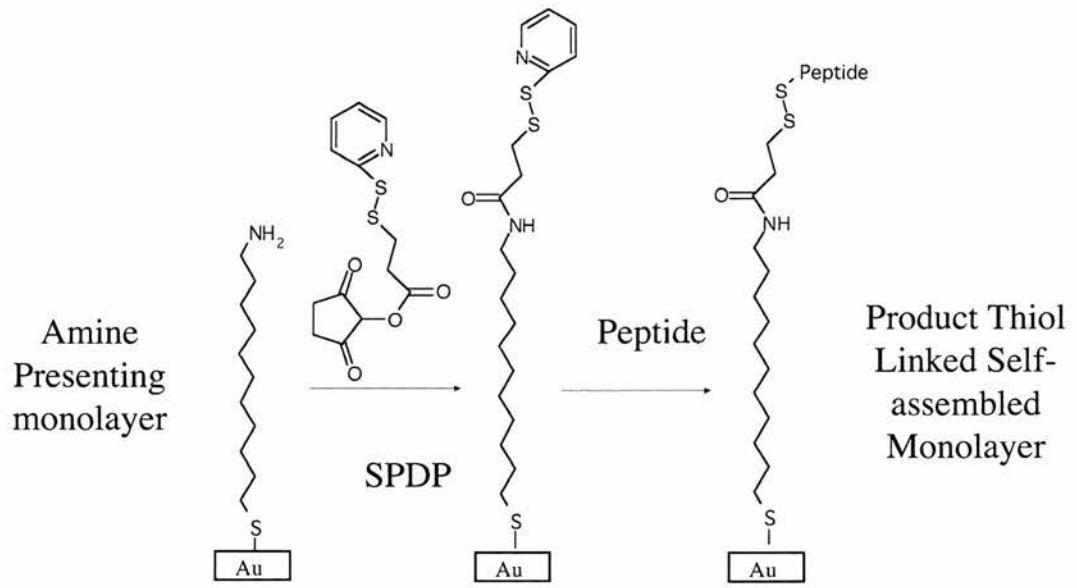

Figure 1.9 The SPDP reaction carried out on an amine terminated monolayer in order to link a sulfhydryl containing peptide to the surface

It may seem counter-intuitive to form a monolayer on the surface and then react it with a thiol. The advantage of doing this is that the spatial distribution of the peptides can be better controlled. This is desirable because a close packed arrangement would prohibit the interaction of the presented peptide with the cell surface.

The use of SPDP for surface immobilisation was not initially considered due to the cost that would be involved in soaking the surface in a solution of SPDP for the formation of the reactive surface. This problem however was solved by the use of a small quantity of solution applied directly to the surface and covered with a cover slip to spread out the solution evenly [129].

1.2.2.2.2.7 C2 Self-assembled Monolayers

SAMs of C2 alkanethiols have been used in this study as they are the only type of commercially available thiols that have the same chain length and different tail group functionalities. Evidence has been presented for the different positioning of the protein PS1 on surfaces dependent on the tail group of the C2 SAM used. MAA and 2-mercaptoethanol (Meth) SAMs had different orientational effects on the protein [130]. This indicates that there is a distinct difference between the surface chemistries of the assembled thiols and this makes them of use for cell adhesion experiments and comparison of the effects of the terminal functionality.

The MAA (COOH) monolayer and the MEA (NH_2) monolayer have been covered in previous sections and it has been concluded that, while there is evidence that significant H-bonding occurs in the monolayers to help stabilisation, the monolayers do not have a very dense structure. A flow experiment found that MAA was better adsorbed to an Au surface than MEA [112]. The ordering of Meth SAMs has been shown by an STM experiment, which visualised the well-ordered monolayers [131].

The structure of ETT has been investigated by STM and ordered domains have been found with the same features as the ODT long chain thiol SAMs [56]. There have also been different ordered structures found in ETT SAMs [55] compared the long chain thiol. The ETT FTIR spectrum shows that the ETT is capable of ordering so that the CH_2 asymmetric peak appears at 2918 cm^{-1}, which indicates a low level of liquid-like character in the SAM.

The very well ordered structures that are presented here for very short chain SAMs could indicate that they are actually better ordered than intermediate length SAMs where there is more conformational flexibility allowed by the hydrocarbon backbone. This is probably due to the strong ordering force of the sulfur head group.

1.2.2.2.2.8 Carbohydrate Self-assembled Monolayers

Carbohydrate thiol monolayers are rare due to the difficulty in forming thiol containing carbohydrates. It has been confirmed that it is possible to make carbohydrate SAMs [116, 132, 133], and it is possible for them to interact with carbohydrate binding proteins (lectins) [116], this makes them promising for use as cell growth substrates.

1.2.2.2.3 *Analysing Self-assembled Monolayers of Alkanethiols*

The monolayers of alkanethiols on Au have a structure that depends intimately on their preparation and storage conditions. It has been noted that small variations in these conditions can produce significant differences in the monolayer [47]. This means that, in order to have a true picture of what type of surface has been produced it has to be analysed with regard to both structure and chemical functionality.

There are many techniques that have been used to analyse alkanethiol SAMs, one of the most powerful and most widely used is STM, particularly when performed in an ultra high vacuum (UHV) environment. The images obtained from this technique have given great insight into the structure of the monolayer (Figure 1.5 and Refs [19, 39, 47, 134-136]). The disadvantage of this technique is that it is very time consuming; it can be difficult to obtain images of molecular resolution. Therefore it

is not a good technique for quality assessment of samples. AFM has much the same advantages and disadvantages [24, 37, 137-140].

The main advantage of IR spectroscopy is that with high quality spectra a great deal can be learned about the surface structures [141]. It first of all indicates what types of moieties are on the surface and it can provide information about the orientation of the surface groups (when the IR beam is reflected off a metal surface in reflection absorption spectroscopy). So it can provide information about composition, structure, and surface homogeneity. It is also a non-invasive technique so the surfaces are undamaged after analysis. This makes it an ideal choice for analysing monolayers for cell growth.

1.3 Fourier Transform Infrared Spectroscopy and Polarisation Modulation Infrared Reflection Absorption Spectroscopy

As mentioned previously, IR spectroscopy is the technique of choice for analysing slides of alkanethiolate monolayers to confirm their composition and structure. The precise form of IR spectroscopy and the sensitivity of the instrument and detector are the key factors in determining the power of the technique.

1.3.1 Infrared Spectroscopy

In a basic IR spectroscopy experiment, the sample is irradiated with a polychromatic IR source: some of the radiation is absorbed and some is passed through (transmitted). A detector registers the radiation that is not absorbed and the amount of radiation absorbed over a range of frequencies is then determined. A spectrum is produced representing the molecular absorption and transmission; this is the molecular fingerprint of the molecule. The frequency, at which the sample absorbs depends on the geometry, stiffness, polarity and length of bonds, and the masses of the atoms involved. More precisely, the absorbed frequencies correspond to the vibrational modes of the molecule and the band intensity depends on the extent to which the dipole moment of the molecule changes during a vibrational period.

A faster and slightly more complex way of collecting a spectrum is by using FTIR spectroscopy. This technique uses an interferometer, which has a beamsplitter that divides an incoming beam from the IR source into two equal parts. One part reflects from mirror A, the other from the moving mirror B. These two beams are then reflected back to the beamsplitter where they are redirected towards the detector. These two beams of radiation combine constructively or destructively depending on the path length of the movable mirror B. The combined beam then passes through the sample and as before certain IR frequencies are absorbed. The detector samples the combined beam.

During an experiment to determine the IR spectrum of a substance the movable mirror is moved a very short distance away from the beam splitter while the other mirror remains stationary. This produces a signal that corresponds to these two beams interfering with one another. This signal is called an interferogram. Every point of the interferogram contains information about every frequency of IR radiation that comes from the source. This interferogram is decoded by Fourier transformation to give the spectral analysis of every wavelength of IR radiation that the source produces and that the detector is able to detect. The Fourier transform converts the interferogram into a spectrum of the intensity of each frequency of radiation present in the detected signal. The signal to noise ratio of the spectra can be improved by constructing a spectrum from the sum of averaged interferograms.

1.3.2 Reflection Absorption Spectroscopy

Due to the high sensitivity of FTIR spectroscopy for low concentrations of analytes, it can be adapted to detect monolayers of organic molecules adsorbed on surfaces. In order to produce high quality spectra (and because the substrate is typically opaque) a technique called reflection-absorption spectroscopy (Figure 1.10) is used.

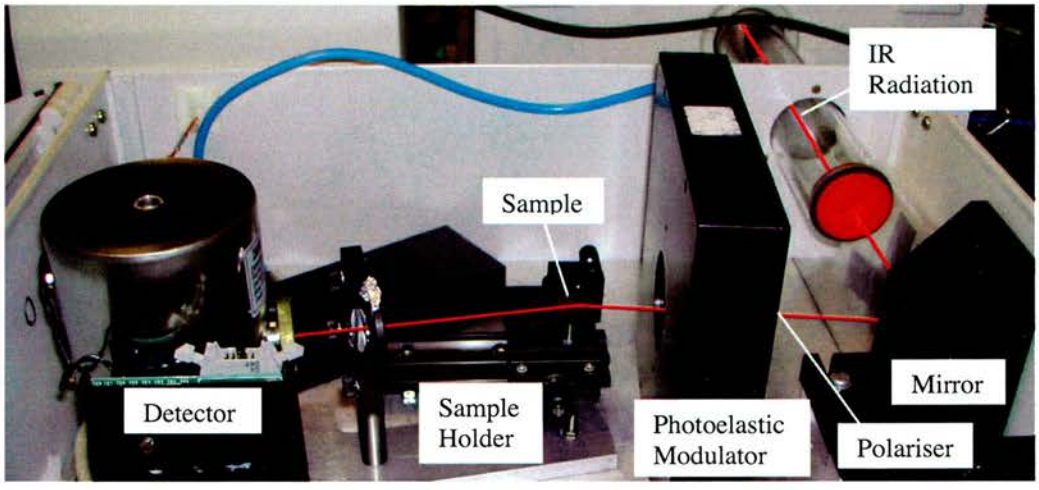

Figure1.10 Polarisation Modulation Infrared Reflection Absorption spectroscopy layout used to collect spectra in this study. The red line depicts the path of the IR radiation.

This type of FTIR spectroscopy involves using mirrors to reflect the IR beam so that it hits the surface at a grazing angle. The grazing angle is important because the phase of the radiation changes when it reflects from the surface and the reflected radiation interferes with the incident beam. For s polarised radiation (there is no polariser in the incident beam but the unpolarised radiation can be resolved into a sum of s- and p- polarised radiation) the interference is destructive (phase change 180 degrees). This creates a node at the surface so that no s radiation can be absorbed. For p polarised radiation the interference is constructive as it has a phase change about 90 degrees although this varies with the incident angle. The optimum incident angle is substrate dependent, but for a metal such as Au it is close to grazing incidence (80-85°). The SAMs on Au are perfect candidates for this technique as it

is only the top layer that is of interest and a reflective surface is required for this technique to work.

Unless all the IR optics, source and detector are operated in a vacuum, it is very rarely possible to get complete removal of the absorbance peaks caused by gas-phase CO_2 and water by ratioing the spectra. The amount of CO_2 and water present in the atmosphere is continuously changing and therefore the amount of atmospheric absorbance of radiation by CO_2 and water is also continuously changing. This means that the amount of atmospheric water and CO_2 absorbance present when the clean, blank sample is run will be completely different from when the SAM sample is run. This is particularly problematic for samples where the number of individual interferograms averaged is large, and the run times are longer.

1.3.3 Polarisation Modulation Infrared Reflection Absorption Spectroscopy

This technique is preferred as atmospheric interferences can be virtually eliminated, and a reference sample is not needed. In PMIRRAS a polariser is used to create linearly polarised radiation, which is passed through a photoelastic material such as ZnSe or CaF_2. On application of a sinusoidal ac voltage, this material changes the polarisation of the radiation between p-polarised and an extremum state, which is optimally s-polarised. Across the spectrum, the relationship to the extremum state is defined by a Bessel function, whose maxima can be selected for optimum s/p

differentiation in the region of interest. IR absorbing species in the gas-phase, principally water and carbon dioxide that can swamp the monolayer signal contribute equally to both s- and p-polarised spectra, while the monolayer is responsive only to p-polarised radiation. There are two reasons for this, both arising from the response of the metal electrons to an (varying) electric or electromagnetic field. Firstly it is because of the 180 degree phase change, which creates a node for s polarised radiation at the surface (described above in more detail). Secondly it is because of the surface dipole selection (Figure 1.11) rule.

The surface dipole selection rule states that only those vibrations of the adsorbed molecules, whose dipole change has a component perpendicular to the surface are active, as the parallel dipoles are screened by the metal surface. This means that the p/s spectral ratio optimally contains only surface-active vibrations. In turn, this is the key to determining functional group molecular orientation at metal surfaces. ***1.3.4***

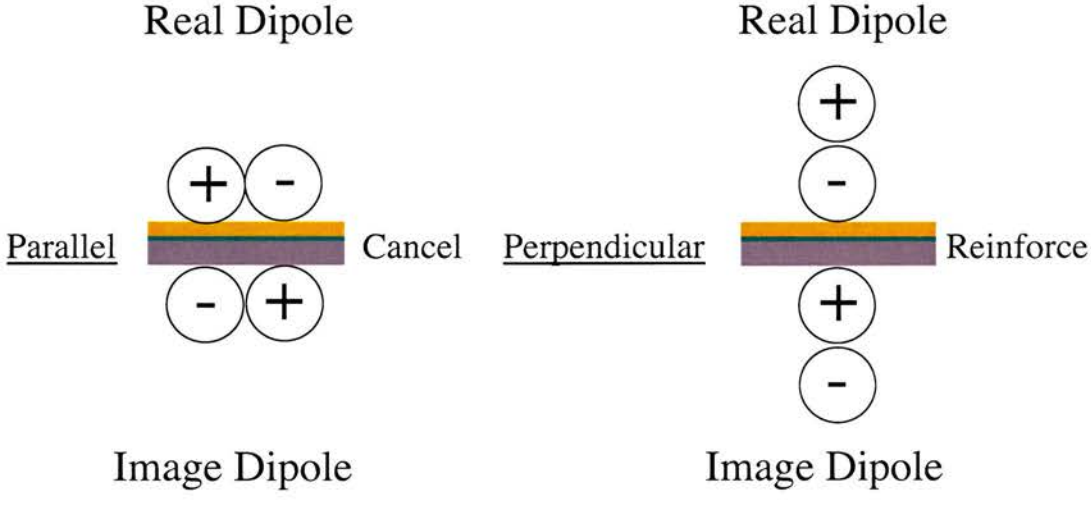

Figure 1.11 Diagram of surface dipole selection. Only those vibrations of the adsorbed molecules, whose dipole change has a component perpendicular to the surface are active as the parallel dipoles are screened by the metal surface

1.3.4 Alkanethiols and IR spectroscopy

The main information about the alkanethiol SAM that can be found by using IR spectroscopy, is the molecular composition of the monolayer and how well ordered it is. A well ordered monolayer will have well defined peaks at specific frequencies. If the monolayer is disordered, these peaks will be shifted to higher wavenumbers than the normal range expected for them, or in a particularly disordered monolayer may not be visible at all. The peaks in the spectra are due to the molecules vibrating and causing a change in dipole. Different types of vibration are observed for each molecular species, these different types of vibration are called vibrational modes (Figure 1.12). The most commonly observed vibrational modes in the spectra of alkanethiol SAMs are caused by stretching and deformation modes of the alkyl chain and functional tail groups. The movement of the atoms that causes the vibrations, is illustrated below.

Another factor, which determines whether or not the peaks will be visible, is the surface dipole selection rule (Figure 1.11). As mentioned before, only vibrations which have a dipole component that is perpendicular to the surface will be seen. It is therefore possible to determine the orientation of molecules on the surface from the position, and the magnitude of the peaks. The chain conformation, the orientation, coverage and packing all contribute to the position and intensity of the absorption bands.

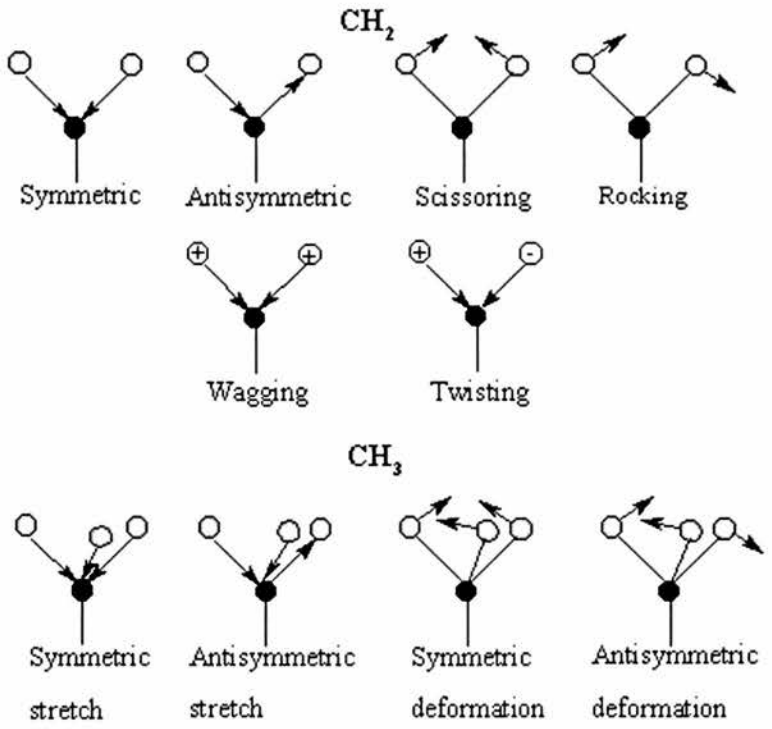

Figure 1.12 Vibrational Modes of alkyl groups. From a figure by A.King

1.4 Cells and Surface Modification

1.4.1 Introduction to Cells and their Natural Environment

The biological surface on which cells grow is called the extracellular matrix (ECM). The main purpose of the ECM is to provide a structural scaffold for cells. In addition, the ECM provides encoded instructions to help direct cell function and growth [142, 143]. The instructions are presented as variations in the chemistry or topography of the ECM. The chemical cues are presented in the form of long peptide chains (proteins) or long polysaccharide chains (glycosaminoglycans GAGs)

that the cell has receptors for. When the receptor binds to a peptide or polysaccharide sequence with the correct chemical structure and conformation this starts a signalling cascade. Many different receptors will bind different sequences and this information and the topographical signals are combined in complex pathways which gives the cell information about what it should do [144-146].

It has been found that the chemical cues in the ECM, particularly those in proteins, can be reduced in some cases to just a few amino acids. One of the most common examples of this is a cell adhesion peptide with the amino acid sequence RGD, which has been found to bind cell surface receptors called integrins. First discovered in fibronectin [147] the RGD peptide sequence has also been found in vitronectin, fibrinogen, laminin and collagen. In all its forms it has been implicated in integrin binding and cell signalling [148].

1.4.2 Cells in Culture

It should be noted that cells in culture (*in vitro*) will not be exactly the same as cells in their natural environment (*in vivo*), however, there are several advantages to working with cell cultures. The first of these is that it is possible to experiment with cell types that are difficult to obtain in large quantities or where it is ethically difficult (and increasingly legally difficult for human cells) to do so. In addition, work can be performed on one cell type at a time so there is a lower likelihood of vague results stemming from errors due to mixed cell types. There is also the

advantage, which will be exploited in this study, that the environment in which the cells are grown can be manipulated and this can be correlated to cell growth characteristics.

There are three type of cultured cells [149]:-

A. Primary cultures which are explants of tissue taken directly from a living organism.

B. Cell strains which are formed when cells from a primary culture are dissociated from one another and plated out.

C. Cell lines which are immortalised cell strains. Cells are or can become immortal by three methods. The first is by the appearance of cells in normal culture that have a genetic variant that allows them to grow forever. The second is by mutating the cells, for instance by irradiating them to cause the genetic changes that occur infrequently naturally. The third is by using explants from tumours tissue, which are naturally immortal.

1.4.2.1 Cell Growth in Culture

The most important factor to be considered when growing cells in culture is that the environment must be kept sterile. Without this consideration cell cultures can quickly become infected with bacteria or fungi. In order for cells to grow in culture, stocks of certain chemicals must be provided. These are supplied to the cells in a liquid solution known as the media. The constituents of the media are inorganic salts, which are principally needed for the maintenance of the osmotic balance; amino acids, which are needed as building blocks; vitamins needed as cofactors; carbohydrates, in particular sugars used as an energy source; buffer, which is needed to maintain the pH and is usually a bicarbonate / gaseous CO_2 system. Phenol red is usually also added as a visual indicator of pH, and antibiotics and antifungals are added as appropriate. In addition to these requirements, serum (the soluble portion of clotted blood plasma) containing important proteins (such as growth factors) is needed [150]. The serum does not have to be species specific and Foetal Bovine Serum (FBS) is generally used for most mammalian cell culture.

1.4.2.2 Topographical Modification- Cell Dependence on Topography

1.4.2.2.1 Patterning of Topography

One way to pattern topography is to have the surface topology produced via molding. An elastomeric mold is placed against the surface and an epoxy prepolymer is allowed to flow by capillary forces into the channels of the mold. This surface can then have a thin layer of a metallic substrate deposited onto it for further modifications [151].

Another way to pattern the surface topographically is by lithography. A resist is applied to the surface. The resist is then exposed through a mask to UV radiation [152] or X-ray radiation [153], or selectively removed by laser ablation [154]. This either solidifies the resist or decomposes it in the exposed areas. The unwanted areas can then be washed away with solvent leaving a pattern. The created pattern can either be used directly in this state [155] or the unprotected parts can be etched. Etching can be performed using hydrofluoric acid or potassium hydroxide, which leave sloping walls, or using reactive ions, which can be directed vertically by an electric field to give vertical sided structures. The depth of etching is measured by optical reflectometry. After etching the resist is removed [152, 156, 157].

A different method of creating topography on a surface is by polymer demixing. The principle of this is that two different polymers are spin coated onto a substrate from a common solution. These polymers phase segregate in different ways depending on the solubility of each polymer in the solution and its affinity for the surface. This produces patterns of islands and plateaux on the substrate [158].

1.4.2.2.2 Control of Cell Growth by Surface Topography

Roughened surfaces produced from the manufacturing processes have been found to show increased osteointegration, reduced fibrous encapsulation, and enhanced integration of breast implants (basically the body doesn't try to reject or wall off the implants as much) compared with smooth surfaces [152]. This is an effect, which arises from the increased adhesion of connective tissue cells onto the roughened surfaces.

The effect that microtexture has on fibroblasts differs with the size of the texture. One group found that fibroblasts orientated along 3 and 10 μm deep grooves but they inserted obliquely into 22 μm grooves [152]. Rat dermal fibroblast cells were cultured on pure Ti wafers, and it was found that those on plasma etched gratings of width 1 and 2 μm oriented the cells and their stress fibres parallel to the surface pattern. This was not seen with gratings of size 5 and 10μm. The bigger the grating the less the cells responded its presence [159].

The effect of topography depth on cell orientation is complex as different cell types react in different manners. It can be difficult to separate the effect of depth from width. In general, it has been found that the extent of cell orientation in response to grooves increases with groove depth up to about 25 μm, though cells can react to depths as shallow as 44 nm [160].

The topography width has a significant effect on cell orientation. When the grooves are wider than the cell the effects on the orientation of the cells are small, though cells may align to an edge. Grooves of width smaller than the cell, have an effect on its orientation and the lower limit for this has not been found [161].

It is thought that the cells may be as sensitive or more sensitive at sensing topography than an AFM. This may be accomplished by compression or deformation being sensed by the cell as the cell conforms or attaches to the topography [161]. It is known that osteoblasts can be activated by mechanical stimuli [162], so other cells could have similar, more sensitive receptors, which allow the cell to respond to the topography of their surroundings.

Whether the chemistry of the surface or the topography is the major determining factor for the orientation of cells has been a topic debated for some time. When a chemical cue was oriented at 90° to a topographical cue the cells reacted mainly to the chemical cue when the grooves were 500 nm deep or less [163]. When the

grooves were deeper the topographical cue became more significant [163]. In general chemical differences seem to have a larger effect on cell behaviour [164], though both topographic chemical and cues are important for cell guidance [165].

This indicates that the effects of topography and chemistry can have different contributing factors and as such should be initially studied separately with the variable not under investigation being carefully controlled.

1.4.2.3 Chemical Modification-Cell Dependence on Chemistry

The growth of cells is influenced by surface chemistry in two ways, firstly by the presentation of specific ligands in the appropriate density and conformation[166], secondly by the hydrophobicity of the surface [167]. Ligand-presenting surfaces are thought to have an effect on the cell by interacting with the cell-signalling receptors and causing a signalling cascade that can affect cellular functions or conformation.

The hydrophobicity of the surface is though to have a less direct effect. The cells are grown in media with FBS with contains proteins. These proteins deposit on the surface in different conformations depending on what the chemistry of the surface is, generally matching the hydrophobic parts of the protein to hydrophobic SAMs. The cells then interact with the surfaces presented by these deposited proteins, and

differences in protein deposition causes differences in cell growth characteristics until the cell secretes its own ECM material to reform the surface.

It is possible that there is no specific interaction between the cell and presented ligands, however this is not likely as there has been found to be significantly more adhesion to cell adhesion peptide (RGD) presenting surfaces than to analogues with the same chemical functionalities in a different order (RDG) [168].

The easiest way in which surfaces can be modified to control their surface chemistry is by the non-specific deposition of single proteins. This process is unfortunately not as simple as it sounds because the conformation in which the proteins deposit themselves on the surface is often influenced by the substrate surface chemistry [169]. This is true for most materials used in cell growth, as even if protein deposition on the surface is not the aim of the study it will still occur as soon as the surface is exposed to a serum containing solution [167].

The proteins deposited in this manner form a heterogeneous layer, which usually contains both conformational and orientational variation [168], This can make it difficult to determine which cell adhesion promoting regions are accessible and correctly oriented. One way to make regions that promote cell adhesion and binding more available is to use only these regions, to incorporate the desired sequences in a more controlled manner.

The first bioactive peptide used to control cell adhesion and spreading was the RGD peptide when in 1988 the peptide was adsorbed onto a polyacrylamide gel [170]. This produced very promising results for use as a model system to study cell adhesion. Several different polymers have since been modified to present the RGD peptide either adsorbed or covalently attached [171-177]. These were found to promote cell attachment and growth and as such were considered to be promising biomaterials for three dimensional cell culture.

1.4.2.3.1 Cell Growth on Polymers

Polymeric materials, which present chemical functionalities to encourage or prevent cell growth are increasingly in demand. The reason for this is that they are relatively inexpensive and can be used for medical applications such as catheters [178] or implants [179]. Polymers are also commonly used for cell culture applications.

1.4.2.3.1.1 Modification of Polymer Constituents for Cell Growth

One way to form a surface presenting the required chemistry is to form a polymer that contains the required groups. One example of this is the modification of a cellulose polymer to give different levels of hydrophobicity [180]; in this case it was found that moderate hydrophilicity gave the best cell adhesion. Another example of

this is a polymer created containing different proportions of a biomimetic peptide (RGD) and a carbohydrate (maltose); the polymer containing the largest amount of RGD was found to be the best cell growth substrate [171].

The advantage of using a polymeric material to present the desired surface chemistry is that the micrometre or nanometre level topography of the surface can be easily controlled by molding the polymer. The first disadvantage of using polymers is that it is difficult to control the way in which conformation that ligands are presented in the polymer surface. The second disadvantage is that the size of the polymeric features that can be controlled is much bigger than the level down to which most cells can sense.

As cells can respond to very small changes in the environment it is possible that two macromers made in the same way could elicit very different responses from cells. A more controlled approach, which also utilises polymers, involves the attachment of polypyrrole modified by an RGD containing peptide to Ti [176]. As this produces a thin film the resultant surface can be more intensively characterised to determine the structure.

1.4.2.3.1.2 Modification of Polymer Surface for Cell Growth

Polymeric surfaces can be modified in three ways after they have been created [181]. The first method is to coat the surface with a material of a different composition such as coating with Au for thiol self-assembly [182]. The second method was mentioned earlier for alkanethiols and involves the reaction of the surface molecules to present an additional type of molecule, usually a ligand.

The third method is the physical modification of the surface by bombarding the surface with ions [183], irradiating with ultraviolet radiation [184] or exposing it to plasma discharge [185]. These procedures lead to the formation of radicals that react with oxygen leading to the formation of oxygen-containing groups such as carbonyl, carboxyl, ester, or hydroxyl groups. The beam modification of the polymers also has the effect of increasing the number of double bonds, this makes the material relatively enriched with carbon which is known to have beneficial effect on cell adhesion [186]. The advantage of this is it is quick and relatively cheap to achieve. The disadvantage is that it is unpredictable what exact surface will be produced; the reactions are not very predictable.

1.4.2.3.2 Cell Growth on Self-assembled Monolayers

Growing cells on SAMs is a good way to control surface chemistry in a way that can be well characterised. The two main types of SAM that are stable enough for use in cell culture are alkylsiloxanes on silicon and alkanethiols on Au. Apart from the bioactive SAMs these studies predominantly have an effect on the protein deposition, although the amount of cellular adhesion seems to correspond to more than just the wettability of the surface.

1.4.2.3.2.1 Self-assembled Monolayers that Promote Cell Adhesion

It was found that cells adhere to both hydrophilic and hydrophobic alkanethiol SAM surfaces [187]. In cell cultures plated from media containing 10% foetal bovine serum, it was found that cells attached better to more hydrophilic SAMs with tail groups of carboxylic acid or $-N(CH)_2$, than those with the methyl tail groups. When cells were plated from media, which did not contain serum, it was found that cells attached equally well to both hydrophilic and hydrophobic SAMs [187]. The same results for serum adsorbed surfaces were also found for alkylsiloxane monolayers which had fibroblasts grown on them [188]. These results both support the theory that protein attachment from serum plays a significant role.

In a different study of cell adhesion, after 24 hours the number of cells attached to a carboxylic acid-terminated alkanethiol SAM were ten times the number adherent to a methyl-terminated SAM. Cells were found to preferentially adhere to carboxylic acid-terminated monolayers, and after 24 hours were observed to bridge regions of 75 μm between carboxylic acid-terminated SAMs [152].

1.4.2.3.2.2 Self-assembled Monolayers that Prevent Cell Adhesion

One of the molecules, which has been most extensively studied for its property of inhibiting cell adhesion, has been oligoethylene glycol (OEG) [189]. A certain amount of OEG alkanethiol needs to be bound in order to prevent the adsorption of cells to the surface [187, 190]. The percentage of the film that has to be OEG in order to resist cell adhesion varies according to the length of the OEG chain; those typically used contain 3 to 6 ethylene oxide units [191]. In cases where the OEG SAMs are presented mixed with another alkanethiol the ratio is typically 100:1 [191].

Initially it was thought that the terminal hydroxyl group on the OEG chain was responsible for the prevention of adsorption [191] but this has been found to be incorrect, as inhibition of cell adhesion was found to occur without it [189]. Another hypothesis that was also proved incorrect was that OEG chains would become less resistant to protein adhesion as they became shorter. In a study using SAMs of

undecylenic thiol presenting OEG groups EG_nOH with n = 2-7, all lengths of n resisted the adsorption of proteins. This implies that the mechanism of repulsion is not purely steric factors [191]. By comparison of OEG terminated alkanethiols on Au (which adopt helical conformation) and Ag (which adopt extended *trans* conformation) it was found that the conformation which was most protein resistant was the helical conformation; the *trans* conformation showed no protein resistance [189]. These observations indicate that the interfacial water adsorption is important in the SAMs ability to resist protein and cell adsorption. Harder *et al* proposed that it could be the solvent ordering which put up the barrier to protein adhesion [192].

Another alkanethiol SAM that resists the adsorption of proteins is a SAM which presents tri(propylene sulfoxide) groups [193]. This SAM was found to be less effective at resisting protein adherence than OEG SAMs [193]. Alkanethiol SAMs presenting the carbohydrate maltose [192] and mannitol groups [192] have also been found to inhibit protein and cell adhesion. Studies with mannitol-terminated alkanethiols have shown that these carbohydrate SAMs are more effective than OEG-terminated SAMs for long-term cell patterning. Chapman *et al* found that in general SAM terminations that resist the adsorption of proteins are H-bond acceptors but not H-bond donors, hydrophilic and conformationally flexible [194].

1.4.2.3.2.3 Bioactive Self-assembled Monolayers

Bioactive chemical surfaces are surfaces that present bioactive ligands that can affect cell function or growth by stimulation or inhibition of the cell receptors producing a cell signalling cascade. The two main types of bioactive ligand are carbohydrates and peptides; these can cause many different cell responses including cell-cell recognition, cell adhesion, cell differentiation or cell migration.

The peptides are usually parts of proteins that have been found to have a specific activity when presented to the cells. As this study is on cell adhesion and growth it is the cell adhesion peptides that are of interest. The most ubiquitous cell adhesion peptide is the RGD peptide. It has been used in many studies to promote cell adherence [170-177].

The easiest way to present the cell adhesion peptide RGD in a SAM is by purchasing the RGDC peptide and assembling it on Au surfaces from ethanolic solution. The peptide attaches via the thiol group of the cysteine residue. Although this is the least time-consuming method it is unlikely to be the most effective at promoting cell adhesion as the peptides are unlikely to be accessible as cellular ligands when packed closely together on the surface. Au-coated polyurethanes were used to present RGD sequences in peptides of different lengths and compositions all linked to the Au surface via the Cys residue [182]. It was found that different cell types spread better

on surfaces adsorbed with different sequences. Also it was noted that there was little or no cell adhesion of 3T3 fibroblasts or human vascular endothelial cells to the bare Au or Cys modified surfaces [182]. A similar approach was also used in order to assemble longer peptides onto Au. A Cys residue was placed after every few residues in order to form loops attached to the surface. The only disadvantage of this approach is that close packed films are not formed so these structures can only loosely be called SAMs.

A more ordered SAM presenting the RGD peptides was made of alkylsiloxanes. This was done in order to obtain a more homogeneous surface that would be better substrate for analysis of cell adhesion [195]. This approach was adapted and used for SAMs of alkanethiols that presenting the RGD peptide at the end of an OEG thiol, in a mixed monolayer with triethyleneglycol-terminated thiols [196]. The OEG groups, as mentioned previously, are used in order to prevent the non-specific adsorption of protein or cells. This gives more control over the conditions and so the factors responsible for adhesion can be more accurately identified.

Langmuir-Blodgett self-assembled films have also been produced presenting the RGD peptide and this study produced the particularly interesting result that the peptide had differential binding to cells dependent on the orientation of the peptide on the surface [197]. The cells spread well on the looped RGD surface in a

concentration dependent manner, they also spread on the carboxyl-coupled surface. There was no cell spreading on amino-coupled surfaces.

A great deal of work has been done on RGD, though it is not the only cell adhesion peptide that has been used as a ligand for cell attachment. The PHSRN sequence from fibronectin has also been used for the adherence of BHK cells [168] and the IKVAV [198] and YIGSR [199] cell attachment domains found in laminin have been adhered to the surface by a terminal Cys residue. These laminin peptide SAMs have been successfully used for the growth of hippocampal neurons.

There have been no reports found of SAMs of carbohydrates used for cell growth.

1.4.2.4 Assessment of Cell Growth

A simple method of assessing cell viability is via membrane integrity using trypan blue exclusion [200]. Cell proliferation can be analysed via the incorporation of labelled nucleotides such as [3H]-thymidine into newly synthesised DNA during cell division [201]. The amount of incorporation can be measured by liquid scintillation counting, and this is a relative measure of cellular proliferation. The disadvantages of this technique are that it is time-consuming, labour-intensive and exposes the researcher to toxic chemicals (scintillation fluid and tritium).

The thymidine analogue 5-bromo-2'-deoxyuridine (BrdU) can be used instead of [3H]-thymidine in proliferation assays. BrdU is incorporated into cellular DNA in a similar manner to thymidine [202]. This technique has the advantage that it is easy to quantify the incorporation of BrdU using anti-BrdU monoclonal antibodies (mAbs) in ELISAs. This eliminates the need to use radioisotopes. ELISAs with both colorimetric [202] and chemiluminescent [203] detection can be used.

There are two main methods to detect BrdU. One described above uses anti-BrdU mAbs to detect BrdU incorporation by denaturing the cellular DNA into single strands in order to expose the BrdU epitope to the antibody, either by heating it to greater than 90°C or by acid (2-4N hydrochloric acid) treatment [204]. This method has disadvantages, if downstream assays are to be used as many cellular proteins are lost or degraded during the denaturation process. The other uses strand break induced photolysis (SBIP), a technique where recombinant DNA denaturation is not as extensive and antigens and other cellular features are preserved. In the SBIP assay, cells are grown in the presence of a BrdU photolyte, which labels the DNA of proliferating cells as in the previous method [205]. An enhancer photolyte is then added which sensitises the DNA- incorporated BrdU to subsequent photolysis. The cells are then harvested, washed and UV-irradiated to induce strand breaks at BrdU-incorporation sites [205]. These break sites are labelled with bromolated deoxyuridine triphosphate (Br-dUTP) in a TUNEL assay-like reaction catalysed by terminal deoxynucleotidyl transferase (TdT), which adds deoxyribonucleotides in a

template-independent manner. The anti-BrdU monoclonal antibody is then used in an ELISA [206].

The MTT assay designed by Mosmann using 3-[4,5-dimethylthiazol-2-yl]-2,5-diphenyltetrasodium bromide (MTT) tetrazolium salts is a viable alternative to the [3H]-thymidine incorporation assay [207, 208]. The tetrazolium ring of MTT is reduced to formazan, which is blue in colour, by the succinate-tetrazolium reductase system active only in viable cells [205]. The intensity of the resulting colour change indicates the enzymatic activity of living cells. In actively proliferating cells the rate of MTT conversion is fast, whereas in senescent and dying cells MTT conversion is slow. Comparison of this value to an untreated control provides a measure of the change in cellular proliferation. To quantify the amount of dye it is solubilised and quantified using a plate reader. The absorbance measured correlates directly with cell number.

Other tetrazolium salts: WST-1, WST-8, XTT, and MTS have been used instead of MTT with the advantage that these tetrazolium salts produce water-soluble formazan salts in the presence of an electron-coupling reagent which makes the analysis faster. This also has the advantage that multiple time points can be taken which was not possible with MTT. The only disadvantage of using these kits is that there has to be extensive use of detailed controls or the results may be misleading. For example, the metabolic activities of certain cell lines may be far different than those of others.

Cells that have a particularly low metabolic activity, such as lymphocytes, must be used in higher numbers than more metabolically active cells, so direct cell-to-cell comparisons are difficult. Also, the assays may not be linear over a broad logarithmic range of cell proliferation because of the use of plate readers with these kits [209]. Finally, despite their widespread use, the details of tetrazolium salt cellular bioreduction are still not well understood [205].

The main disadvantage of all these techniques, which are common indicators of cell proliferation, is that they are toxic to the cells. Due to this factor other non-toxic methods of analysis were investigated.

1.4.2.4.1 BCECF Assay

BCECF is a fluorescent indicator that can be irreversibly loaded into cells. In order to load the BCECF into the cells it is given in the form of the BCECF-AM ester, which can enter cells without permeabilization. It does not leave because once it has entered the cell the AM-ester is cleaved by an esterase leaving the BCECF trapped. Once the BCECF has been loaded into the cells the level of fluorescence can be used to quantify the number of cells present. This can be used to assess the number of cells adhering to a surface by taking readings of fluorescence before and after washing the surface.

The main advantage of this compound is that it is non-toxic [210] and it has not been shown to affect cell growth, therefore cultures can be used for other experiments. Another slight advantage is that as well as providing quantitative results it can be used to provide pictures of cell adhesion, which can be particularly useful on an opaque surface. The major disadvantage of this compound is that the fluorescence declines significantly within a period of 12 hours so readings cannot be taken over long periods of time. A slight disadvantage is that the loading process can be affected by the addition of either media or FBS and the absence of these can decrease the viability of the cells, which could adversely affect their adhesion potential [210].

1.4.2.4.2 AlamarBlue Assay

AlamarBlue is a product used to measure the respiration of cells. Respiration is a good indicator of cell proliferation because it is both an indicator of cell growth and cell condition. The main component of alamarBlue is resazurin which is a blue, non-fluorescent compound which reduces irreversibly to become a pink, fluorescent compound called resorufin [211]. The other component(s) that are included in the alamarBlue mix are poisoning agents which are added to absorb excess electrons which would reduce the pink, fluorescent resorfin to colourless non-fluorescent dihydroresorfrin [212]. The preferred poisoning agents are potassium ferrocyanide,

ferric salt or ferricinium, though methylene blue, toluidine blue, azure I and gallocyanide can also be present [213].

The major advantage of this particular indicator of cell growth is that it is non-cytotoxic [214]. This means that it does not kill the cells, so the growth of cells can be measured over time rather than as an end-point. It is also easy to use with samples that are not transparent as it has a change in the level of fluorescence (which it is possible to excite and measure from above) as well as a visible colour change with cell proliferation. The major disadvantage is that the major component, resazurin has been found to have problems with the resorfin reversibly reducing to dihydroresorufin [212]. These problems have only been attenuated, not solved by the addition of the poisoning agents. It should also be noted that the medium containing reduced glutathione [215] (such as RPMI 1640) also significantly reduces resazurin over time.

1.5 Aim

The main aim of this project is to clarify the effect that surface chemistry and structure of alkanethiols on Au has on the proliferation of cells in culture. In doing this it is hoped that there can be some clear correlations found between the type of

alkanethiol used to produce a SAM, the structure of that thiol on a Au surface, and the amount of cell adhesion and growth.

1.6 References

1. Wolff, S.L., *Molecular and cellular biology*, Publshed by Wadsworth

2. Jackson, R., *Tissue culture used as bioproducts factories*. 2003, CSIRO.

3. Lodish, H., A. Berk, L.S. Zipursky, P. Matsudaira, D. Baltimore, and J. Darnel, *Manipulating cells and viruses in culture*, in *Molecular cell biology*. 2000, W. H. Freeman & Company: New York.

4. Riehle, M., *Animal cell culture lab*. 2005, Glasgow University.

5. Frank, U. and B. Rinkevich, *Scyphozoan jellyfish's mesoglea supports attachment, spreading and migration of anthozoans' cells in vitro*. Cell Biology International, 1999. **23**(4): p. 307-311.

6. Ruegsegger, M.A. and R.E. Marchant, *Student research award in the doctoral degree candidate category, 27th annual meeting of the society for biomaterials, St. Paul, ,MN, April 24-29, 2001 - Reduced protein adsorption and platelet adhesion by controlled variation of oligomaltose surfactant polymer coatings*. Journal of Biomedical Materials Research, 2001. **56**(2): p. 159-167.

7. Bonzon, N., X. Carrat, C. Deminiere, G. Daculsi, F. Lefebvre, and M. Rabaud, *New artificial connective matrix made of fibrin monomers, elastin peptides and type I+ III collagens - Structural study, biocompatibility and use as tympanic membranes in rabbit*. Biomaterials, 1995. **16**(11): p. 881-885.

8. VandeVondele, S., J. Voros, and J.A. Hubbell, *RGD-grafted poly-l-lysine-graft -(polyethylene glycol) copolymers block non-specific protein adsorption while promoting cell adhesion*. Biotechnology and Bioengineering, 2003. **82**: p. 784 –790.

9. Logeart-Avramoglou, D. and J. Jozefonvicz, *Carboxymethyl benzylamide sulfonate dextrans (cmdbs), a family of biospecific polymers endowed with numerous biological properties: A review*. Journal of Biomedical Materials Research, 1999. **48**(4): p. 578-590.

10. Bigelow, W.C., D.L. Pickett, and W.A. Zisman, *Oleophobic mono-layers: 1. Films adsorbed from solution in non-polar liquids*. Journal of Colloid and Interface Science, 1946. **1**: p. 513-538.

11. Engquist, I., *Self-assembled monolayers*. 1996. p. 5.

12. Franco, M., P.F. Nealey, S. Campbell, A.I. Teixeira, and C.J. Murphy, *Adhesion and proliferation of corneal epithelial cells on self- assembled monolayers*. Journal of Biomedical Materials Research, 2000. **52**(2): p. 261-269.

13. Wagner, P., S. Nock, J.A. Spudich, W.D. Volkmuth, S. Chu, R.L. Cicero, C.P. Wade, M.R. Linford, and C.E.D. Chidsey, *Bioreactive self-assembled monolayers on hydrogen-passivated Si(111) as a new class of atomically flat substrates for biological scanning probe microscopy*. Journal of Structural Biology, 1997. **119**(2): p. 189-201.

14. Wasserman, S.R., Y.-T. Tao, and G.M. Whitesides, *Structure and reactivity of alkylsiloxane monolayers formed by reaction of alkyltrichlorosilanes on silicon substrates*. langmuir, 1989. **5**: p. 1074-1087.

15. Kane, R.S., S. Takayama, E. Ostuni, D.E. Ingber, and G.M. Whitesides, *Patterning proteins and cells using soft lithography*. Biomaterials, 1999. **20**(23-24): p. 2363-2376.

16. Riederer, D.E., R. Chatterjee, S.W. Rosencrance, Z. Postawa, T.D. Dunbar, D.L. Allara, and N. Winograd, *Thermal desorption induced by kiloelectron volt ion bombardment of thiol-bound self-assembled monolayers on gold.* Journal of the American Chemical Society, 1997. **119**(34): p. 8089-8094.

17. Ulman, A., *Formation and structure of self-assembled monolayers*. Chemical Reviews, 1996. 96(4): p. 1533-1554.

18. Dubois, L.H., B.R. Zegarski, and R.G. Nuzzo, *Molecular ordering of organosulfur compounds on Au(111) and Au(100) - adsorption from solution*

and in ultrahigh-vacuum. Journal of Chemical Physics, 1993. **98**(1): p. 678-688.

19. Qian, Y.L., G.H. Yang, J.J. Yu, T.A. Jung, and G.Y. Liu, *Structures of annealed decanethiol self-assembled monolayers on Au(111): An ultrahigh vacuum scanning tunneling microscopy study*. Langmuir, 2003. **19**(15): p. 6056-6065.

20. Kawasaki, M., T. Sato, T. Tanaka, and K. Takao, *Rapid self-assembly of alkanethiol monolayers on sputter-grown Au(111)*. Langmuir, 2000. **16**(4): p. 1719-1728.

21. Follonier, S., W.J.W. Miller, N.L. Abbott, and A. Knoesen, *Characterization of the molecular orientation of self-assembled monolayers of alkanethiols on obliquely deposited gold films by using infrared-visible sum-frequency spectroscopy*. Langmuir, 2003. **19**(25): p. 10501-10509.

22. Hutt, D.A. and G.J. Leggett, *Desorption of butanethiol from Au(111) during storage in ultrahigh vacuum: Effects on surface coverage and stability toward displacement by solution-phase thiols*. Langmuir, 1997. **13**(11): p. 3055-3058.

23. Bensebaa, F., T.H. Ellis, A. Badia, and R.B. Lennox, *Thermal treatment of n-alkanethiolate monolayers on gold, as observed by infrared spectroscopy*. Langmuir, 1998. **14**(9): p. 2361-2367.

24. Alves, C.A., E.L. Smith, and M.D. Porter, *Atomic scale imaging of alkanethiolate monolayers at gold surfaces with atomic force microscopy.* Journal of the American Chemical Society, 1992. **114**(4): p. 1222-1227.

25. Wagner, P., M. Hegner, P. Kernen, F. Zaugg, and G. Semenza, *Covalent immobilization of native biomolecules onto Au(111) via N-hydroxysuccinimide ester functionalized self-assembled monolayers for scanning probe microscopy.* Biophysical Journal, 1996. **70**(5): p. 2052-2066.

26. Zerulla, D., I. Uhlig, R. Szargan, and T. Chasse, *Competing interaction of different thiol species on gold surfaces.* Surface Science, 1998. **404**(1-3): p. 604-608.

27. Ishida, T., N. Nishida, S. Tsuneda, M. Hara, H. Sasabe, and W. Knoll, *Alkyl chain length effect on growth kinetics of n-alkanethiol self-assembled monolayers on gold studied by x-ray photoelectron spectroscopy.* Japanese Journal of Applied Physics Part 2-Letters, 1996. **35**(12B): p. L1710-L1713.

28. Camillone, N., T.Y.B. Leung, P. Schwartz, P. Eisenberger, and G. Scoles, *Chain length dependence of the striped phases of alkanethiol monolayers self-assembled on Au(111): An atomic beam diffraction study.* Langmuir, 1996. **12**(11): p. 2737-2746.

29. Lavrich, D.J., S.M. Wetterer, S.L. Bernasek, and G. Scoles, *Physisorption and chemisorption of alkanethiols and alkyl sulfides on Au(111).* Journal of Physical Chemistry B, 1998. **102**(18): p. 3456-3465.

30. Schreiber, F., *Self-assembled monolayers: From 'simple' model systems to biofunctionalized interfaces.* Journal of Physics-Condensed Matter, 2004. **16**(28): p. R881-R900.

31. Noh, J. and M. Hara, *Nanoscale observation of dissociative adsorption during self-assembly processes of dialkyl disulfides on Au(111).* RIKEN Review, 2001. **37**: p. 54-57.

32. Poirier, G.E. and M.J. Tarlov, *The c(4x2) superlattice of n-alkanethiol monolayers self- assembled an Au(111).* Langmuir, 1994. **10**(9): p. 2853-2856.

33. Arce, F.T., M.E. Vela, R.C. Salvarezza, and A.J. Arvia, *Dynamic characteristics of adsorbed monolayers of 1- dodecanethiol on gold (111) terraces from in-situ scanning tunneling microscopy imaging.* Electrochimica Acta, 1998. **44**(6-7): p. 1053-1067.

34. Arce, F.T., M.E. Vela, R.C. Salvarezza, and A.J. Arvia, *The dynamic behavior of butanethiol and dodecanethiol adsorbates on Au(111) terraces.* Journal of Chemical Physics, 1998. **109**(14): p. 5703-5706.

35. Danisman, M.F., L. Casalis, G. Bracco, and G. Scoles, *Structural investigation of monolayers prepared by deposition of (Ch_3s)(2) on the (111) face of single-crystal gold*. Journal of Physical Chemistry B, 2002. **106**(45): p. 11771-11777.

36. Yourdshahyan, Y. and A.M. Rappe, *Structure and energetics of alkanethiol adsorption on the Au(111) surface*. Journal of Chemical Physics, 2002. **117**(2): p. 825-833.

37. Barrena, E., C. Ocal, and M. Salmeron, *Evolution of the structure and mechanical stability of self- assembled alkanethiol islands on Au(111) due to diffusion and ripening*. Journal of Chemical Physics, 1999. **111**(21): p. 9797-9802.

38. Camillone, N., C.E.D. Chidsey, G.Y. Liu, and G. Scoles, *Superlattice structure at the surface of a monolayer of octadecanethiol self-assembled on Au(111)*. Journal of Chemical Physics, 1993. **98**(4): p. 3503-3511.

39. Noh, J. and M. Hara, *Final phase of alkanethiol self-assembled monolayers on Au(111)*. Langmuir, 2002. **18**(6): p. 1953-1956.

40. Yeganeh, M.S., S.M. Dougal, R.S. Polizzotti, and P. Rabinowitz, *Interfacial atomic structure of a self-assembled alkyl thiol monolayer/ Au(111): A sum-frequency generation study*. Physical Review Letters, 1995. **74**(10): p. 1811-1814.

41. 2003, North Carolina State University.

42. Hayashi, T., Y. Morikawa, and H. Nozoye, *Adsorption state of dimethyl disulfide on Au(111): Evidence for adsorption as thiolate at the bridge site.* Journal of Chemical Physics, 2001. **114**(17): p. 7615-7621.

43. Morikawa, Y., T. Hayashi, C.C. Liew, and H. Nozoye, *First-principles theoretical study of alkylthiolate adsorption on Au(111).* Surface Science, 2002. **507-510**: p. 46-50.

44. Mrksich, M., *Tailored substrates for studies of attached cell culture.* Cellular and Molecular Life Sciences, 1998. **54**(7): p. 653-662.

45. Liao, S., Y. Shnidman, and A. Ulman, *Adsorption kinetics of rigid 4-mercaptobiphenyls on gold.* Journal of the American Chemical Society, 2000. **122**: p. 3688-3694.

46. Ulman, A., *Self-assembled monolayers of 4-mercaptobiphenyls.* Accounts of Chemical Research, 2001. **34**: p. 855-863.

47. Schreiber, F., *Structure and growth of self-assembling monolayers.* Progress in Surface Science, 2000. **65**(5-8): p. 151-256.

48. Bryant, M.A. and J.E. Pemberton, *Surface raman scattering of self-assembled monolayers formed from 1-alkanethiols: Behavior of films at Au and*

comparison to films at Ag. Journal of the American Chemical Society, 1991. **113**: p. 8284-8293.

49. Porter, M.D., T.B. Bright, D.L. Allara, and C.E.D. Chidsey, *Spontaneously organized molecular assemblies .4. Structural characterization of normal-alkyl thiol monolayers on gold by optical ellipsometry, infrared-spectroscopy, and electrochemistry*. Journal of the American Chemical Society, 1987. **109**(12): p. 3559-3568.

50. Fenter, P., A. Eberhardt, K.S. Liang, and P. Eisenberger, *Epitaxy and chainlength dependent strain in self-assembled monolayers*. Journal of Chemical Physics, 1997. **106**(4): p. 1600-1608.

51. Aoki, K., *Theory of phase separation of binary self-assembled films*. Journal of Electroanalytical Chemistry, 2001. **513**(1): p. 1-7.

52. Bindu, V. and T. Pradeep, *Characterisation of alkanethiol (C_nH_{2n}+1SH, n = 3, 4, 6, 8, 10, 12 and 18) self assembled monolayers by x-ray photoelectron spectroscopy*. Vacuum, 1998. **49**(1): p. 63-66.

53. Rosenbaum, A.W., M.A. Freedman, S.B. Darling, I. Popova, and S.J. Sibener, *Surface vibrations in alkanethiol self-assembled monolayers of varying chain length*. Journal of Chemical Physics, 2004. **120**(8): p. 3880-3886.

54. Kato, H.S., J. Noh, M. Hara, and M. Kawai, *An hreels study of alkanethiol self-assembled monolayers on Au(111)*. Journal of Physical Chemistry B, 2002. **106**(37): p. 9655-9658.

55. Kawasaki, M. and H. Nagayama, *Observation of highly ordered 3 x 4 phase of ethanethiol self- assembled monolayer on Au(111)*. Chemistry Letters, 2001(9): p. 942-943.

56. Widrig, C.A., C.A. Alves, and M.D. Porter, *Scanning tunneling microscopy of ethanethiolate and normal- octadecanethiolate monolayers spontaneously adsorbed at gold surfaces*. Journal of the American Chemical Society, 1991. **113**(8): p. 2805-2810.

57. Lee, S.Y., J. Noh, M. Hara, and H. Lee, *An STM study on solvent effects in forming self-assembled cysteamine and propanethiol monolayers on Au(111)*. Molecular Crystals and Liquid Crystals, 2002. **377**: p. 177-180.

58. Kang, J. and P.A. Rowntree, *Molecularly resolved surface superstructures of self-assembled butanethiol monolayers on gold*. Langmuir, 1996. **12**(11): p. 2813-2819.

59. Allara, D.L. and R.G. Nuzzo, *Spontaneously organized molecular assemblies .2. Quantitative infrared spectroscopic determination of equilibrium structures of solution-adsorbed normal-alkanoic acids on an oxidized aluminum surface*. Langmuir, 1985. **1**(1): p. 52-66.

60. Bain, C.D., E.B. Troughton, Y.T. Tao, J. Evall, G.M. Whitesides, and R.G. Nuzzo, *Formation of monolayer films by the spontaneous assembly of organic thiols from solution onto gold*. Journal of the American Chemical Society, 1989. **111**(1): p. 321-335.

61. Nishi, N., D. Hobara, M. Yamamoto, and T. Kakiuchi, *Chain-length-dependent change in the structure of self- assembled monolayers of n-alkanethiols on Au(111) probed by broad-bandwidth sum frequency generation spectroscopy*. Journal of Chemical Physics, 2003. **118**(4): p. 1904-1911.

62. Nuzzo, R.G., L.H. Dubois, and D.L. Allara, *Fundamental studies of microscopic wetting on organic surfaces. 1. Formation and structural characterization of a self-consistent series of polyfunctional organic monolayers*. Journal of the American Chemical Society, 1990. **112**: p. 558-569.

63. Angelico, V.J., S.A. Mitchell, and V.H. Wysocki, *Low-energy ion-surface reactions of pyrazine with two classes of self-assembled monolayers: Influence of alkyl chain orientation*. Analytical Chemistry, 2000. **72**(11): p. 2603-2608.

64. Wolf, K.V., D.A. Cole, and S.L. Bernasek, *Low-energy collisions of pyrazine and d(6)-benzene molecular ions with self-assembled monolayer surfaces: The odd-even chain length effect*. Langmuir, 2001. **17**(26): p. 8254-8259.

65. Duwez, A.S., J. Riga, J. Ghijsen, J.J. Pireaux, and J.J. Verbist, *Surface molecular structure of self-assembled alkanethiols evidenced by UPS, synchrotron radiation and HREELS*. Journal of Electron Spectroscopy and Related Phenomena, 1995. **76**: p. 523-528.

66. Castiglioni, c., M. Gussoni, and G. Zerbi, *Charge mobility in sigma bonded molecules: The infrared spectrum of polymethylene chains in the solid and liquid phases*. Journal of chemical Physics, 1991. **95**(10): p. 7144-7149.

67. Duwez, A.S., L.M. Yu, J. Riga, J. Delhalle, and J.J. Pireaux, *Vibrational structure and organization of various self- assembled alkanethiol monolayers: A HREELS study*. Langmuir, 2000. **16**(16): p. 6569-6576.

68. Kohli, P., K.K. Taylor, J.J. Harris, and G.J. Blanchard, *Assembly of covalently-coupled disulfide multilayers on gold*. Journal of the American Chemical Society, 1998. **120**(46): p. 11962-11968.

69. Chah, S., J.H. Fendler, and J. Yi, *In-situ analysis of stepwise self-assembled1,6-hexanedithiol multilayers by surface plasmon resonance measurements*. Chemical Communications, 2002. **18**: p. 2094-2095.

70. Esplandiu, M.J., H. Hagenstrom, and D.M. Kolb, *Functionalized self-assembled alkanethiol monolayers on Au(111) electrodes: 1. Surface structure and electrochemistry*. Langmuir, 2001. **17**(3): p. 828-838.

71. Rieley, H., G.K. Kendall, F.W. Zemicael, T.L. Smith, and S.H. Yang, *X-ray studies of self-assembled monolayers on coinage metals. 1. Alignment and photooxidation in 1,8-octanedithiol and 1- octanethiol on Au*. Langmuir, 1998. **14**(18): p. 5147-5153.

72. Leung, T.Y.B., M.C. Gerstenberg, D.J. Lavrich, G. Scoles, F. Schreiber, and G.E. Poirier, *1,6-hexanedithiol monolayers on Au(111): A multitechnique structural study*. Langmuir, 2000. **16**(2): p. 549-561.

73. Joo, S.W., S.W. Han, and K. Kim, *Multilayer formation of 1,2-ethanedithiol on gold: Surface-enhanced Raman scattering and ellipsometry study*. Langmuir, 2000. **16**: p. 5391-5396.

74. Joo, S.W., S.W. Han, and K. Kim, *Adsorption characteristics of aliphatic dithiols on silver and gold revealed by ellipsometry and FT-IR spectroscopy*. Molecular Crystals and Liquid Crystals, 2001. **371**: p. 355-358.

75. MacDairmid, A.R., M.C. Gallagher, and J.T. Banks, *Structure of dithiothreitol monolayers on Au(111)*. Journal of Physical Chemistry B, 2003. **107**(36): p. 9789-9792.

76. Ihs, A. and B. Liedberg, *Chemisorption of L-cysteine and 3-mercaptopropionic acid on gold and copper surfaces: An infrared reflection - absorption study*. Journal of Colloid and Interface Science, 1991. **144**(1): p. 283-292.

77. Cavalleri, O., G. Gonella, S. Terreni, M. Vignolo, L. Floreano, A. Morgante, M. Canepa, and R. Rolandi, *High resolution x-ray photoelectron spectroscopy of L-cysteine self-assembled films*. Physical Chemistry Chemical Physics, 2004. **6**(15): p. 4042-4046.

78. Zhang, J.D., Q.J. Chi, J.U. Nielsen, E.P. Friis, J.E.T. Andersen, and J. Ulstrup, *Two-dimensional cysteine and cystine cluster networks on Au(111) disclosed by voltammetry and in situ scanning tunneling microscopy*. Langmuir, 2000. **16**(18): p. 7229-7237.

79. Cavalleri, O., G. Gonella, S. Terreni, M. Vignolo, P. Pelori, L. Floreano, A. Morgante, M. Canepa, and R. Rolandi, *High resolution XPS of the s 2p core level region of the L- cysteine/gold interface*. Journal of Physics-Condensed Matter, 2004. **16**(26): p. S2477-S2482.

80. Xu, Q.M., L.J. Wan, C. Wang, C.L. Bai, Z.Y. Wang, and T. Nozawa, *New structure of L-cysteine self-assembled monolayer on Au(111): Studies by in situ scanning tunneling microscopy*. Langmuir, 2001. **17**(20): p. 6203-6206.

81. Zhang, J., Q. Chi, J.U. Nielsen, A.G. Hansen, J.E.T. Andersen, H. Wackerbarth, and J. Ulstrup, *Organized monolayers of biological macromolecules on Au(111) surfaces*. Russian Journal of Electrochemistry, 2002. **38**(1): p. 68-76.

82. Sorribas, H., C. Padeste, T. Mezzacasa, L. Tiefenauer, L. Leder, D. Fitzli, and P. Sonderegger, *Neurite outgrowth on microstructured surfaces functionalized by a neural adhesion protein*. Journal of Materials Science: Materials in Medicine, 1999. **10**(12): p. 787-791.

83. Uvdal, K. and T.P. Vikinge, *Chemisorption of the dipeptide Arg-Cys on a gold surface and the selectivity of g-protein adsorption*. Langmuir, 2001. **17**(6): p. 2008-2012.

84. Wallwork, M.L., D.A. Smith, J. Zhang, J. Kirkham, and C. Robinson, *Complex chemical force titration behavior of amine-terminated self-assembled monolayers*. Langmuir, 2001. **17**(4): p. 1126-1131.

85. Lee, S.Y., J. Noh, E. Ito, M. Hara, and H. Lee, *Solvent effect on formation of cysteamine self-assembled monolayers on Au(111)*. Japanese Journal of Applied Physics Part 1-Regular Papers Short Notes & Review Papers, 2003. **42**(1): p. 1-6.

86. Leff, D.V., L. Brandt, and J.R. Heath, *Synthesis and characterization of hydrophobic, organically-soluble gold nanocrystals functionalized with primary amines*. Langmuir, 1996. **12**(20): p. 4723-4730.

87. Kawasaki, M., T. Sato, and T. Yoshimoto, *Controlled layering of two-dimensional j-aggregate of anionic cyanine dye on self-assembled cysteamine monolayer on Au(111)*. Langmuir, 2000. **16**(12): p. 5409 -5417.

88. Sigma-Aldrich, *Product Catalog*. 2004, Sigma-Aldrich.

89. Smalley, J.F., *Indirect laser-induced temperature jump study of the chain- length dependence of the pk(a)'s of omega-mercaptoalkanoic acid monolayers self-assembled on gold*. Langmuir, 2003. **19**(22): p. 9284-9289.

90. Bain, C.D. and G.M. Whitesides, *A study by contact angle of the acid-base behavior of monolayers containing omega-mercaptocarboxylic acids adsorbed on gold: An example of reactive spreading*'. Langmuir, 1989. **5**: p. 1370-1378.

91. Dai, Z. and H.X. Ju, *Effect of chain length on the surface properties of omega- carboxy alkanethiol self-assembled monolayers*. Physical Chemistry Chemical Physics, 2001. **3**(17): p. 3769-3773.

92. Schmitt, H., A. Badia, L. Dickinson, L. Reven, and R.B. Lennox, *The effect of terminal hydrogen bonding on the structure and dynamics of nanoparticle*

self-assembled monolayers (SAMs): An NMR dynamics study. Advanced Materials, 1998. **10**(6): p. 475-480

93. Arnold, R., W. Azzam, A. Terfort, and C. Woll, *Preparation, modification, and crystallinity of aliphatic and aromatic carboxylic acid terminated self-assembled monolayers*. Langmuir, 2002. **18**(10): p. 3980-3992.

94. Dannenberger, O., K. Weiss, H.J. Himmel, B. Jager, M. Buck, and C. Woll, *An orientation analysis of differently endgroup-functionalised alkanethiols adsorbed on Au substrates*. Thin Solid Films, 1997. **307**(1-2): p. 183-191.

95. Giz, M.J., B. Duong, and N.J. Tao, *In situ STM study of self-assembled mercaptopropionic acid monolayers for electrochemical detection of dopamine*. Journal of Electroanalytical Chemistry, 1999. **465**(1): p. 72-79.

96. Sawaguchi, T., Y. Sato, and F. Mizutani, *Ordered structures of self-assembled monolayers of 3- mercaptopropionic acid on Au(111): In situ scanning tunneling microscopy study*. Physical Chemistry Chemical Physics, 2001. **3**(16): p. 3399-3404.

97. Petri, M., D.M. Kolb, U. Memmert, and H. Meyer, *Adsorption of mercaptopropionic acid onto Au(111) - Part I. Adlayer formation, structure and electrochemistry*. Electrochimica Acta, 2003. **49**(1): p. 175-182.

98. Hobara, D., O. Miyake, S. Imabayashi, K. Niki, and T. Kakiuchi, *In-situ scanning tunneling microscopy imaging of the reductive desorption process of alkanethiols on Au(111)*. Langmuir, 1998. **14**(13): p. 3590-3596.

99. Xia, J., W. Wei, Y. Hu, H. Tao, and L. Wu, *A novel voltammetric method for the direct determination of copper in complex environmental samples*. Analytical Sciences, 2004. **20**: p. 1037-1041.

100. Laibinis, P.E., R.G. Nuzzo, and G.M. Whitesides, *Structure of monolayers formed by coadsorption of 2 normal- alkanethiols of different chain lengths on gold and its relation to wetting*. Journal of Physical Chemistry, 1992. **96**(12): p. 5097-5105.

101. Bertilsson, L. and B. Liedberg, *Infrared study of thiol monolayer assemblies on gold - preparation, characterization, and functionalization of mixed monolayers*. Langmuir, 1993. **9**(1): p. 141-149.

102. Creager, S.E. and J. Clarke, *Contact-angle titrations of mixed omega-mercaptoalkanoic acid alkanethiol monolayers on gold - reactive vs nonreactive spreading, and chain-length effects on surface pk(a) values*. Langmuir, 1994. **10**(10): p. 3675-3683.

103. Chen, S.F., L.Y. Li, C.L. Boozer, and S.Y. Jiang, *Controlled chemical and structural properties of mixed self- assembled monolayers of alkanethiols on Au(111)*. Langmuir, 2000. **16**(24): p. 9287-9293.

104. Laibinis, P.E., M.A. Fox, J.P. Folkers, and G.M. Whitesides, *Comparisons of self-assembled monolayers on silver and gold - mixed monolayers derived from $HS(CH_2)21x$ and $HS(CH_2)10y$ (x, y = CH_3, CH_2OH) have similar properties*. Langmuir, 1991. **7**(12): p. 3167-3173.

105. Collard, D.M. and M.A. Fox, *Use of electroactive thiols to study the formation and exchange of alkanethiol monolayers on gold*. Langmuir, 1991. **7**(6): p. 1192-1197.

106. Folkers, J.P., P.E. Laibinis, and G.M. Whitesides, *Self-assembled monolayers of alkanethiols on gold - comparisons of monolayers containing mixtures of short-chain and long-chain constituents with CH_3 and CH_2OH terminal groups*. Langmuir, 1992. **8**(5): p. 1330-1341.

107. Bain, C.D. and G.M. Whitesides, *Formation of 2-component surfaces by the spontaneous assembly of monolayers on gold from solutions containing mixtures of organic thiols*. Journal of the American Chemical Society, 1988. **110**(19): p. 6560-6561.

108. Stranick, S.J., S.V. Atre, A.N. Parikh, M.C. Wood, D.L. Allara, N. Winograd, and P.S. Weiss, *Nanometer-scale phase separation in mixed composition self-assembled monolayers*. Nanotechnology, 1996. **7**(4): p. 438-442.

109. Imabayashi, S., N. Gon, T. Sasaki, D. Hobara, and T. Kakiuchi, *Effect of nanometer-scale phase separation on wetting of binary self-assembled thiol monolayers on Au(111)*. Langmuir, 1998. **14**(9): p. 2348-2351.

110. Kakiuchi, T., M. Iida, N. Gon, D. Hobara, S. Imabayashi, and K. Niki, *Miscibility of adsorbed 1-undecanethiol and 11- mercaptoundecanoic acid species in binary self-assembled monolayers on Au(111)*. Langmuir, 2001. **17**(5): p. 1599-1603.

111. Li, L.Y., S.F. Chen, and S.Y. Jiang, *Molecular-scale mixed alkanethiol monolayers of different terminal groups on Au(111) by low-current scanning tunneling microscopy*. Langmuir, 2003. **19**(8): p. 3266-3271.

112. Fleming, M.S. and D.R. Walt, *Stability and exchange studies of alkanethiol monolayers on gold-nanoparticle-coated silica microspheres*. Langmuir, 2001. **17**(16): p. 4836-4843.

113. Bain, C.D., J. Evall, and G.M. Whitesides, *Formation of monolayers by the coadsorption of thiols on gold - variation in the head group, tail group, and solvent*. Journal of the American Chemical Society, 1989. **111**(18): p. 7155-7164.

114. El-Deab, M.S. and T. Ohsaka, *Molecular-level design of binary self-assembled monolayers on polycrystalline gold electrodes*. Electrochimica Acta, 2004. **49**(13): p. 2189-2194.

115. Chechik, V., R.M. Crooks, and C.J.M. Stirling, *Reactions and reactivity in self-assembled monolayers*. Advanced Materials, 2000. **12**(16): p. 1161-1171.

116. Revell, D.J., J.R. Knight, D.J. Blyth, A.H. Haines, and D.A. Russell, *Self-assembled carbohydrate monolayers: Formation and surface selective molecular recognition*. Langmuir, 1998. **14**(16): p. 4517-4524.

117. Wagner, P., P. Kernen, M. Hegner, E. Ungewickell, and G. Semenza, *Covalent anchoring of proteins onto gold-directed NHS- terminated self-assembled monolayers in aqueous buffers - SFM images of clathrin cages and Triskelia*. Febs Letters, 1994. **356**(2-3): p. 267-271.

118. Nakano, K., H. Taira, M. Maeda, and M. Takagi, *Covalent attachment of proteins on self-assembled monolayer electrodes as characterized by electrochemical impedance measurements and FT-IR spectroscopy*. Bunseki Kagaku, 1998. **47**(12): p. 929-935.

119. Chen, L.H., Y.S. Choi, J.W. Park, J. Kwon, R.S. Wang, T. Lee, and S.H. Ryu, *Effect of linker for immobilization of glutathione on BSA- assembled controlled pore glass heads*. Bulletin of the Korean Chemical Society, 2004. **25**(9): p. 1366-1370.

120. Lee, W., B.K. Oh, Y.M. Bae, S.H. Paek, W.H. Lee, and J.W. Choi, *Fabrication of self-assembled protein a monolayer and its application as an immunosensor*. Biosensors & Bioelectronics, 2003. **19**(3): p. 185-192.

121. Frey, B.L. and R.M. Corn, *Covalent attachment and derivatization of poly(L-lysine) monolayers on gold surfaces as characterized by polarization-modulation FT-IR spectroscopy*. Analytical Chemistry, 1996. **68**(18): p. 3187-3193.

122. Pierce, *Determine reactivity of NHS ester biotinylation and cross-linking reagents*. 2003, Pierce Biotechnology Inc.

123. Biebuyck, H.A., C.D. Bain, and G.M. Whitesides, *Comparison of organic monolayers on polycrystalline gold spontaneously assembled from solutions containing dialkyl disulfides or alkenethiols*. Langmuir, 1994. **10**(6): p. 1825-1831.

124. Biebuyck, H.A. and G.M. Whitesides, *Interchange between monolayers on gold formed from unsymmetrical disulfides and solutions of thiols - evidence for sulfur sulfur bond-cleavage by gold metal*. Langmuir, 1993. **9**(7): p. 1766-1770.

125. Ishida, T., *Evidence for cleavage of disulfides in the self-assembled monolayer on Au(111)*. Langmuir, 1997. **13**(13): p. 3261-3265.

126. Wang, J.H., J.R. Kenseth, V.W. Jones, J.B.D. Green, M.T. McDermott, and M.D. Porter, *SFM tip-assisted hydrolysis of a dithiobis(succinimidoundecanoate) monolayer chemisorbed on a Au(111)*

surface. Journal of the American Chemical Society, 1997. **119**(52): p. 12796-12799.

127. Miller, B.T., T.J. Collins, M.E. Rogers, and A. Kurosky, *Peptide biotinylation with amine-reactive esters: Differential side chain reactivity.* Peptides, 1997. **18**(10): p. 1585-1595.

128. Uptima, *SPDP, LC-SPDP, sulfo-LC-SPDP heterobifunctional cross-linkers*, Uptima.

129. Wegner, G.J., *SPDP reaction*, W. Crocker, Editor. 2004: Madison Wisconsin.

130. Lee, I., J.W. Lee, and E. Greenbaum, *Biomolecular electronics: Vectorial arrays of photosynthetic reaction centers*. Physical Review Letters, 1997. **79**(17): p. 3294-3287.

131. Hyun, M. and C.K. Rhee, *STM study of 2-mercaptoethanol self-assembled monolayer on Au(111)*. Bulletin of the Korean Chemical Society, 2001. **22**(2): p. 213-218.

132. de Jong, M.R., J. Huskens, and D.N. Reinhoudt, *Influencing the binding selectivity of self-assembled cyclodextrin monolayers on gold through their architecture*. Chemistry-a European Journal, 2001. **7**(19): p. 4164-4170.

133. Fritz, M.C., G. Hahner, N.D. Spencer, R. Burli, and A. Vasella, Self-assembled hexasaccharides: Surface characterization of thiol-terminated sugars adsorbed on a gold surface. Langmuir, 1996. **12**(25): p. 6074-6082.

134. Poirier, G.E., W.P. Fitts, and J.M. White, *Two dimensional phase diagram of decanethiol on Au(111)*. Langmuir, 2001. **17**(4): p. 1176-1183.

135. Yamada, R., H. Wano, and K. Uosaki, *Effect of temperature on structure of the self-assembled monolayer of decanethiol on Au(111) surface*. Langmuir, 2000. **16**(13): p. 5523-5525.

136. Yang, G.H. and G.Y. Liu, *New insights for self-assembled monolayers of organothiols on Au(111) revealed by scanning tunneling microscopy*. Journal of Physical Chemistry B, 2003. **107**(34): p. 8746-8759.

137. Barrena, E., C. Ocal, and M. Salmeron, *Structure and stability of tilted-chain phases of alkanethiols on Au(111)*. Journal of Chemical Physics, 2001. **114**(9): p. 4210-4214.

138. Barrena, E., E. Palacios-Lidon, C. Munuera, X. Torrelles, S. Ferrer, U. Jonas, M. Salmeron, and C. Ocal, *The role of intermolecular and molecule-substrate interactions in the stability of alkanethiol nonsaturated phases on Au(111)*. Journal of the American Chemical Society, 2004. **126**(1): p. 385-395

139. Brewer, N.J., B.D. Beake, and G.J. Leggett, *Friction force microscopy of self-assembled monolayers: Influence of adsorbate alkyl chain length, terminal group chemistry, and scan velocity*. Langmuir, 2001. **17**(6): p. 1970-1974.

140. Xu, S., S.J.N. Cruchon-Dupeyrat, J.C. Garno, G.Y. Liu, G.K. Jennings, T.H. Yong, and P.E. Laibinis, *In situ studies of thiol self-assembly on gold from solution using atomic force microscopy*. Journal of Chemical Physics, 1998. **108**(12): p. 5002-5012.

141. Ulman, A., J.E. Eliers, and N. Tillman, *Packing and molecular orientation of alkanethiol monolayers on gold surfaces*. Langmuir, 1989. **5**(5): p. 1147-1152.

142. Venstrom, K.A. and L.F. Reichardt, Extracellular-matrix .2. Role of extracellular-matrix molecules and their receptors in the nervous-system. Faseb Journal, 1993. 7(11): p. 996-1003.

143. Streuli, C., *Extracellular matrix remodelling and cellular differentiation*. Current Opinion in Cell Biology, 1999. **11**(5): p. 634-640.

144. Giancotti, F.G. and E. Ruoslahti, *Transduction - integrin signaling*. Science, 1999. **285**(5430): p. 1028-1032.

145. Roskelley, C.D. and M.J. Bissell, *Dynamic reciprocity revisited: A continuous, bidirectional flow of information between cells and the*

extracellular matrix regulates mammary epithelial cell function. Biochemistry and Cell Biology-Biochimie Et Biologie Cellulaire, 1995. **73**(7-8): p. 391-397.

146. Lin, C.Q. and M.J. Bissell, *Multifaceted regulation of cell-differentiation by extracellular-matrix.* Faseb Journal, 1993. **7**(9): p. 737-743.

147. Pierschbacher, M.D. and E. Ruoslahti, Nature, 1984. **309**: p. 30-33.

148. Ruoslahti, E., *RGD and other recognition sequences for integrins.* Annual Review of Cell and Developmental Biology, 1996. **12**: p. 697-715.

149. Heald, R., *Laboratory 5: Fluorescence microscopy of the cytoskeleton in cultured cells.* 2004, University of California Berkeley.

150. ECACC, *Fundamental techniques in cell culture . . . A laboratory handbook.* 2005, Sigma Aldrich.

151. Ostuni, E., L. Yan, and G.M. Whitesides, *The interaction of proteins and cells with self-assembled monolayers of alkanethiolates on gold and silver.* Colloids and Surfaces B-Biointerfaces, 1999. **15**(1): p. 3-30.

152. Ito, Y., *Surface micropatterning to regulate cell functions.* Biomaterials, 1999. **20**(23-24): p. 2333-2342.

153. Yang, X.M., R.D. Peters, T.K. Kim, and P.F. Nealey, *Patterning of self-assembled monolayers with lateral dimensions of 0.15 mu using advanced lithography*. Journal of Vacuum Science & Technology B, 1999. **17**(6): p. 3203-3207.

154. Martele, Y., K. Callewaert, K. Naessens, P. Van Daele, R. Baets, and E. Schacht, *Controlled patterning of biomolecules on solid surfaces*. Materials Science & Engineering C-Biomimetic and Supramolecular Systems, 2003. **23**(3): p. 341-345.

155. Chen, G., Y. Ito, Y. Imanishi, A. Magnani, S. Lamponi, and R. Barbucci, *Photoimmobilization of sulfated hyaluronic acid for antithrombogenicity*. Bioconjugate Chemistry, 1997. **8**(5): p. 730-734.

156. Craighead, H.G., C.D. James, and A.M.P. Turner, *Chemical and topographical patterning for directed cell attachment*. Current Opinion in Solid State & Materials Science, 2001. **5**(2-3): p. 177-184.

157. Flemming, R.G., C.J. Murphy, G.A. Abrams, S.L. Goodman, and P.F. Nealey, *Effects of synthetic micro- and nano-structured surfaces on cell behavior*. Biomaterials, 1999. **20**(6): p. 573-588.

158. Walheim, S., M. Boltau, J. Mlynek, G. Krausch, and U. Steiner, *Structure formation via polymer demixing in spin-cast films*. Macromolecules, 1997. **30**(17): p. 4995-5003.

159. den Braber, E.T., J.E. de Ruijter, L.A. Ginsel, A.F. von Recum, and J.A. Jansen, *Orientation of ECM protein deposition, fibroblast cytoskeleton, and attachment complex components on silicone microgrooved surfaces*. Journal of Biomedical Materials Research, 1998. **40**(2): p. 291-300.

160. WojciakStothard, B., A. Curtis, W. Monaghan, K. Macdonald, and C. Wilkinson, *Guidance and activation of murine macrophages by nanometric scale topography*. Experimental Cell Research, 1996. **223**(2): p. 426-435.

161. Curtis, A. and C. Wilkinson, *Topographical control of cells*. Biomaterials, 1997. **18**(24): p. 1573-1583.

162. Charras, G.T., P.P. Lehenkari, and M.A. Horton, *Atomic force microscopy can be used to mechanically stimulate osteoblasts and evaluate cellular strain distributions*. Ultramicroscopy, 2001. **86**(1-2): p. 85-95.

163. Britland, S., H. Morgan, B. WojiakStodart, M. Riehle, A. Curtis, and C. Wilkinson, *Synergistic and hierarchical adhesive and topographic guidance of BHK cells*. Experimental Cell Research, 1996. **228**(2): p. 313-325.

164. Magnani, A., A. Priamo, D. Pasqui, and R. Barbucci, *Cell behaviour on chemically microstructured surfaces*. Materials Science & Engineering C-Biomimetic and Supramolecular Systems, 2003. **23**: p. 315-328.

165. Steele, J.G., G. Johnson, K.M. McLean, G.J. Beumer, and H.J. Griesser, *Effect of porosity and surface hydrophilicity on migration of epithelial tissue over synthetic polymer*. Journal of Biomedical Materials Research, 2000. **50**(4): p. 475-482.

166. Becker, O.M., Y. Levy, and O. Ravitz, *Flexibility, conformation spaces, and bioactivity*. Journal of Physical Chemistry B, 2000. **104**(9): p. 2123-2135.

167. Evans, M.D.M. and J.G. Steele, *Polymer surface chemistry and a novel attachment mechanism in corneal epithelial cells*. Journal of Biomedical Materials Research, 1998. **40**(4): p. 621-630.

168. Feng, Y.Z. and M. Mrksich, *The synergy peptide PHSRN and the adhesion peptide RGD mediate cell adhesion through a common mechanism.* Biochemistry, 2004. **43**(50): p. 15811-15821.

169. Steele, J.G., B.A. Dalton, G. Johnson, and P.A. Underwood, *Adsorption of fibronectin and vitronectin onto primariatm and tissue culture polystyrene and relationship to the mechanism of initial attachment of human vein endothelial cells and BHK-2 1 fibroblasts*. Biomaterials, 1995.

170. Brandley, B.K. and R.L. Schnaar, Analytical Biochemistry, 1988. **172**: p. 270-278.

171. Sagnella, S., F. Kligman, E.H. Anderson, J.E. King, G. Murugesan, R.E. Marchant, and K. Kotte-Marchant, *Human microvascular endothelial cell growth and migration on biomimetic surfactant polymers*. Biomaterials, 2004. **25**(7-8): p. 1249-1259.

172. Patel, N., R. Bhandari, K.M. Shakesheff, S.M. Cannizzaro, M.C. Davies, R. Langer, C.J. Roberts, S.J.B. Tendler, and P.M. Williams, *Printing patterns of biospecifically-adsorbed protein*. Journal of Biomaterials Science-Polymer Edition, 2000. **11**(3): p. 319-331.

173. Irvine, D.J., A.M. Mayes, and L.G. Griffith, *Nanoscale clustering of RGD peptides at surfaces using comb polymers. 1. Synthesis and characterization of comb thin films*. Biomacromolecules, 2001. **2**(1): p. 85-94.

174. Maheshwari, G., G. Brown, D.A. Lauffenburger, A. Wells, and L.G. Griffith, *Cell adhesion and motility depend on nanoscale RGD clustering*. Journal of Cell Science, 2000. **113**(10): p. 1677-1686.

175. Banerjee, P., D.J. Irvine, A.M. Mayes, and L.G. Griffith, *Polymer latexes for cell-resistant and cell-interactive surfaces*. Journal of Biomedical Materials Research, 2000. **50**(3): p. 331-339.

176. Jo, S., P.S. Engel, and A.G. Mikos, *Synthesis of poly(ethylene glycol)-tethered poly(propylene fumarate) and its modification with GRGD peptide.* Polymer, 2000. **41**(21): p. 7595-7604.

177. Mann, B.K., A.S. Gobin, A.T. Tsai, R.H. Schmedlen, and J.L. West, *Smooth muscle cell growth in photopolymerized hydrogels with cell adhesive and proteolytically degradable domains: Synthetic ECM analogs for tissue engineering*. Biomaterials, 2001. **22**(22): p. 3045-3051.

178. Flemming, R.G., C.C. Capelli, S.L. Cooper, and R.A. Proctor, *Bacterial colonization of functionalized polyurethanes*. Biomaterials, 2000. **21**(3): p. 273-281.

179. Fitton, J.H., B.A. Dalton, G. Beumer, G. Johnson, H.J. Griesser, and J.G. Steele, *Surface topography can interfere with epithelial tissue migration.* Journal of Biomedical Materials Research, 1998. **42**(2): p. 245-257.

180. van Wachem, P.B., T. Beugeling, J. Feijen, A. Bantjes, J.P. Detmers, and W.G. van Aken, *Interaction of cultured human endothelial cells with polymeric surfaces of different wettabilities*. Biomaterials, 1985. **6**(6): p. 403-408.

181. Ratner, B.D., *Surface modification of polymers - chemical, biological and surface analytical challenges*. Biosensors & Bioelectronics, 1995. **10**(9-10): p. 797-804.

182. McMillan, R., B. Meeks, F. Bensebaa, Y. Deslandes, and H. Sheardown, *Cell adhesion peptide modification of gold-coated polyurethanes for vascular endothelial cell adhesion*. Journal of Biomedical Materials Research, 2001. **54**(2): p. 272-283.

183. Assero, G., C. Satriano, G. Lupo, C.D. Anfuso, G. Marletta, and M. Alberghina, *Pericyte adhesion and growth onto polyhydroxymethylsiloxane surfaces nanostructured by plasma treatment and ion irradiation.* Microvascular Research, 2004. **68**(3): p. 209-220.

184. Welle, A. and E. Gottwald, *UV-based patterning of polymeric substrates for cell culture applications*. Biomedical Microdevices, 2002. **4**(1): p. 33-41.

185. Griesser, H.J., R.C. Chatelier, T.R. Gengenbach, G. Johnson, and J.G. Steele, *Growth of human-cells on plasma polymers - Putative role of amine and amide groups*. Journal of Biomaterials Science-Polymer Edition, 1994. **5**(6): p. 531-554.

186. Bacakova, L., E. Filova, F. Rypacek, V. Svorcik, and V. Stary, *Cell adhesion on artificial materials for tissue engineering*. Physiological Research, 2004. **53**: p. S35-S45.

187. Lopez, G.P., M.W. Albers, S.L. Schreiber, R. Carroll, E. Peralta, and G.M. Whitesides, *Convenient methods for patterning the adhesion of mammalian-*

cells to surfaces using self-assembled monolayers of alkanethiolates on gold. Journal of the American Chemical Society, 1993. **115**(13): p. 5877-5878.

188. Faucheux, N., R. Schweiss, K. Lutzow, C. Werner, and T. Groth, *Self-assembled monolayers with different terminating groups as model substrates for cell adhesion studies*. Biomaterials, 2004. **25**(14): p. 2721-2730.

189. Harder, P., M. Grunze, R. Dahint, G.M. Whitesides, and P.E. Laibinis, *Molecular conformation in oligo(ethylene glycol)-terminated self-assembled monolayers on gold and silver surfaces determines their ability to resist protein adsorption*. Journal of Physical Chemistry B, 1998. **102**(2): p. 426-436.

190. Lopez, G.P., H.A. Biebuyck, R. Harter, A. Kumar, and G.M. Whitesides, *Fabrication and imaging of 2-dimensional patterns of proteins adsorbed on self-assembled monolayers by scanning electron- microscopy*. Journal of the American Chemical Society, 1993. **115**(23): p. 10774-10781.

191. Prime, K.L. and G.M. Whitesides, *Adsorption of proteins onto surfaces containing end-attached oligo(ethylene oxide) - a model system using self-assembled monolayers*. Journal of the American Chemical Society, 1993. **115**(23): p. 10714-10721.

192. Luk, Y.Y., M. Kato, and M. Mrksich, *Self-assembled monolayers of alkanethiolates presenting mannitol groups are inert to protein adsorption and cell attachment*. Langmuir, 2000. **16**(24): p. 9604-9608.

193. Deng, L., M. Mrksich, and G.M. Whitesides, *Self-assembled monolayers of alkanethiolates presenting tri(propylene sulfoxide) groups resist the adsorption of protein*. Journal of the American Chemical Society, 1996. **118**(21): p. 5136-5137.

194. Chapman, R.G., E. Ostuni, S. Takayama, R.E. Holmlin, L. Yan, and G.M. Whitesides, *Surveying for surfaces that resist the adsorption of proteins*. Journal of the American Chemical Society, 2000. **122**(34): p. 8303-8304.

195. Massia, S.P. and J.A. Hubbell, Journal of Cell Biology, 1991. **114**: p. 1089-1100.

196. Roberts, C., C.S. Chen, M. Mrksich, V. Martichonok, D.E. Ingber, and G.M. Whitesides, *Using mixed self-assembled monolayers presenting RGD and (EG)(3)OH groups to characterize long-term attachment of bovine capillary endothelial cells to surfaces*. Journal of the American Chemical Society, 1998. **120**(26): p. 6548-6555.

197. Pakalns, T., K.L. Haverstick, G.B. Fields, J.B. McCarthy, D.L. Mooradian, and M. Tirrell, *Cellular recognition of synthetic peptide amphiphiles in self-assembled monolayer films*. Biomaterials, 1999. **20**(23-24): p. 2265-2279.

198. Heller, D.A., V. Garga, K.J. Kelleher, T.C. Lee, S. Mahbubani, L.A. Sigworth, T.R. Lee, and M.A. Rea, *Patterned networks of mouse hippocampal neurons on peptide- coated gold surfaces*. Biomaterials, 2005. **26**(8): p. 883-889.

199. Saneinejad, S. and M.S. Shoichet, *Patterned glass surfaces direct cell adhesion and process outgrowth of primary neurons of the central nervous system*. Journal of Biomedical Materials Research, 1998. **42**(1): p. 13-19.

200. Combrier, E., P. Metezeau, X. Ronot, H. Kiefergachelin, and M. Adolphe, *Comparative-assessment of invitro toxicity of xenobiotics using flow-cytometry and spectrophotometry*. Toxicology in Vitro, 1990. **4**(6): p. 751-755.

201. Aznarsalatti, J., E. Bastida, G. Escolar, L. Almirall, M. Diazricart, P. Anton, R. Castillo, and A. Ordinas, *Dipyridamole induces changes in the thrombogenic properties of extracellular-matrix generated by endothelial-cells in culture*. Thrombosis Research, 1991. **64**(3): p. 341-353.

202. Maghni, K., O.M. Nicolescu, and J.G. Martin, *Suitability of cell metabolic colorimetric assays for assessment of CD4+T cell proliferation: Comparison to 5-bromo- 2-deoxyuridine (BrdU) ELISA*. Journal of Immunological Methods, 1999. **223**(2): p. 185-194.

203. Steward, G.F. and F. Azam, *Bromodeoxyuridine as an alternative to H-3-thymidine for measuring bacterial productivity in aquatic samples*. Aquatic Microbial Ecology, 1999. **19**(1): p. 57-66.

204. Gonchoroff, N.J., J.A. Katzmann, R.M. Currie, E.L. Evans, D.W. Houck, B.C. Kline, P.R. Greipp, and M.R. Loken, *S-phase detection with an antibody to bromodeoxyuridine - Role of dnase pretreatment*. Journal of Immunological Methods, 1986. **93**(1): p. 97-101.

205. Cunningham, B.A., The Scientist, 2001. **15**: p. 26.

206. Systems, P.F. 2000, Phoenix Flow Systems.

207. Mosmann, Journal of Immunological Methods, 1983. **65**: p. 55-63.

208. Hussain, R.F., A.M.E. Nouri, and R.T.D. Oliver, *A new approach for measurement of cytotoxicity using colorimetric assay*. Journal of Immunological Methods, 1993. **160**(1): p. 89-96.

209. Odintsova, N.A., A.V. Ermak, and L.G. Tsal, *Substrate selection for long-term cultivation of marine invertebrate cells*. Comparative Biochemistry and Physiology a-Physiology, 1994. **107**(4): p. 613-619.

210. Probes, M., *BCECF*. 2004, Molecular Probes.

211. Tratnyek, P.G., T.E. Reilkoff, A.W. Lemon, M.M. Scherer, B.A. Balko, L.M. Feik, and B.D. Henegar, *Visualizing redox chemistry: Probing environmental oxidation–reduction reactions with indicator dyes*. The Chemical Educator, 2001. **6**(3).

212. O'Brien, J., I. Wilson, T. Orton, and F. Pognan, *Investigation of the alamar blue (resazurin) fluorescent dye for the assessment of mammalian cell cytotoxicity*. European Journal of Biochemistry, 2000. **267**(17): p. 5421-5426.

213. Lancaster, M.V. and R.D. Fields, *Antibiotic and cytotoxic drug suceptibility assays using resazurin and poisoning agents*. 1996, Alamar Biosciences Laboratory, Inc. (Chicago, IL): United States of America.

214. Seifalian, A.M., H.J. Salacinski, G. Punshon, B. Krijgsman, and G. Hamilton, *A new technique for measuring the cell growth and metabolism of endothelial cells seeded on vascular prostheses*. Journal of Biomedical Materials Research, 2001. **55**(4): p. 637-644.

215. Rasmussen, E.S. and G.M. Nicolaisen, *Stability of resazurin in buffers and mammalian cell culture media*. In Vitro & Molecular Toxicology-a Journal of Basic and Applied Research, 1999. **12**(4): p. 195-202.

Chapter 2

Analysis of Self-Assembled Monolayers of Alkanethiols on Gold

2.1 Introduction

The aim of this work is to investigate the structures formed by self-assembled monolayers (SAMs) of alkanethiols on gold (Au). These structures have been investigated because it has been hypothesised that the structure of the alkanethiol SAM on the Au surface has an effect on cellular adhesion and growth on that surface. This characterisation is particularly important because SAMs of alkanethiols have been shown to have many different structures [1]. The chemistry and possible structural forms of different alkanethiol SAMs are discussed in this chapter. The effect that the chemistry and angstrom scale topography of these structures have on cell growth is addressed in chapter 3.

For the purposes of this study when short-chain thiols are referred to this means thiols with a carbon chain length of C8 or less and when long chain thiols are referred to this means thiols with a carbon chain length of C10 or more. Where thiols with an intermediate chain length are referred to this means thiols with a carbon chain length of between C6 and C10. The intermediate region overlaps the long and short regions due to more than one structure (Figure 1.5) being present in self-assembled monolayers (SAMs) of these thiols. In cases where other studies are

referred to the chain length will be reported using the definitions given by the experimenters and these will be clarified with their definitions of short or long chain thiols.

2.1.1 Infrared Spectra

The interpretation of the infrared (IR) spectra has been carried out by assigning vibrational bands to peaks using representative examples from literature. The position of peaks in the spectra changes with the structure of the SAM. For methyl-terminated thiols, the CH_2 asymmetric peak is generally used as a measure of the degree of liquid-like character in the SAM [2]. For a SAM, which has a high degree of crystallinity, this band will generally be found around 2918 cm^{-1} and for a SAM with a significant amount of liquid-like character the band will be found around 2924 cm^{-1} [2]. When peaks are particularly broad this is usually an indication that there is a significant amount of hydrogen bonding (H-Bonding) found in the SAM.

2.2 Experimental

Fourier Transform Infrared (FTIR) spectroscopy measurements were performed on a Magna 860 ESP spectrometer (Nicolet, Madison WI, U.S.A) with a narrow band mercury cadmium telluride (MCT) detector (Nicolet, Madison WI, U.S.A) cooled

with liquid nitrogen. For measurements made by polarisation modulation infrared reflection adsorption spectroscopy (PMIRRAS) the above spectrometer was used in conjunction with a photoelastic modulator (Hinds Hillsboro, OR, U.S.A) and a synchronous sampling demodulator (GWC Instruments, Madison WI, U.S.A).

The silicon wafers coated with 5 nm Titanium (Ti) and 100 nm of gold (Au) deposited under UHV conditions were supplied by Georg Albert PVD-Beschichtungen (Heidelberg, Germany).

The thiols used were purchased from Sigma (Poole, Dorset, U.K.) unless otherwise stated. The RGDC was obtained from American Peptide Company, Inc. (Sunnyvale, CA, U.S.A). The dithiobis(succinimidyl undecanoate) (Ditbsu) and the 11-aminoundecanethiol hydrochloride (AUT.HCl) were purchased from NBS Biologicals (Huntingdon, Cambs., U.K.) These thiols were used without further purification. The 4-mercaptobutyric acid (MBA) and the dithiols were all obtained from the University of St. Andrews chemical store cupboard. The mercaptooctanoic acid (MOA), the 10-aminoundecanethiol (ADT) and the 10-aminoundecanethiol hydrochloride (ADT.HCl) were synthesised with the help of Dr Alan Aitken.

The (*N*-succinimidyl 3-[2-pyridyldithio]-propionamido) (SPDP) used was purchased from Pierce (Rockford, IL, U.S.A). All other reagents were purchased from Sigma (Poole, Dorset, U.K.).

The nitrogen (N_2) used was purchased from BOC Gases Ltd (Rotherham, South Yorkshire,U.K.). All solvents were supplied by Bamford Laboratories (Rochdale, U.K.) except N,N - dimethylformamide (DMF) which was purchased from Sigma (Poole, Dorset, U.K.).

The lidded beakers and the glassware were purchased from Fisher Scientific U.K. Ltd. (Loughborough, Leicestershire, U.K.). The pipettes were finnpipettes purchased from Lab 3 Ltd. (Northampton, U.K.). The Hamilton syringe and needles were obtained from Cole-Parmer (Hanwell, London, U.K.).

2.3 Methods

2.3.1 Cutting Gold-coated Slides

The wafers were carefully removed from the packaging and placed on a piece of graph paper. A slide cutter was then used to fracture the wafer into pieces of approximately 1 X 2 cm using graph paper as a guide. The fact that silicon (Si) (100) has points of fracture at 90° to each other was used to useful effect in producing these slides. However, the exact positioning of the fracture in relation to the position of the cutter varied slightly producing a variation of up to 3 mm in the

dimensions of the slide. After cutting the slides were checked for imperfections and stored for up to 3 weeks before use. It should be noted that only plastic tweezers were used when handling the slides to avoid damage.

2.3.2 Making Solutions of Alkanethiols

In order to produce the stock solutions the amount of thiol needed to produce a 1.15 mM solution in 250 mL was measured out; solid thiols were weighed out on a balance, while liquid thiols were measured using a Hamilton syringe. The thiols were then transferred to a 250 mL volumetric flask and made up to 250 mL with absolute ethanol. In cases where there was an insufficient amount of thiol to make 250 mL of 1.15 mM solution the amount was scaled down to either 25 mL or 10 mL as appropriate for the amount of thiol available. The solution was always shaken well to ensure full dissolution. When the thiols were difficult to dissolve they were sonicated until no particles were visible. When sonicating, parafilm was put over the neck of the volumetric flask instead of the stopper to prevent explosion or evaporation.

The stock solution was stored in a fume cupboard in sealed volumetric flasks until needed. The working solution was produced by making a 1 in 100 dilution of the stock solution. In general, 1 mL of the stock solution was made up to 100 mL in a

volumetric flask with absolute ethanol to make a 0.0115 mM (11.5 μM) solution. This was also well shaken to ensure even distribution of the thiol in the solution.

2.3.3 Making Mixed Thiol Solutions

In order to produce monolayers containing multiple thiols, more than one component is added into the working solution. For example, to make 100 mL of a 50 : 50 solution of 11-mercaptoundecanoic acid (MUA) : 11-aminoundecanethiol hydrochloride (AUT.HCl), 1 mL of MUA and 1 mL of AUT.HCl were mixed and made up to 100 mL with absolute ethanol in a volumetric flask.

2.3.4 Making Self-assembled Monolayers

Lidded beakers were prepared for use by sonicating with cyclohexane then ethanol for at least 5 minutes each to remove any possible contaminants. Before the first use the beakers were rinsed with the appropriate alkanethiol solution. In order to produce SAMs approximately 20 mL of the alkanethiol working solution was poured into the prepared beaker and the Si/Ti/Au slides were transferred into it. The beaker was then closed and put in a dark cupboard at room temperature. The slides were left to soak for at least 24 hours before being removed, thoroughly washed with ethanol and dried with N_2. Prior to running FTIR spectra the slides were put in a vacuum

desiccator with phosphorous pentoxide for at least 30 minutes to remove any traces of ethanol.

2.3.5 Reacting Self-assembled Monolayers of 11-Mercaptoundecanoic Acid

SAMs of MUA on Au-coated slides were produced as described above and after drying with N_2, the slides were transferred to a glass Petri dish containing a solution of 75 mM 1-ethyl-3 [3(dimethylamino)propyl] carbodiimide hydrochloride (EDC) and 15 mM N-hydroxysuccinimide (NHS) in purified water. The dish was covered and left to react for at least 30 minutes after which time the slide was removed and washed with purified water. The slide was then transferred to an ammonia or buffered amine solution and left to react for at least 90 minutes. The ammonia solution was composed of ammonium chloride 0.5 M adjusted to pH 7.5 with sodium hydroxide (NaOH). The buffered amine solution was made up of triethanolamine hydrochloride 0.05 M, sodium chloride 0.25 M and amino acid/peptide 0.005 M adjusted to pH 8 with NaOH. After removal from the reaction solution the slide was washed with purified water. If no further reactions were to be performed the slide was washed with ethanol, dried with N_2 and put in vacuum desiccator with phosphorous pentoxide for at least 30 minutes before FTIR spectra could be run.

2.3.6 Reacting Self-assembled Monolayers of 11-Aminoundecanethiol Hydrochloride

1 mg of SPDP was weighed out directly before the experiment and dissolved in 100 μl of DMF and 400 μl of phosphate buffered saline (PBS). The slides of AUT.HCl SAMs were transferred to a glass Petri dish after drying with N_2. 20 μl of the SPDP solution was pipetted onto each slide. Cover slips were placed on the slides to spread the solution evenly over the surface before they were left to react for at least 90 minutes. It is important to put the lid on the Petri dish during this reaction to stop the evaporation of the liquid and the adherence of the cover slip to the slide. After the reaction the cover slips were removed carefully, the slides were rinsed well with purified water and dried with N_2. The slides were then transferred to another Petri dish and 20 μl of 10 mM Cys containing peptide in PBS was pipetted onto the surface, a cover slip placed on top and the Petri dish lidded. The thiol was left to react for at least 90 minutes before the cover slip was removed and the slide washed thoroughly with purified water and dried with N_2. The slide was then put in a vacuum desiccator with phosphorous pentoxide for at least 30 minutes before FTIR spectra could be run.

2.3.7 Collecting Spectra using Polarisation Modulation Infrared Reflection Absorption Spectroscopy

The dried slide was removed from the vacuum desiccator and the Si side of the slide was placed onto a clean piece of mounted silicon, which had been wet slightly with purified water. When pieces of flat, slightly wet silicon are rubbed gently together they adhere. The mounted silicon had been previously adfixed to a screw that fitted into the sample holder. Once the sample had been mounted the sample holder was adjusted so that the signal reaching the MCT detector was optimised. The photoelastic modulator was then placed between the IR source and the sample. The amount of signal reaching the detector was again maximised. The box holding the slide mount etc. was then closed and flushed with a steady stream of N_2. The spectra were then collected for 1024 scans at a resolution of 2 cm^{-1} with the photoelastic modulator set to an optimal (see below) wavelength; first at 2857 cm^{-1} then at 1851 cm^{-1}. The spectrometer was controlled and the spectra viewed using Omnic software.

The spectra produced are formed from Rp +Rs where Rp is the reflectance of P polarised light and Rs is the reflectance of S polarised light and J2(ø)(Rp-Rs), which is the difference in reflectivity between the p and s polarised light, modified by a second order Bessel function of the separation from the optimal wavelength. The Rp signal is an absorption spectra of the monolayer and the background, which includes

surface and gas phase absorption. The Rs signal is an absorption spectra of the background. (Rp +Rs) needs to be divided by J2(ø)(Rp-Rs) in order to obtain the reflectance of the surface without the background including gas-phase absorption. The processed spectra of the absorbed species were then examined for features. If there were no distinct features above the noise level or the features were indistinct, then 5 or 10 spectra were taken of the same slide and averaged to produce spectra with lower noise level.

2.3.8 Processing Spectra

The influence of the Bessel function was removed from the spectra using a program designed by Dr Steve Francis (University of St. Andrews) for this purpose. The spectra were then transferred back into the Omnic software for comparison.

2.4 Results

As a general rule the intensities of the spectra are not directly comparable to each other. This is due to the vagaries of the sample holder and the FTIR equipment; there were difficulties in attaining consistency of sample orientation and in maximising the intensity of the transmitted IR radiation to a consistent level.

The assignments of the spectral peaks are taken from papers by Kluth *et al* [2] and Choi *et al* [3]. The assignments given by Choi *et al* have been reproduced in Table 2.1.

Vibrational Assignment	**Peak position (cm^{-1})**
CH_2 Asym stretching	2918
CH_2 Sym stretching	2847
CH_2 (all-*trans*) scissoring	1467
CH_2 (next to gauche) scissoring	1451
CH_2 (adjacent to S) scissoring	1426
CH_2 wagging for kink defect	1366
CH_2 wagging for double-gauche defect	1349
CH_2 wagging	1327
CH_2 wagging	1298
CH_2 wagging	1266
CH_2 wagging	1232
CH_2 wagging	1202
CH_2 wagging	1180
C-C-C stretching	1093
C-C-C stretching	1056

Table 2.1 IR assignments for reference from a study by Choi *et al* [3] on 1,9-nonanedithiol on silver.

2.4.1 Methyl-terminated Self-assembled Monolayers

2.4.1.1 Chain Length Effect

The short chain, methyl-terminated thiol SAMs up to 1-octanethiol (C8) all have the CH_2 asymmetric stretch at 2926 cm^{-1} except for ethanethiol (ETT) which has the stretch at 2924 cm^{-1} (Figure 2.1).

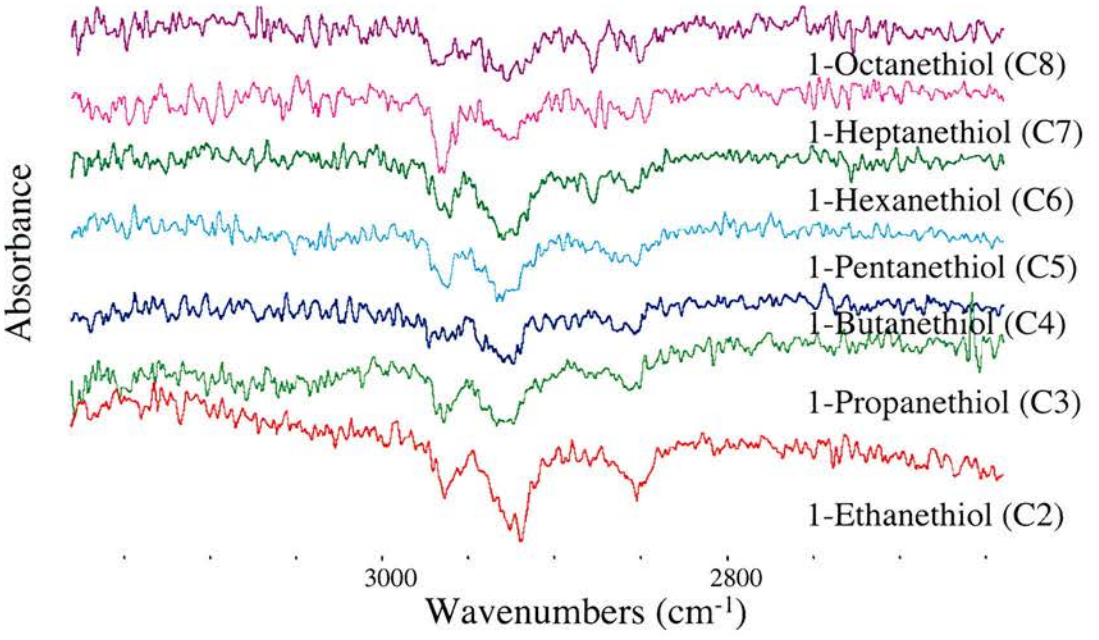

Figure 2.1 PMIRRAS spectra of all short chain methyl-terminated thiol SAMs from ethanethiol (C2) to octanethiol (C8), optimised at 2857 cm^{-1}.

The symmetric CH_3 peak is absent for ETT and 1-butanethiol (BTT) and only becomes clearly defined from C6 (1-hexanethiol (HXT)) to C8 (1-octanethiol (OTT)) (Figure 2.1).

In the lower CH bending region (Figure 2.2) there is also a difference between the spectra from the shortest thiol SAMs and those from HXT (C6) to OTT (C8) SAMs. This difference is shown in two ways: the first is that the intensities of the peaks are much smaller for SAMs with chain lengths longer than C5 (1-Pentanethiol (PTT)) in a way that cannot be accounted for by instrumental differences. The second is that the positioning of the CH_2 wag changes to lower values for SAMs of carbon chain length C6 (HXT)-C8 (OTT) (Table 2.2, Figure 2.2).

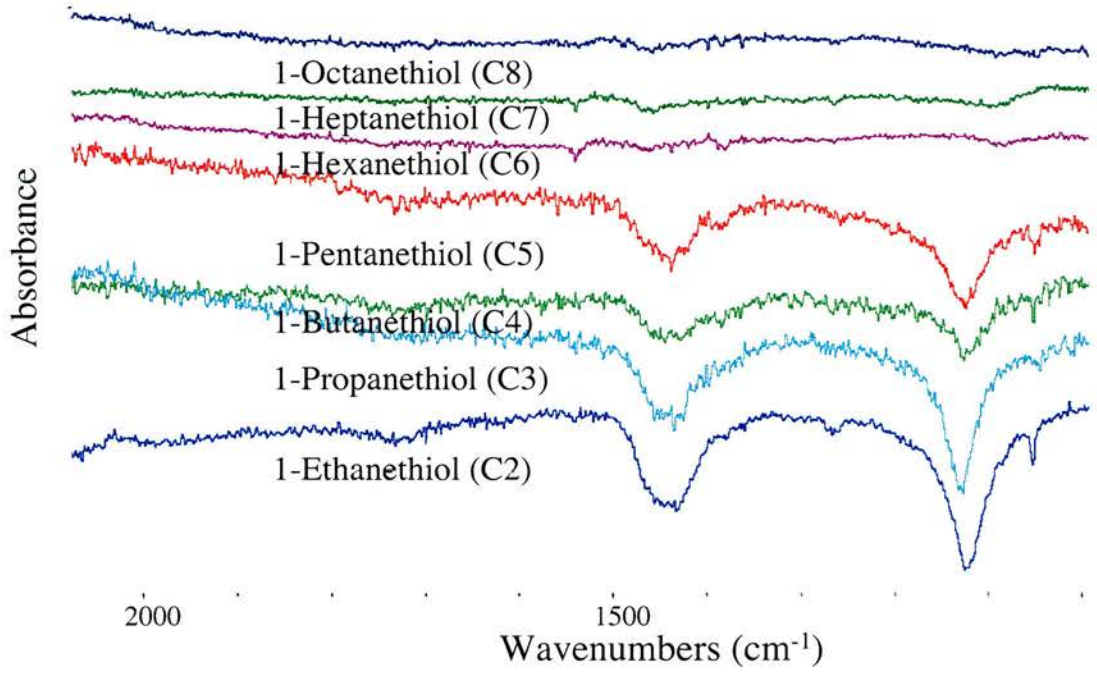

Figure 2.2 PMIRRAS spectra of all short chain methyl-terminated thiol SAMs from ethanethiol (C2) to octanethiol (C8), optimised at 1851 cm^{-1}.

Carbon Number	CH_2 Asym Stretch	CH_3 Asym Stretch	CH_3 Sym Stretch	CH_2 Sym Stretch	CH_2 sym + CH_3 Asym Scissor	CH_3 Sym Scissor	CH_2 Wag	CH_2 Rock	C-C-C Stretch
2	2924	2963	-	2849	1442	1381	1124	1268	1052
3	2926	2962	2880	2852	1440	1383	1130	1270	1043
4	2926	2970	-	2852	1440	1386	1121	1269	1050
5	2926	2962	2880	2859	1447	1387	1124	1260	1047
6	2926	2964	2875	2854	1460	1381	1095	1267	1047
7	2926	2964	2877	2857	1454	1387	1096	1266	1044
8	2926	2967	2879	2850	1457	1387	1083	1257	1048
10	2927	2964	2880	2860	1438	1378	1124	1268	1052
11	2926	2963	2876	2854	1443	1384	1146	1261	1048
16	2925	2963	2876	2854	1445	1382	1122	1261	1048 / 1027
18	2919	2963	2877	2849	1485	1382	1093	1261	1065

Table 2.2 Table of peak positions for methyl-terminated thiol SAMs from figures 2.1-2.4.

The position of the CH_2 wag peak changes between the C6-C8 SAMs and the longer chain thiol SAMs (Figure 2.3); for C10 (1-decanethiol (DCT)) to C16 (1-hexadecanethiol (HDT)) the CH_2 wag is in the 1125 cm^{-1} area then for the 1-octadecanethiol (ODT) (C18) SAM it reverts back to the lower 1090 cm^{-1} area seen for C6-C8 SAMs (Table 2.2).

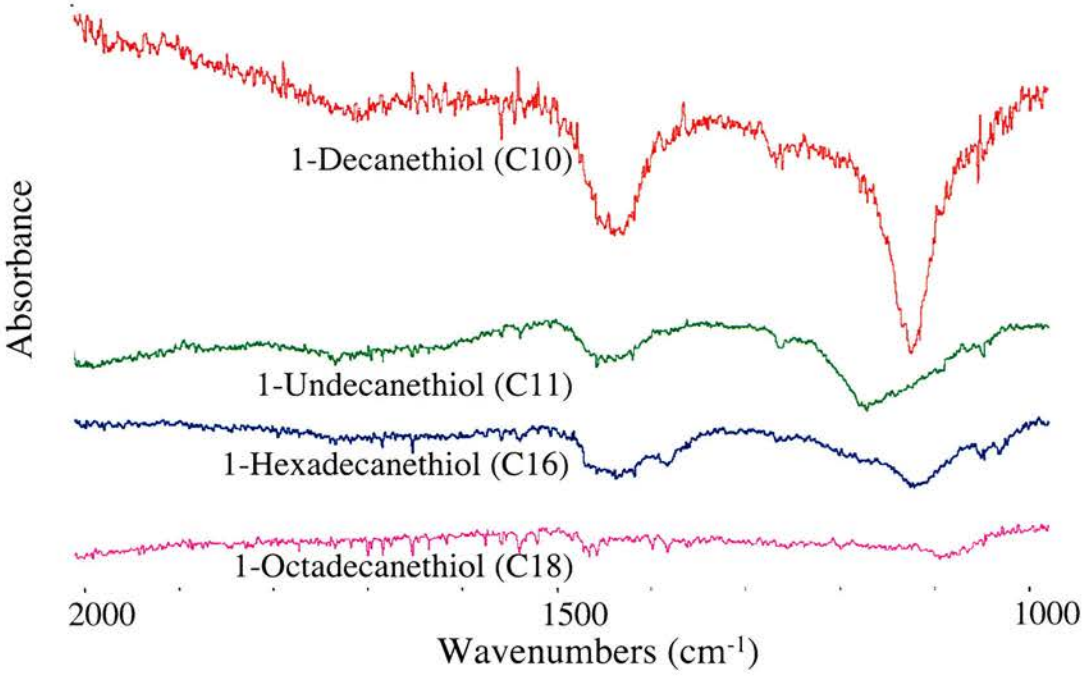

Figure 2.3 PMIRRAS spectra of a selection of long chain methyl-terminated thiol SAMs, optimised at 1851 cm^{-1}.

In the upper CH stretching region of the long chain thiol SAM spectra the frequency of the CH_2 asymmetric stretch decreases with increased carbon chain length (Figure 2.4). There is a particularly large change seen between C16 (HDT) and C18 (ODT); the peak decreases in frequency from 2925 cm^{-1} to 2919 cm^{-1} (Table 2.2).

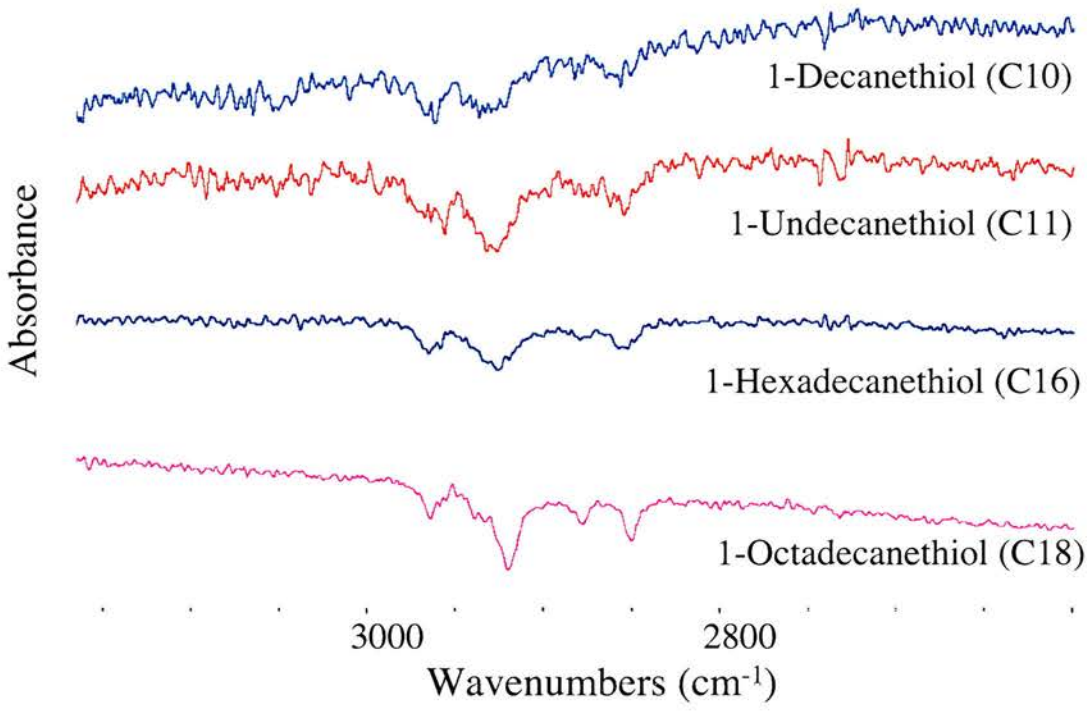

Figure 2.4 PMIRRAS spectra of a selection of long chain methyl-terminated thiol SAMs, optimised at 2857 cm^{-1}.

2.4.1.2 Odd-Even Effect

The CH_3 asymmetric peak rises and falls between SAMs with even carbon chain lengths and SAMs with odd carbon chain lengths displaying the odd-even effect. This effect is also seen in the symmetric CH_2 peaks where there appears to be a

difference between the odd carbon chain length SAMs and the even carbon chain length SAMs. It is difficult to tell if the effect is present for the shortest SAMs as the symmetric CH_3 peak is absent for ETT and BTT.

2.4.2 Dithiol Self-assembled Monolayers

There is little variation in the positioning of the asymmetric CH_2 peaks, only the 1,2-ethanedithiol and the 1,5-pentanedithiol have this peak at a higher frequency (Table 2.3). The main interesting feature of the upper wavenumber CH stretching region of the dithiol SAMs spectra is that there is a peak at around 2965 cm^{-1} which bears distinct resemblance to the CH_3 asymmetric peak seen in the methyl spectra in both position and size relative to the CH_2 asymmetric peak (Figures 2.1 & 2.5). In addition, the 1,4-butanedithiol (BTDT) and 1,5-pentanedithiol (PTDT) SAM spectra (Figure 2.5) show this anomalous peak to be larger than the CH_2 asymmetric peak.

	CH_2 Asym Stretch	**Fermi Resonance**	**CH_2 Sym Stretch**	**CH_2 Sym Scissoring**	**CH_2 Wag**	**CH_2 Rock**	**C-C-C Stretch**
2	2931	2963	2858	1480	1108	1261	1062
3	2929	2965	2857	1446	1185	1259	1058
4	2929	2965	2862	-	1141	1274	swamped
5	2933	2960	2864	1442	1149	1274	1050
6	2929	2968	2863	1450	1185	1263	1050

Table 2.3 Table of peak positions for dithiol SAMs from figures 2.5 & 2.6.

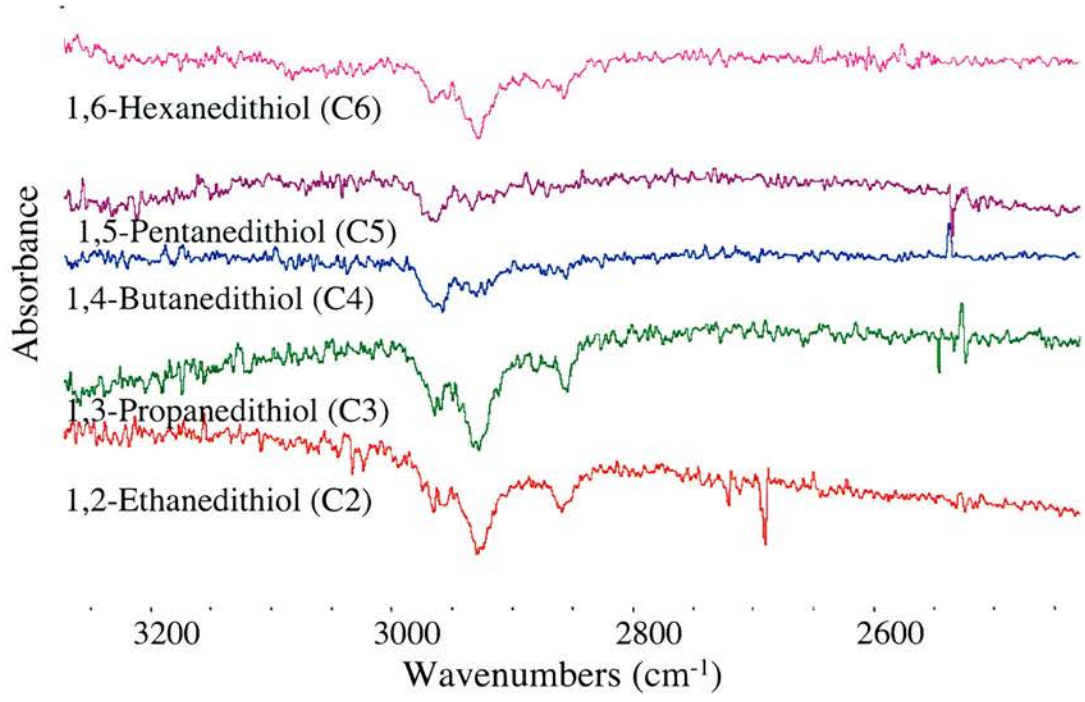

Figure 2.5 PMIRRAS spectra of a selection of short chain dithiol SAMs. These are optimised at 2857cm^{-1}.

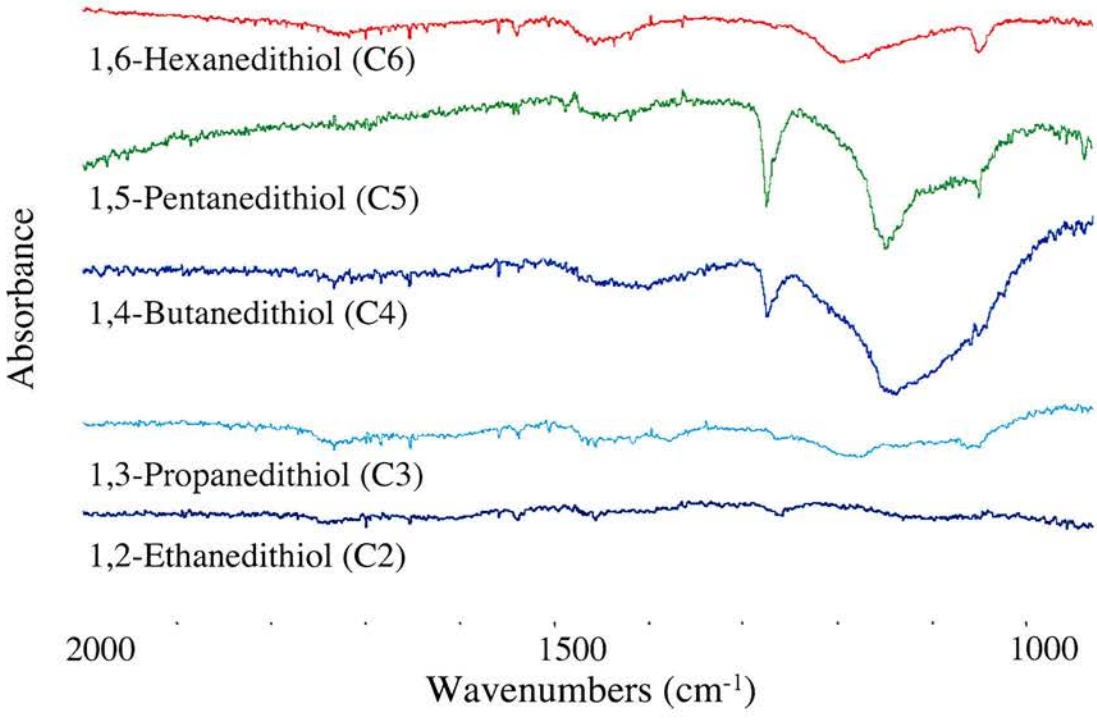

Figure 2.6 PMIRRAS spectra of a selection of short chain dithiol SAMs. These are optimised at 1851cm^{-1}.

In the 1851 cm^{-1} optimised spectra (Figure 2.6) the most distinctive peak is the one between 1250 cm^{-1} and 1051 cm^{-1}. This peak is attributed to the CH_2 wagging bands [3]. This peak in BTDT (C4) and PTDT (C5) SAMs is much larger and broader, indicating a different structure. In the case of BTDT the peak is so big that it has overwhelmed the adjacent peak that would have appeared at around 1055 cm^{-1} (the C-C backbone stretch). The other lower region peaks do not show any particular trends (Table 2.3).

2.4.3 Mixed RGDC and Cysteine SAM Structures

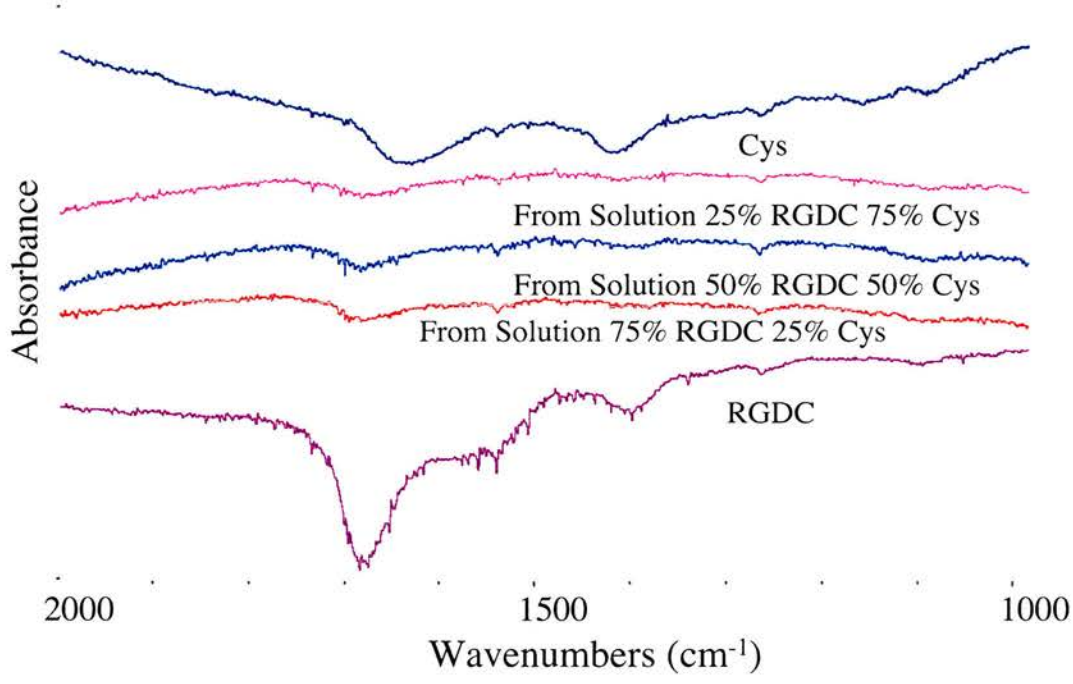

Figure 2.7 PMIRRAS spectra of SAMs formed from a mixed solution of the peptide arginyl glycyl aspartyl cysteine RGDC and the thiol containing amino acid cysteine. The percentage composition indicates the composition of the solution these SAMs were formed from, not necessarily the composition on the surface. In both these substances the SAM is formed by attachment of the thiol from the cysteine group. These are optimised at 2857 cm^{-1}.

For the 1851 cm^{-1} optimised spectra of cysteine (Cys) SAMs (Figure 2.7) distinctive bands are seen at 1418 cm^{-1} and 1633 cm^{-1}. These peaks correspond to the CO_2^- symmetric stretch and the NH_3^+ degenerate deformation respectively. The free C=O peak at 1736 cm^{-1} is barely visible compared to the other bands (Figure 2.7). The peak at 1540 cm^{-1} is attributed to the N-H bend /C-N stretches.

The peaks of the RGDC SAMs have been assigned using a spectra of an RC SAM [4] that exhibits a similar pattern of peaks, as a guide. The peak at 1680 cm^{-1} is assigned to the amide I stretch, the peak at 1541 cm^{-1} to the amide II stretch and the peak at 1402 cm^{-1} to the symmetric CO_2^- stretch. The free C=O peak at 1733 cm^{-1} is barely visible compared to the other bands.

The peaks of the mixed monolayers correspond to those of the RGDC monolayer SAM, showing the amide I stretch at around 1680 cm^{-1}, the amide II at around 1540 cm^{-1} and the CO_2^- stretch at around 1400 cm^{-1}. The free C=O peak around 1735 cm^{-1} is again barely visible compared to the other bands. There are no particular trends seen for the CH_2 asymmetric stretch peak. (Table 2.4 & Figure 2.8).

SAM	CH_2 Asym	CH_2 Sym	Fermi Resonance	Free CO_2	NH^{3+} Deformation	N-H Bend(60%) C-N Stretch (40%)	Amide I	Amide II	CO_2 Sym	CH_2 Rock	CH_2 Wag	C-C-C Stretch
Cys	2927	2858	2964	1736	1633	1540	-	-	1418	1262	1156	1090
Cys75% RGDC25%	2924	2857	2965	1735	-	-	1674	1536	1404	1260	1154	1085
Cy50% RGDC25%	2927	2857	2961	1735	-	-	1683	1540	1398	1263	1128	1082
Cys25% RGDC75%	2926	2859	2960	1739	-	-	1680	1540	1407	1265	1129	1089
RGDC	2931	2859	2963	1733	-	-	1680	1541	1402	1260	1156	1096

Table 2.4 Table of peak positions for mixed Cys and RGDC SAMs from figures 2.7 & 2.8.

For both the 1851 cm^{-1} and 2857 cm^{-1} optimised spectra the peaks for the single component monolayers are much bigger relative to the noise level than the dual component monolayers (Figures 2.7 & 2.8).

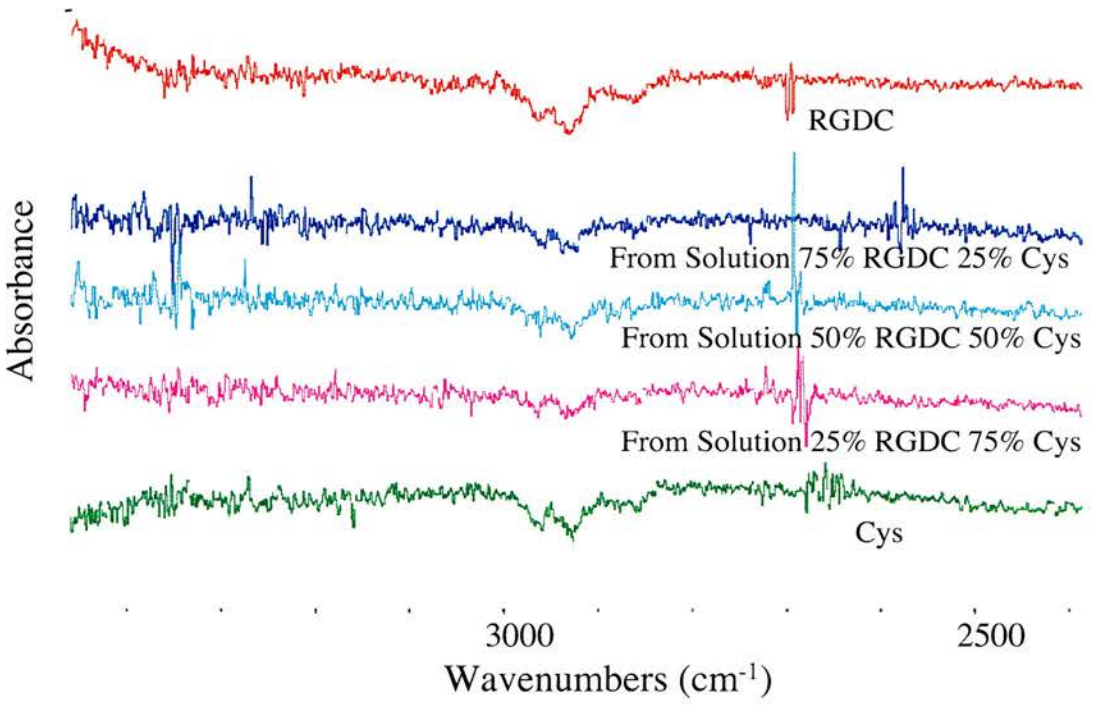

Figure 2.8 PMIRRAS spectra of SAMs formed from a mixed solution of the peptide arginyl glycyl aspartyl cysteine RGDC and the thiol containing amino acid cysteine. The percentage composition indicates the composition of the solution these SAMs were formed from, not necessarily the composition on the surface. In both these substances the SAM is formed by attachment of the thiol from the cysteine group. These are optimised at 2857 cm^{-1}.

2.4.4 Amine- and Amine Hydrochloride-terminated Self-assembled Monolayers

The CH_2 asymmetric peaks for the AUT.HCl and the 10-aminodecanethiol hydrochloride (ADT.HCl) SAMs are positioned in the same place at 2926 cm^{-1}

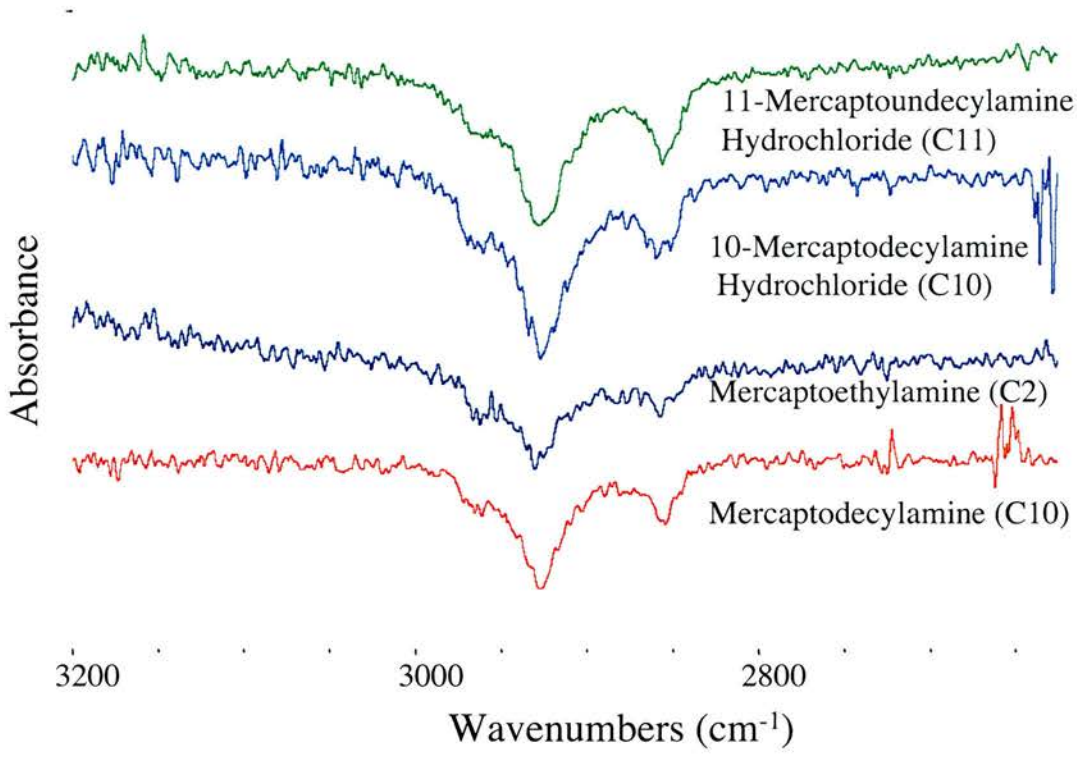

Figure 2.9 PMIRRAS spectra of a selection of amine- and amine hydrochloride-terminated SAMs. These are optimised at 2857 cm^{-1}.

(Figure 2.9 & Table 2.5). While the spectra for the 1851 cm^{-1} maximised region are not identical, particularly in the size of the methylene scissors peak relative to the N-H bend /C-N stretches, there are no particularly significant changes of peak position or intensity (Figure 2.9).

Carbon Number	CH_2 Asym	CH_2 Sym	Fermi Resonance	NH^{3+} Deformation	N-H Bend(60%) C-N Stretch (40%)	CH_2 Scissors	CH_2 Rock	CH_2 Wag
11 HCl	2926	2855	2964	1655	1538	1465	1263	-
10 HCl	2926	2856	2967	1657	1541	1462	1265	1165
10	2928	2855	2969	1601	1536	1431	1265	-
2	2930	2857	2963	1653	1538	1464	1267	1171

Table 2.5 Table of peak positions for amine- and amine hydrochloride-terminated SAMs spectra from figures 2.9 & 2.10

The 2-mercaptoethylamine (MEA (C2)) has its CH_2 asymmetric peak at 2930 cm^{-1} (Figure 2.10). It also has very broad peaks in the 1851 cm^{-1} optimised region.

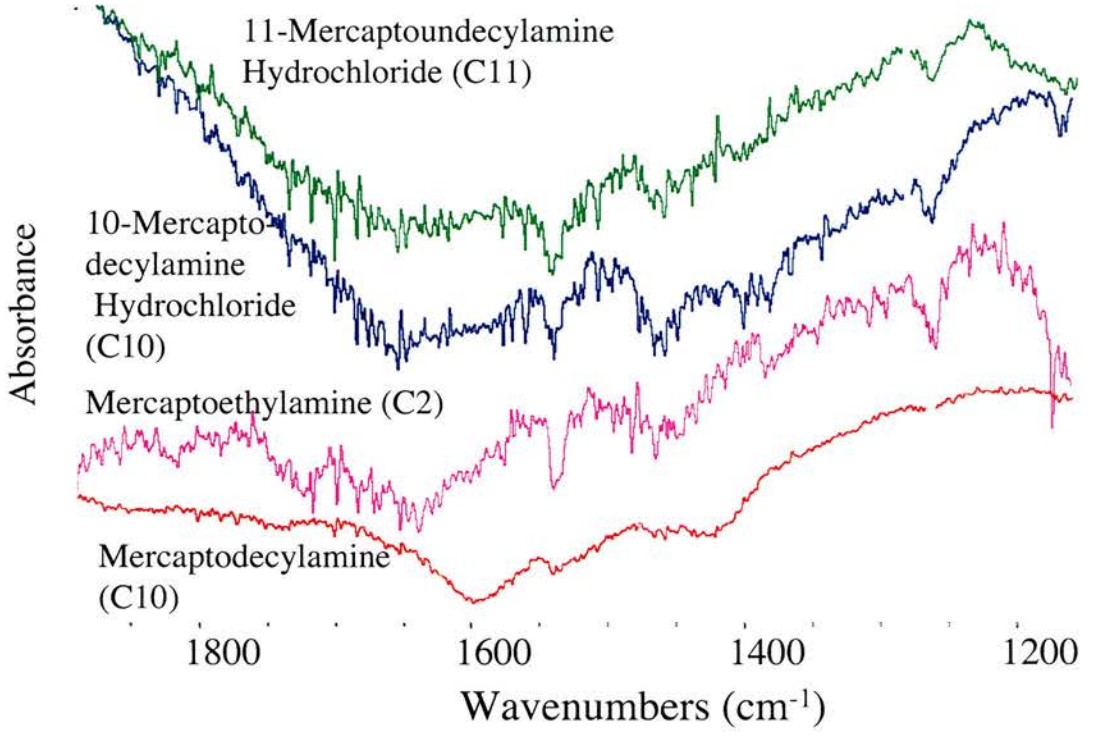

Figure 2.10 PMIRRAS spectra of a selection of amine- and amine hydrochloride-terminated SAMs. These are optimised at 1851 cm^{-1}.

The ADT SAM spectrum optimised at 1851 cm^{-1} also has peak broadening. ADT has a significantly different spectrum from ADT.HCl, the largest change is the shift of the band assigned as the NH_3^+ band in the ADT.HCl SAM from 1657 cm^{-1} to 1601 cm^{-1}. The assignment of this band is addressed further in the discussion. Other peaks that also change significantly are the methylene scissors vibration, the CH_2 asymmetric peak position of 2928 cm^{-1} (Table 2.5) and the wagging bands from 1300-1100 cm^{-1}. The latter cannot be seen in ADT.

2.4.5 Carboxylic Acid-terminated Monolayers

The position of the CH_2 asymmetric peak decreases in wavenumber with increasing carboxylic acid SAM carbon chain length for short-chain thiols (Table 2.5). The MUA (C11) and the 16-mercaptohexadecanoic acid (MHDA (C16)) SAMs have the CH_2 asymmetric peak in the same position (Figure 2.11) indicating that there are no chain length or odd-even effects occurring for long chain alkanethiol SAMs.

Carbon Number	CH_2 Asym	CH_2 Sym	C=O H-Bonded	C=O Free	CO_2 Sym	CO_2 Asym	CH_2 Scissors	CH_2 Rock	CH_2 Wag	C-C Stretch
2	2929	2859	1712	1746	1381	1537	1465	1257	1151	1081
3	2928	2856	1721	1739	1379	1538	1465	1259	1160	1074
4	2926	2853	1721	1744	1377	1539	1450	1256	1147	1077
8	?	?	1740	1757	-	1539	1455	1263	-	1109
11	2924	2854	1716	1737	-	1548	1458	1266	1174	1072
16	2924	2850	1697	1737	1390	1545	1469	-	1179	1083

Table 2.6 Table of peak positions for carboxylic acid-terminated SAMs spectra from figures 2.11 & 2.12.

The C11 and C16 SAMs also have the same peak position for the free C=O peak (1737 cm^{-1}) (Figure 2.12) which indicates more similarity between the two monolayers.

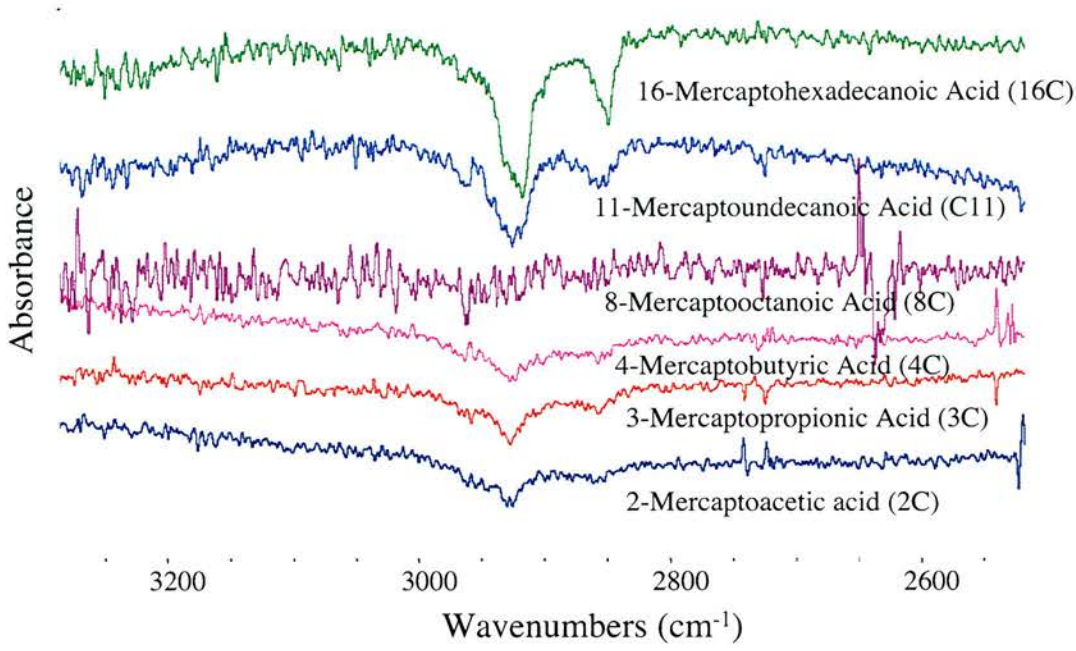

Figure 2.11 PMIRRAS spectra of a selection of carboxylic acid-terminated SAMs. These are optimised at 2857 cm^{-1}.

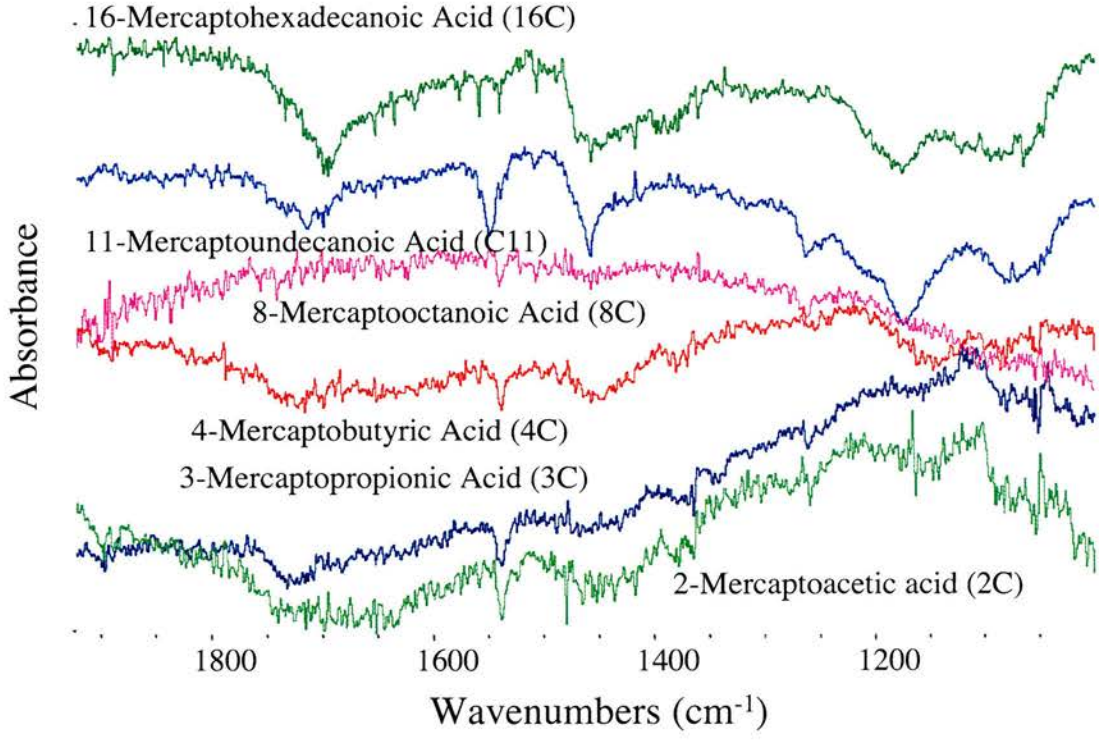

Figure 2.12 PMIRRAS spectra of a selection of carboxylic acid-terminated SAMs. These are optimised at 1851 cm^{-1}.

The type of H-bonding present in the C11 and C16 long-chain thiol SAMs is called into question by the position of the H-bonded C=O peaks at 1697 cm^{-1} and 1716 cm^{-1} [15]. These are the lowest positions found for this peak except for 2-mercaptoacetic acid (MAA) (C2) (at 1712 cm^{-1}) and these indicate the presence of cyclic dimers [15] (Table 2.6). The MAA has the highest frequency CH_2 asymmetric peak position for the carboxylic acid-terminated SAMs.

The 3-mercaptopropionic acid (MPA) (C3) SAM spectrum shows peaks at 1739 cm^{-1} for free C=O and 1721 cm^{-1} for H-bonded C=O. This indicates that there is predominantly acyclic H-bonding in this monolayer. There is some increase in the free C=O peak frequency between MPA (C3) and 4-mercaptobutyric acid (MBA) (C4) SAMs, but the H-bonding peak remains at 1721 cm^{-1}. This indicates that there may be a slightly more cohesive structure for the MBA (C4) SAM but the same degree and type of H-bonding is still present which indicates that the structures will predominantly be the same.

The MOA (8C) SAM spectrum is particularly unclear and peak positions are mostly estimates for this monolayer due to the level of noise. It is certain that the monolayer has been bound to the surface in some manner due to the peaks at 1557 cm^{-1} and 1263 cm^{-1} (Figure 2.12) that are easily distinguished above the noise level. The positions of the C=O peaks are also clearly visible though they are shifted to a much higher frequency than would be expected.

2.4.6 Mixed Monolayers

2.4.6.1 Mixed MUA and AUT Self-assembled Monolayers

The 2857 cm^{-1} maximised spectra (Figure 2.13) show that the peaks corresponding to the CH_2 asymmetric stretch are all centred between 2927 cm^{-1} and 2929 cm^{-1} for the CH_2 asymmetric stretch.

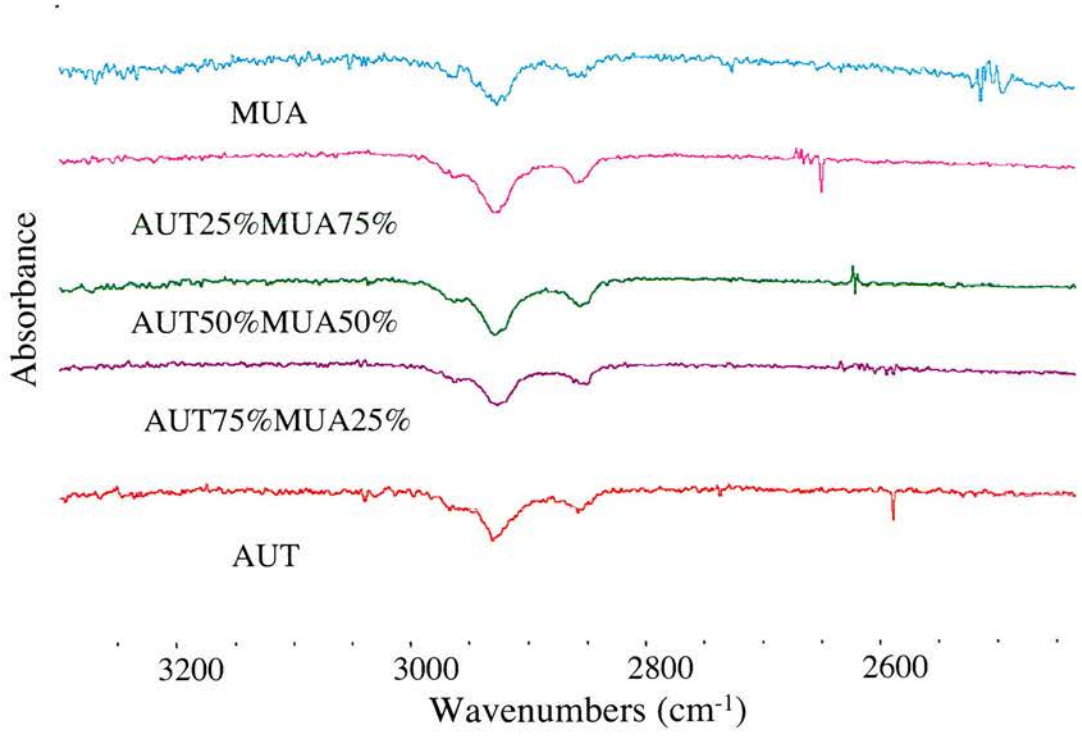

Figure 2.13 PMIRRAS spectra of SAMs formed from 11-Mercaptoundecanoic Acid (MUA), 11-Aminoundecanethiol (AUT) or a mixed solution of these. The percentage composition indicates the composition of the solution these SAMs were formed from, not necessarily the composition on the surface. These are optimised at 2857 cm^{-1}.

SAM Composition	C=O Free	C=O H-bonded	NH^{3+} Deformation	N-H Bend(60%) C-N Stretch (40%)	CO_2 Sym	CO_2 Asym	Methylene Scissors	CH_2 Rock	CH_2 Wag	C-C Stretch
MUA	1737	1718	-	-	1414	1551	1460	1263	1175	1077
MUA 75% / AUT 25%	1734	1718	1653	1540	in Meth scissors	1558	1444	1265	1105	1105
MUA 50% / AUT 50%	1732	1716	1653	1539	in Meth scissors	1558	1446	1261	1150	1105
MUA 25% / AUT 75%	1744	1718	1653	1537	in Meth scissors	1558	1444	1263	1103/ 1186	1056
AUT	-	-	1655	1540	-	-	1451	1265	1161	-

Table 2.7 Table of peak positions for spectra of SAMs formed from 11-Mercaptoundecanoic Acid (MUA), 11-Aminoundecanethiol (AUT) or a mixed solution of these. The percentage composition indicates the composition of the solution these SAMs were formed from, not necessarily the composition on the surface.

In the mixed monolayers the peaks for both the NH_3^+ degenerate deformation and the CO_2^- asymmetric stretch are present at around 1653 cm^{-1} and 1558 cm^{-1} respectively (Figure 2.14).

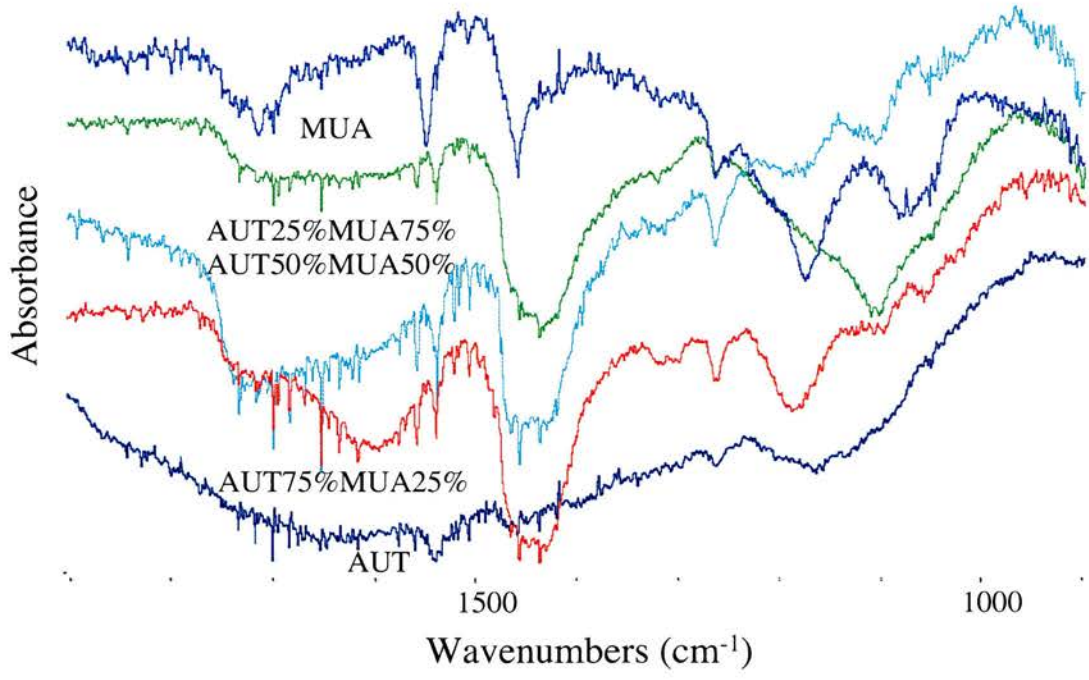

Figure 2.14 PMIRRAS spectra of SAMs formed from 11-Mercaptoundecanoic Acid (MUA), 11-Aminoundecanethiol (AUT) or a mixed solution of these. The percentage composition indicates the composition of the solution these SAMs were formed from, not necessarily the composition on the surface. These are optimised at 1851 cm^{-1}.

The peak present at around 1540 cm^{-1} is seen in both the mixed monolayers and AUT.HCl (Figure 2.14, Table 2.7). This has been attributed to 60% N-H bending and 40% C-N stretch. This peak has been shown to be very sensitive to H-bonding [5] and is therefore probably one of the broadening factors for the peak that centres on the NH_3^+ degenerate deformation at 1653 cm^{-1}.

The peak seen at around 1729 cm^{-1} in the mixed monolayers and MUA can be split into two peaks; one peak corresponding to for the C=O H-bonded vibration at around 1735 cm^{-1} and one peak for the C=O free vibration at around 1720 cm^{-1}.

The peak shape of the mixed SAMs is very different from the single component SAMs. An entirely new peak appears in the mixed SAMs; a very broad peak at around 1445 cm^{-1} that can be seen in all three mixed monolayers. The closest peak, which appears in both MUA and AUT.HCl is the CH_2 methylene scissors vibration at 1460 cm^{-1} and 1451 cm^{-1} respectively.

2.4.6.2 Reacting Mixed Monolayers

2.4.6.2.1 Reacting 11-Mercaptoundecanoic Acid Self-assembled Monolayers

The spectra produced from the reaction of the MUA SAM with the NHS/EDC solution are shown in figures 2.15 and 2.16 and the peaks are listed in table 2.8.

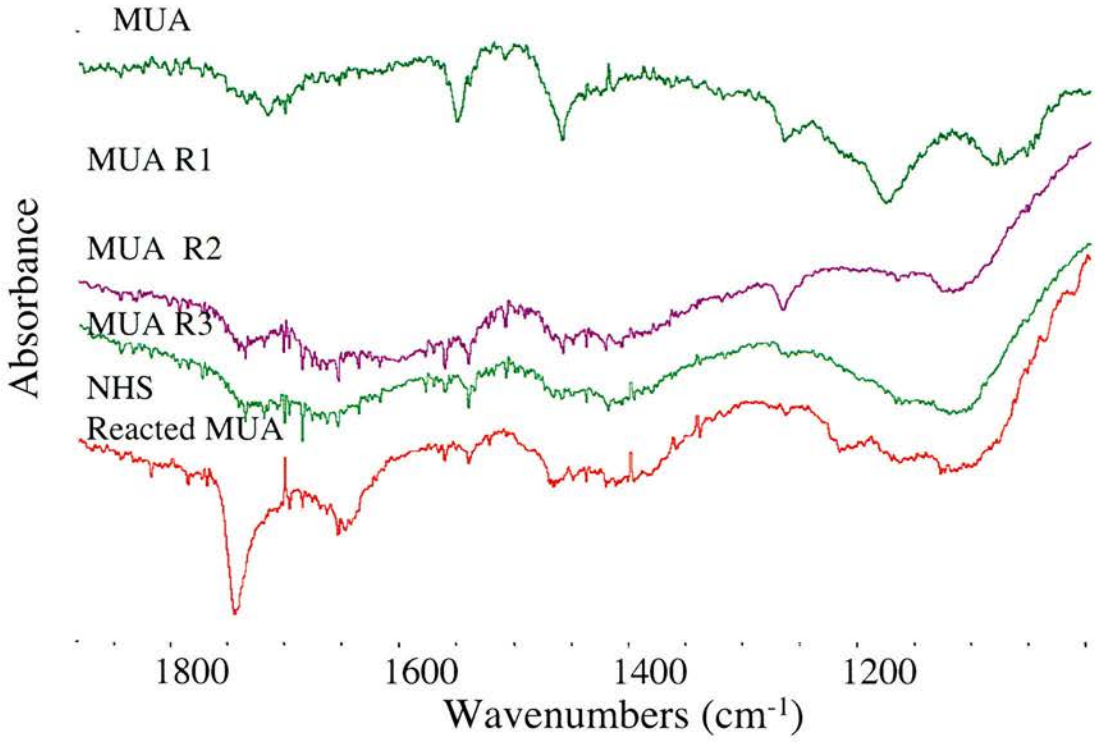

Figure 2.15 PMIRRAS spectra of the progression of reactions of a MUA monolayer with NHS/EDC then Ammonia solution. Firstly an NHS ester is formed then this is reacted with an ammonia solution. These two reactions are then repeated. Only the first NHS ester presenting monolayer is shown at the top, subsequent reactions are shown only after they have been reacted with the ammonia solution. These spectra are optimised at 1851cm^{-1}

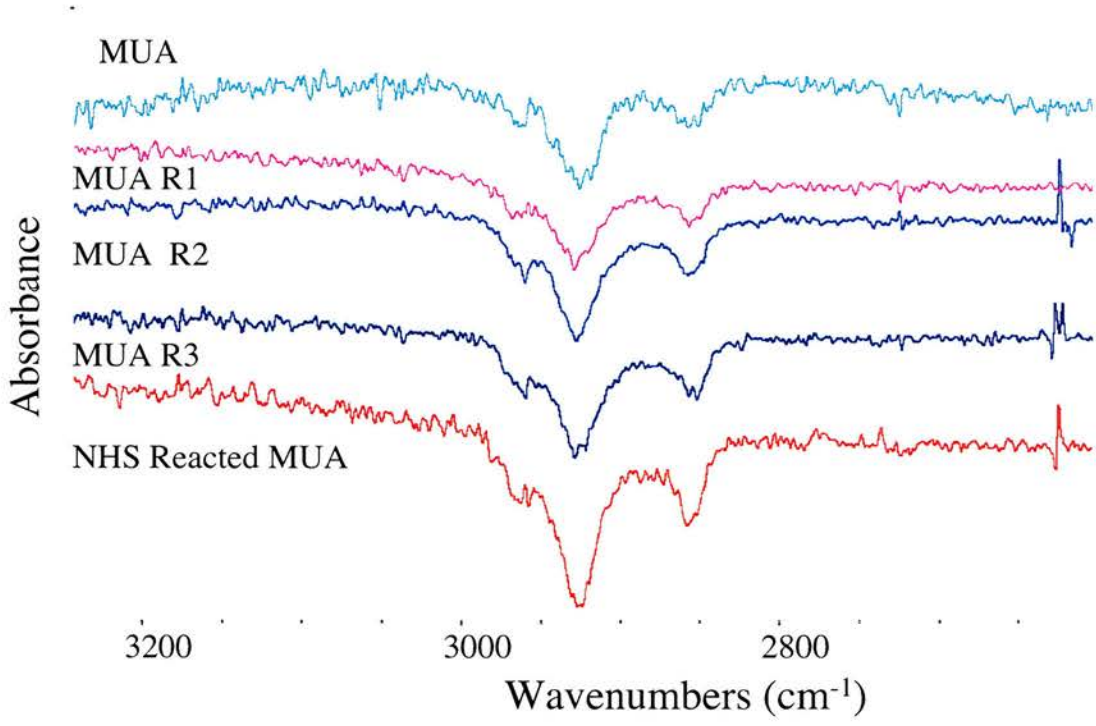

Figure 2.16 PMIRRAS spectra of the progression of reactions of a MUA monolayer with NHS/EDC then Ammonia solution. Firstly an NHS ester is formed then this is reacted with an ammonia solution. These two reactions are then repeated. Only the first NHS ester presenting monolayer is shown at the top, subsequent reactions are shown only after they have been reacted with the ammonia solution. These spectra are optimised at 2857cm^{-1}

SAM	CH_2 Sym	CH_2 Asym	C=O Free	C=O H-bonded	Methylene Scissors	CO_2 Asym	CH_2 Rock	Amide C=O / Amide NH	Amide CN	CH_2 Wag	C-C-C Stretch	C-N-C ASym	C-N-C Sym	NHS Asym C=O	NHS Sym C=O	C=O stretch of NHS ester of MUA
NHS	2854	2926	-	-	1463	-	1261	1644	1408	1163	1118	1212	1380	1744	1785	1817
MUA	2856	2924	1738	1717	1457	1549	1261	-	-	1172	1078	-	-	-	-	-
MUA R1	2855	2927	1740	1719	1459	1542	1265	1655	1419	1165	1110	-	-	-	-	-
MUA R2	2855	2927	1740	1719	1459	1540	1265	1604/ 1655	1410	1163	1121	-	-	-	-	-
MUA R3	2854	2926	1738	1721	1459	1538	1259	1661	1414	1157	1112	-	-	-	-	-
Ditbsu	2853	2924	-	-	1465	-	1265	1627	1417	1178	1063	1223	1378	1742	-	-
Ditbsu R1	2853	2924	-	-	1465	-	1255	1646	1417	1187	-	-	1382	1742	-	-

Table 2.8 Table of peak positions for Ditbsu and NHS reacted spectra from figures 2.15 -2.18.

The MUA SAM has a CH_2 asymmetric stretching peak at a lower wavenumber than any of the equivalent peaks in the reacted monolayers. As SAMs of alkanethiols are very resilient it is unlikely the reaction detaches any of the MUA from the surface to allow the formation of a completely different structure. This means that decrease in the position of the CH_2 asymmetric stretching peak can only be attributed to an increase in the liquid-like character (disorder) in the reacted SAMs compared to the MUA SAM. The least ordered SAMs appear to be the MUA reacted with NHS/EDC then ammonia solution (MUA R1) and the MUA reacted with NHS/EDC then ammonia solution twice (MUA R2).

The reaction of the MUA SAM to form an NHS ester is confirmed by the appearance of the distinctive band around 1200 cm^{-1} (Figure 2.15) which is accounted for by the C-N-C asymmetric stretch and the shifting of the C=O peak to higher frequency.

When the NHS reacts with ammonia solution an amide can clearly be seen to appear (MUA R1 on figure 2.15) and the large NHS related peaks disappear. This is the

case for all the MUA R SAMs. There are no distinct differences between the MUA R1, MUA R2 and MUA R3.

2.4.6.2.2 Comparing NHS Reacted Self-assembled Monolayers and Ditbsu Self-assembled Monolayers

In figures 2.17 & 2.18 the MUA reacted SAM is compared to the Ditbsu reacted SAM.

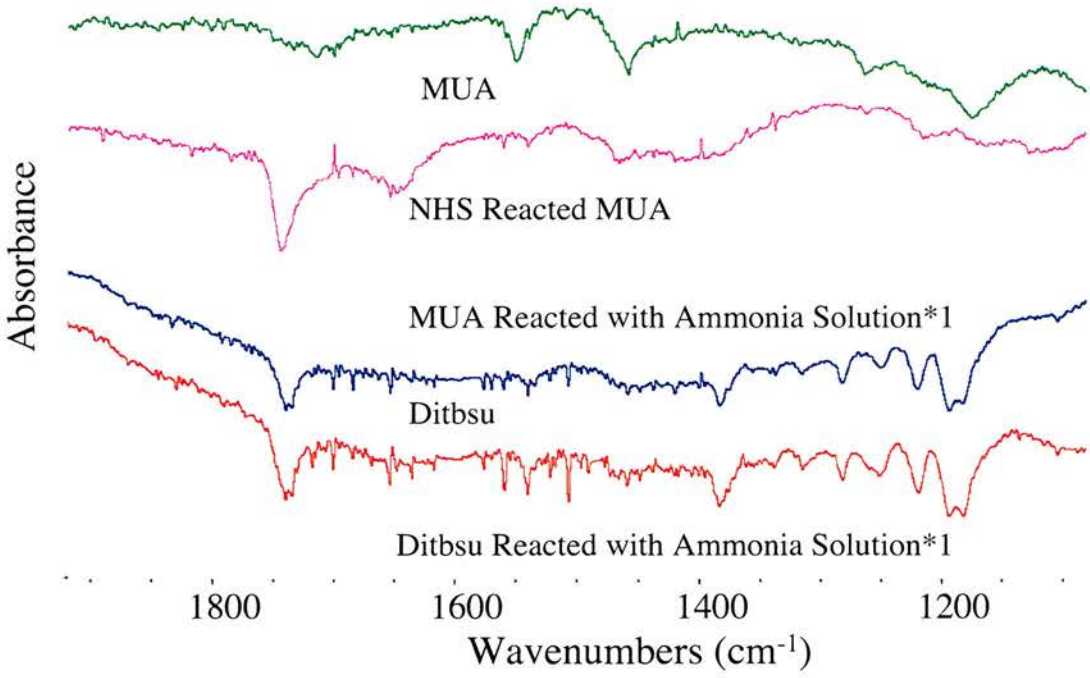

Figure 2.17 PMIRRAS spectra of the reaction of a MUA monolayer first with NHS/EDC then ammonia solution, compared to the reaction of a Ditbsu monolayer with the same ammonia solution. These spectra are optimised at 1851cm^{-1}.

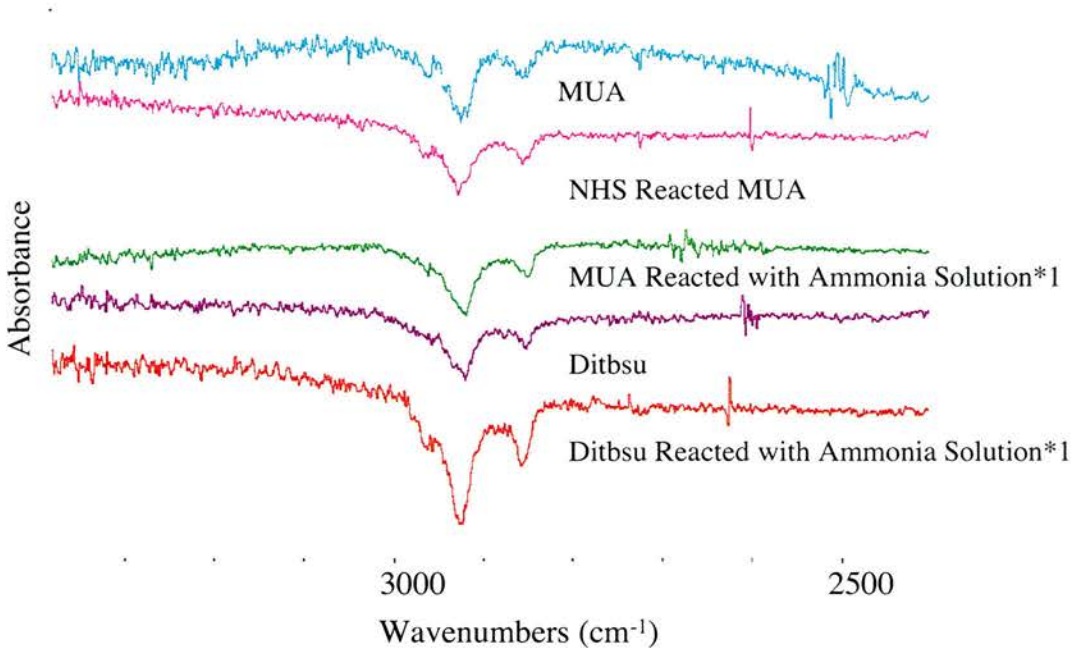

Figure 2.18 PMIRRAS spectra of the reaction of a MUA monolayer first with NHS/EDC then Ammonia solution, compared to the reaction of a Ditbsu monolayer with the same ammonia solution. This spectra is optimised at 2857cm^{-1}.

From figure 2.18 it can be seen that the CH_2 asymmetric peak is in the same position (2924 cm^{-1}) for both the MUA and the Ditbsu SAMs. There is no difference in the position of this peak between the Ditbsu SAM and the Ditbsu SAM reacted with ammonia solution (Ditbsu R1) (Table 2.8). The MUA SAM, as mentioned previously, has a different (CH_2 asymmetric) peak position after reaction.

The 1851 cm^{-1} optimised spectra (Figure 2.17) shows that the MUA SAM reacted with NHS has a different spectra compared to Ditbsu SAM. One of the most marked changes is the lack of a peak at around 1650 cm^{-1} in the Ditbsu SAM spectra. The other point that should be noted is that the spectra for the Ditbsu SAM do not change upon immersion in ammonia solution whereas the NHS reacted MUA changes

drastically upon immersion. This suggests that there is no reaction occurring when the Ditbsu monolayer is immersed in the ammonia solution. The final difference between the MUA reacted SAMs and the Ditbsu SAM is wagging bands between 1300 cm^{-1} and 1200 cm^{-1} that are not very distinct in the MUA SAM reacted with NHS and MUA R1 but appear very clearly in the Ditbsu SAMs.

2.4.6.2.3 SPDP Reaction

The 2857 cm^{-1} optimised region shows slight variation between the spectra for the SPDP/RGDC reacted SAMs (Figure 2.19).

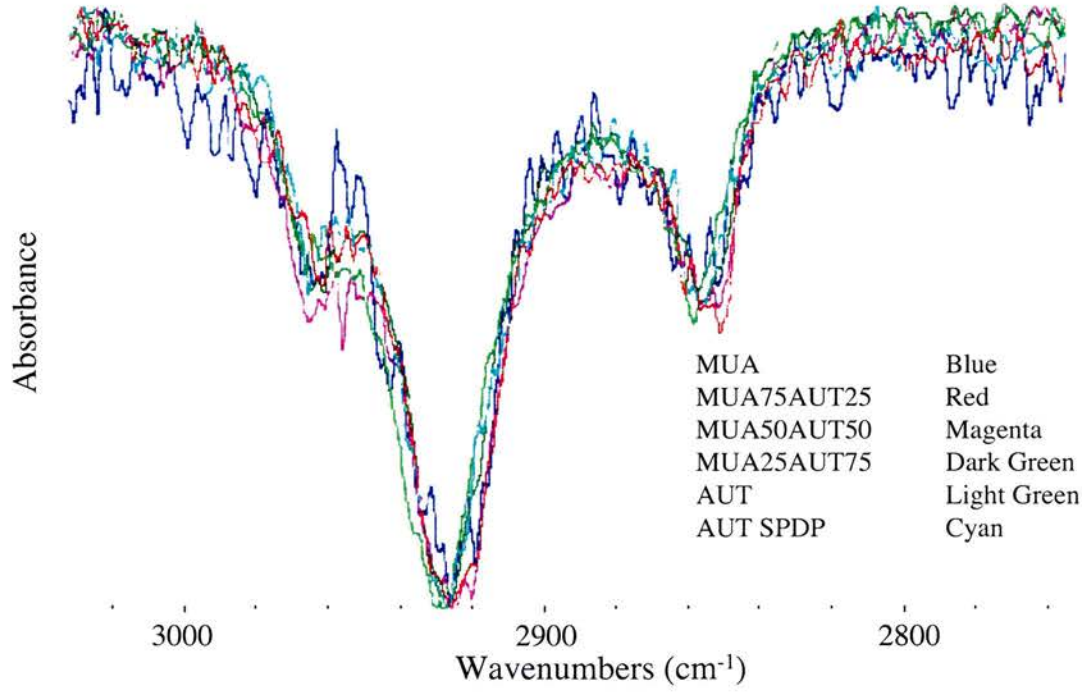

Figure 2.19 PMIRRAS spectra of mixed monolayers made from AUT and MUA reacted firstly with SPDP then with RGDC to form an RGDC presenting surface. The spectra have been scaled so that all the peaks can be seen clearly so the intensities are not comparable. These spectra are optimised at 2857 cm^{-1}.

The spectra that have the lowest frequency CH_2 asymmetric stretches (2924 cm^{-1}) are the MUA and the MUA50%AUT50% SAMs. It is unlikely that the basic structure of the SAM has changed upon reaction, therefore the position of the CH_2 asymmetric peak indicates the amount of disorder in these SAMs. This means that that the MUA and MUA50%AUT50% SAMs are the most ordered. This is expected for the MUA SAM due to it being unable to react with the SPDP, no increase in disorder would be seen by its attempted reaction. The position of the CH_2 asymmetric stretch peak increases in frequency with the proportion of AUT.HCl in the sample except for the MUA50%AUT50% SAM (Table 2.9).

SPDP/ RGDC Reacted SAM	CH_2 Asym	CH_2 Sym	C=O H-bonded	C=O Free	Amide I	Aromatic C=C	CO_2 Asym	Amide II	CO_2 Sym	CH_2 Scissors	CH_2 Rock	CH_2 Wag	C-C-C Stretch
MUA	2924	2856	1718	1737	-	-	1551	-	1414	1460	1263	1175	1077
MUA75% AUT25%	2925	2855	1717	1737	1667	1574	1559	1540	1420	1468	1262	1185	1047
MUA50% AUT50%	2924	2854	1717	1733	1653	1574	1559	1540	1420	1468	1260	1115	Inc. wag
MUA25% AUT75%	2927	2855	1715	1735	1653	1576	1559	1538	1420	1464	1262	1169/ 1101	1045
AUT	2929	2858	1719	1735	1672	1576	1559	1540	1420	1459	1264	1160	1095/ 1047
AUT NO RGDC	2927	2855	1717	1739	1654	1576	1559	1540	1420	1457	1264	1119	1081/ 1042

Table 2.8 Table of peak positions for mixed AUT/MUA SAMs reacted with SPDP and RGDC SAM. Data from the spectra from figures 2.19 &2.20

In the 1851 cm^{-1} optimised region the SPDP/ RGDC reacted SAMs show few particularly distinct wagging peaks and those that are seen are not significantly above the noise level (Figure 2.20). This indicates that the SAMs are not very well ordered.

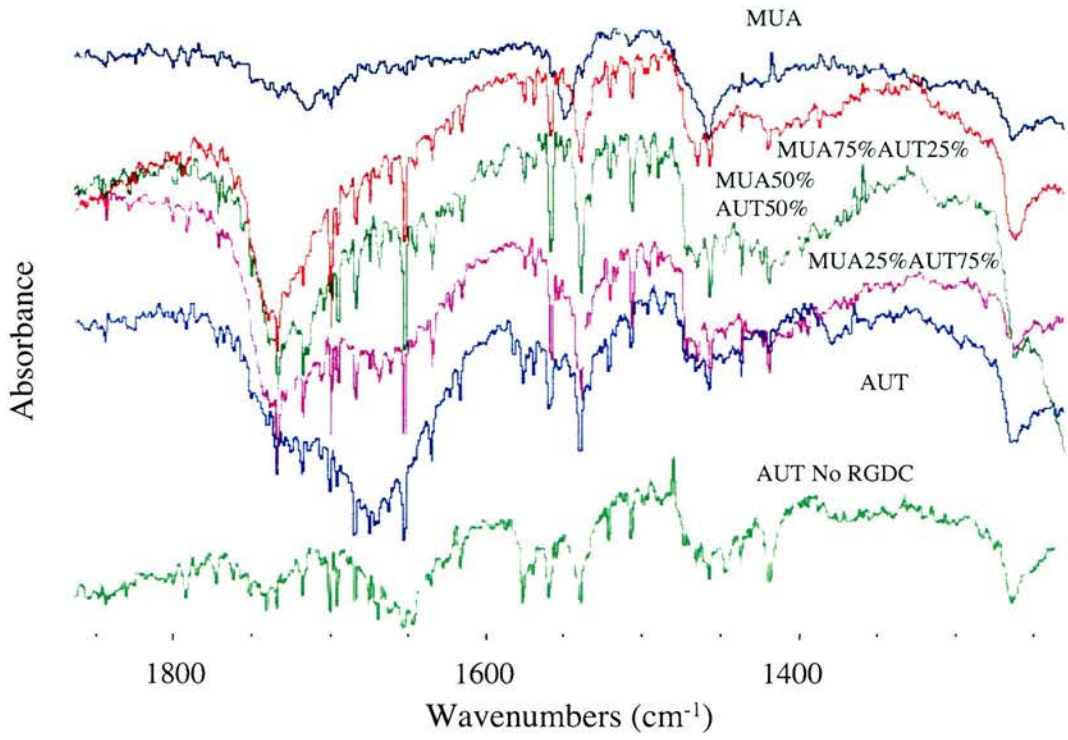

Figure 2.20 PMIRRAS spectra of mixed monolayers made from AUT and MUA reacted firstly with SPDP then with RGDC to form an RGDC presenting surface. The bottom spectrum of reacted AUT has not been reacted with RGDC only SPDP for comparison. The spectra have been scaled so that all the peaks can be seen clearly so the intensities are not comparable. These spectra are optimised at 1851 cm^{-1}.

One notable feature of the spectra shown in figure 2.20 is the aromatic ring stretching at 1574 cm^{-1}. This indicates the presence of the aromatic ring from the pyridyl group. This means that not all the SPDP moieties reacted within the time given.

An indication that the reaction is proceeding proportionally to the amount of AUT.HCl present is the steady increase of the size of the amide peaks at around 1660 cm^{-1} (amide I) and 1540 cm^{-1} (amide II) relative to the C=O stretch at around 1735 cm^{-1}.

Unusually there are bands seen at 1735 cm^{-1} and 1719 cm^{-1} (Figure 2.20) for the AUT.HCl SAM reacted with SPDP. This indicates the presence of a carboxylic acid or other carbonyl moiety, and cannot be accounted for by the amide as the amide C=O band is seen around 1660 cm^{-1}.

2.4.7 C2 Self-Assembled Monolayers

Closer examination of the ETT SAM CH_2 asymmetric stretch peak shows it to be split. While this split was originally classified as a single peak at 2924 cm^{-1} with noise (Figure 2.21), it is possible that these actually represent two different frequencies of the CH_2 group. Assuming that the peak is split, the different positions are 2918cm^{-1} and 2827 cm^{-1}.

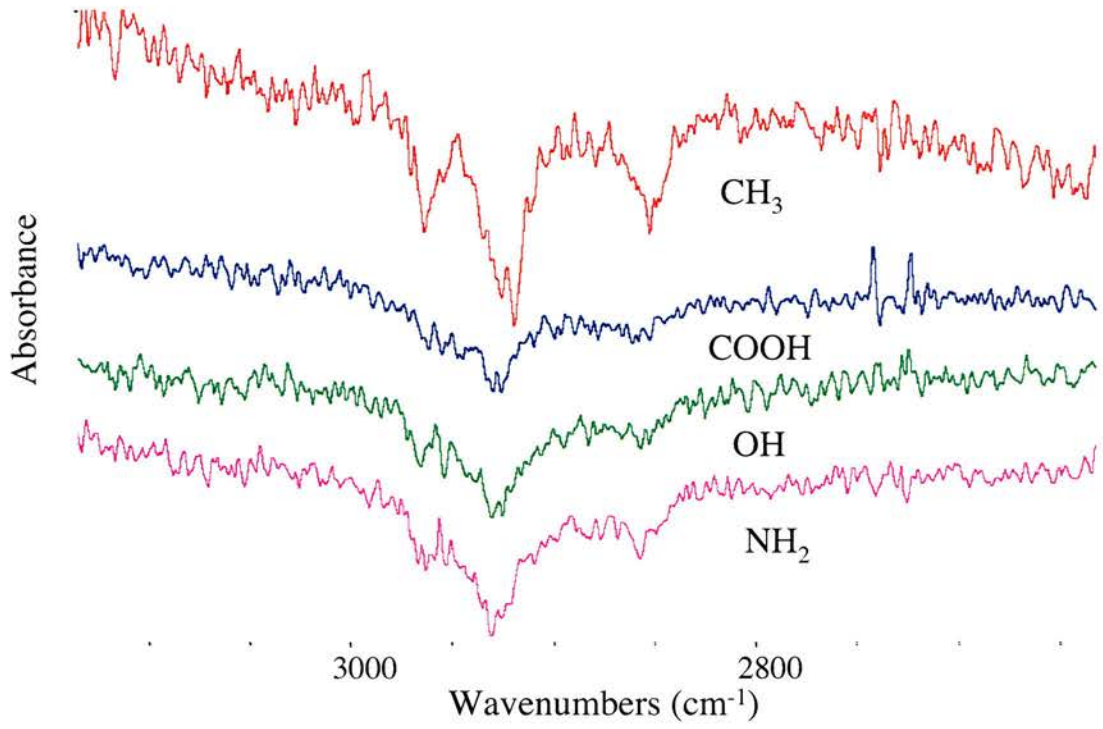

Figure 2.21 PMIRRAS spectra of the differences between spectra of 2 carbon chain length self-assembled monolayers presenting different functionalities. This spectra is optimised at 2857cm^{-1}

This may also be the case for the other C2 SAMs with Meth SAM having asymmetric CH_2 bands at 2926 cm^{-1} and 2930 cm^{-1}, and both MEA and MAA SAMs having these bands at 2925 cm^{-1} and 2930 cm^{-1} (Table 2.9). In all but MEA SAM the intensities of these bands are roughly equal; the 2925 cm^{-1} band for the MEA SAM is very small.

SAM Termination	CH_2 Asym	CH_2 Sym	CH_3 Sym	C=O Free	C=O H-bonded	NH^{3+} Deformation	N-H Bend(60%) C-N Stretch (40%)	CO_2 Asym	Methylene Scissors	CO_2 Sym	CH_3 Sym Scissors	CH_2 Rock	CH_2 Wag
NH_2	2930	2857	-	-	-	1653	1538	-	1464	-	-	1267	1171
CH_3	2924	2849	2963	-	-	-	-	-	1442	-	1381	1268	1124
COOH	2929	2859	-	1746	1712	-	-	1537	1465	1381	-	1257	1151
OH	2927	2857	-	1740	-	-	-	1535	1463	-	-	1256	1154

Table 2.9 Table of peak positions for C2 SAM spectra from figures 2.21 & 2.22.

The most obvious point about the spectra in the 1851 cm^{-1} (Figure 2.22) optimised region is that the Meth SAM has a peak at 1730 cm^{-1} where there should be no absorbance in this spectrum. The origin of this peak could be the oxidation of Meth to MAA. This is also indicated by the presence of a peak at 1535 cm^{-1}. This SAM shall still be designated by the term Meth even though how much of that type of monolayer is present is uncertain.

The other spectra in the 1851 cm^{-1} optimised region (Figure 2.22) indicate peaks in the regions where they are expected to be and the MAA SAM indicates some level of

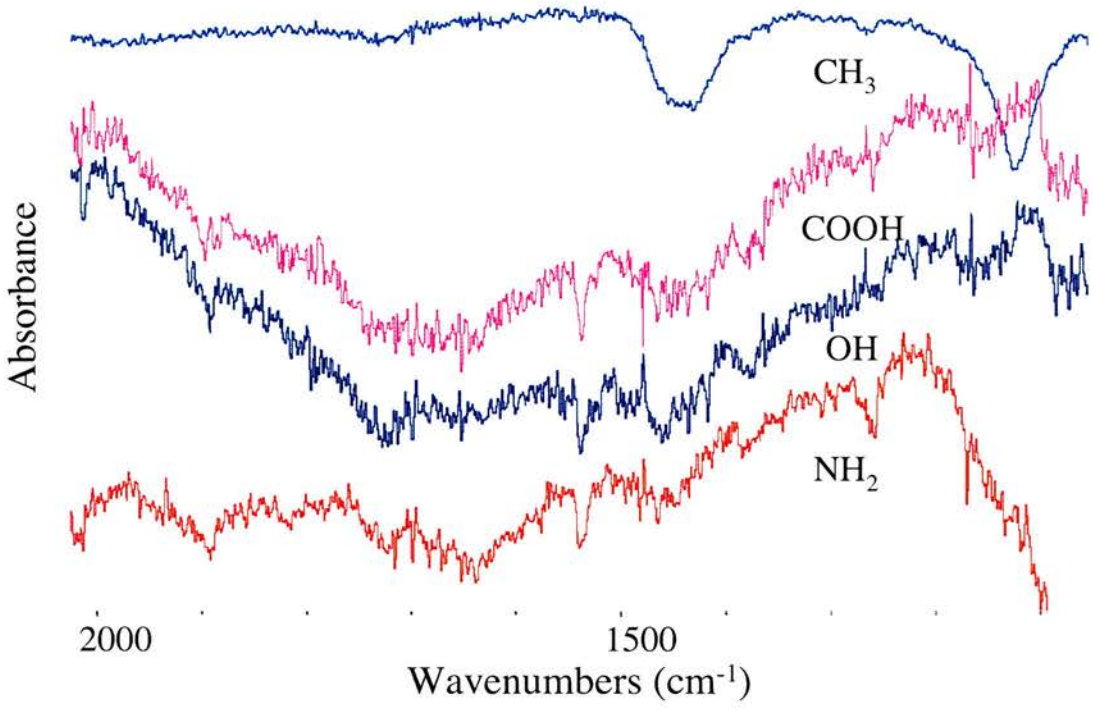

Figure 2.22 PMIRRAS spectra of the differences between spectra of 2 carbon chain length self-assembled monolayers presenting different functionalities. It should be noted that the intensities on this scale have been adjusted in order to have all the relevant peaks clearly visible. This spectra is optimised at 1851cm^{-1}.

disorder due to acyclic dimers as indicated earlier. The 1730 cm^{-1} peak for the Meth SAM is well defined and does not taper off to a lower level, this indicates that it probably does not form acyclic dimers.

2.5 Discussion

2.5.1 Methyl-terminated Self-Assembled Monolayers

2.5.1.1 Chain Length Effect

The short chains, methyl-terminated thiol SAMs up to C8 nearly all have a CH_2 asymmetric peak positioning of 2926 cm^{-1}. It is traditionally thought that SAMs with a CH_2 asymmetric peak positioning above 2920 cm^{-1} are particularly disordered [2], however, there is a growing body of evidence that suggests this may not be the case. [23] A possible explanation for the high frequency of the CH_2 symmetric peaks is that different structures are present of lower molecular densities than those seen in the longer chain alkanethiols. This could mean that the high CH_2 symmetric peak position that shows significant liquid-like character does not necessarily mean disorder, but possibly a structure with a lower packing density of thiols.

The spectra of HXT (C6) to OTT (C8) SAMs show more definition in the CH_3 symmetric stretch. This may be evidence that the monolayer is becoming more ordered or that there is a change in structure. Since the position of the CH_2 asymmetric stretch remains constant (C6-C8) implying that there is an equal amount of liquid-like structure, it is more probable that this is the beginning of a region of change in structure. This idea is supported by the drastic shift of the CH_2 wag peak

from around 1125 cm^{-1} to around 1090 cm^{-1} (Figure 2.2) between PTT (C5) and HXT (C6) SAMs with no change in the data collection procedure to account for this. The slides were not moved between the collection of the spectra optimised at 2857 cm^{-1} and those optimised at 1851 cm^{-1}, and in general if the spectra at one wavelength has a high intensity of absorbance then the spectra at the other will too. This suggests that there is a genuine intensity effect. The change is sudden between these two thiol SAMs and not gradual over several lengths of SAM, this indicates that there may be a point where the structure takes on a completely different form as opposed to more than one structure being present simultaneously. In addition, this argues against there being a gradual increase of order as the chain length of the SAM increases, as there would be no obvious explanation for this phenomenon in that model.

The change of wagging peak position in the longer chain thiol SAMs is also interesting, with the position stable at around 1125 cm^{-1} for C10-C16 and different for ODT (C18). This could mean that the wagging peak frequency changes in areas of structural change to a lower frequency (Figure 2.3). This would be supported by the large change in asymmetric CH_2 peak position from 2925 cm^{-1} at HDT (C16) to 2919 cm^{-1} at ODT (C18).

The decrease in the frequency of the CH_2 asymmetric stretch peak positioning over increased carbon chain length for long chain methyl-terminated thiol SAMs indicates that the self-assembled monolayer is apparently losing liquid-like character and

becoming more crystalline. This is a common phenomenon that has been seen for many thiols though it is markedly absent in this experiment for the shorter chain thiols [2]. This is may be due to the difficulties involved in getting high quality spectra from short chain thiols.

An interesting result is that the ETT SAM is the next least liquid-like thiol studied here after ODT. This is probably due to the sulfur head group having a larger stabilising and ordering influence in the ETT than in the other SAMs, while the carbon chain is not long enough to cause any ordering problems. As this explanation accounts for the difference of value it would fit with either theory about the degree of order in short chain thiol SAMs.

2.5.1.2 Odd-Even Effect

It can be seen (Table 2.2) that there is a difference between the spectra of SAMs of odd chain length and those with an even chain length. This phenomenon is called the odd-even effect. The effect is particularly clear for the CH_2 symmetric stretching peak. The effect is also present for the asymmetric CH_3 because although the effect is still present in the asymmetric peak, it could be coincidence as the positions fluctuate over the range without any particular pattern (Table 2.2).

The fact that ETT and BTT SAMs have no clear symmetric CH_3 stretching peak (Figure 2.1) while 1-propanethiol (PPT) and PTT SAMs do is likely to be another indication of the differences in structure between the odd chain length SAMs and the even chain length SAMs. If the dipole of the CH_3 stretch was close to parallel to the surface then the peak would not be seen above the noise.

The difference shown between the CH_2 symmetric peak position for odd chain length SAMs and for even chain length SAMs (odd-even effect) (Table 2) may also be evidence that the SAM is not particularly disordered. If there was a significant degree of disorder there could not be an observable difference based on the orientation of the tail group as a large degree of disorder would overwhelm the effect and control the peak position.

Due to the small size of this effect more experiments would need to be done to determine whether or not this effect is significant. Very long chain thiol SAMs (C18+) would be particularly useful for this type of experiment as they would be less susceptible to chain length effects.

2.5.2 Dithiol Self-assembled Monolayers

One point of interest about dithiols is that the Aldrich guideline spectra for 1,2-ethanedithiol (ETDT) (C2) to 1,6-hexanedithiol (HXDT) (C6) (not including PTDT

(C5)) show a great deal of variance in peak intensity and position. It is therefore surprising to get such a high level of similarity between the spectra of these different lengths of dithiol SAMs. This is particularly unexpected as they are thought to have a great deal of liquid-like character based on their CH stretching region (optimised at 2857 cm^{-1} (Figure 2.5)); the CH_2 asymmetric stretching peaks are around 2930 cm^{-1}, which is thought to indicate liquid-like structures and complete disorder.

The appearance of a peak at around 2965 cm^{-1} is one of the most unusual features of the dithiol spectra. This is the region typically associated with the CH_3 group, which is not present in these molecules. There is no logical way in which a methyl group could have become attached. It is assumed, due to a thorough washing and drying procedure, that no contaminants will be adhered to the surface. This combined with the fact that sulfur has such an affinity for gold that previous contaminants are generally displaced means that the surfaces are likely to only have thiols adsorbed. That there could be such a large concentration of contaminants is unlikely as there should be other spectral evidence of them.

It has been considered that the 2965 cm^{-1} peak could be Fermi resonance but it not very likely at such a high frequency. However this is the most likely conclusion so far. One study showing FTIR spectra of dithiol SAMs on gold shows a shoulder [6] which is around the same frequency, but it is not well enough resolved to clarify whether the peak is related to some sort of CH_3 contaminant. Further work would be

needed to determine whether the peaks are reproducible and whether or not there is a contaminant present in the dithiol SAM.

The most dominant feature in the CH bending region of the 1851 cm^{-1} maximised spectra is the large broad band between 1250 cm^{-1} and 1051 cm^{-1} that has been attributed to the CH_2 wagging modes [3]. In the case of BTDT and PTDT, this peak is at lower frequency, (Figure 2.6) and is much broader. This shift has a great deal of significance because the wagging peaks are thought to be a good indicator of the amount of order in the SAM. In one study on 1,12-dodecanedithiol, it was thought that the wagging bands were weaker when the SAM had an all *trans* configuration due to sigma conjugation between the alkane chains [7]. In another study [3], when 1,9-nonanedithiolate was heated to high temperature gauche defects were introduced, which significantly weakened the intensity of the peaks. The authors also stated that the very presence of these bands indicated that the chains on the surface were in an all *trans* conformation [3]. The breadth of the bands and the fact that they are not well resolved could be taken as a sign of the amount of disorder in this SAM. Further work is required to clarify the region sufficiently to identify individual peaks.

Another possibility for the difference between BTDT/PTDT and the other dithiols is that some of the dithiols could be forming bi- or multi- layers. Multi-layers have been shown to have clearer peaks in FTIR which are larger and better defined [6], The peaks in the CH stretching region are large and well defined for the self-

assembled ETDT, 1,3-propanedithiol (PPDT) and HXDT (Figure 2.5). It would therefore be reasonable to assume that the self-assembled PTDT and BTDT have not formed multilayers whereas the others have. Since the mechanism whereby multilayers are formed from dithiols deposited on gold under air is unclear, and the literature is often contradictory, it is not entirely unreasonable to expect multilayer formation despite the fact that the conditions used for the preparation of the dithiols were all identical. It should be mentioned that any anomalies in the dithiol spectra could be due to the amount of time the dithiol had been stored for, as over this time dithiol oxidation could have occurred. This probability of this is fairly low as the containers were very well sealed due to the pungent nature of the dithiols.

Whichever explanation is correct, it is certain that the BTDT and PTDT have a different structure from the other dithiols investigated. It is also certain that this structure - and that for all dithiols- has significant liquid-like properties. It is possible that the presence of the CH_2 wagging bands is a feature of an ordered structure that also has a low molecular density, which would explain the high frequency position of the CH_2 asymmetric stretching peaks.

2.5.3 Mixed RGDC and Cysteine Self-assembled Monolayers

The Cys SAM spectrum (Figure 2.7) shows the symmetric CO_2^- stretching band at 1418 cm^{-1} and the NH_3^+ deformation at 1633 cm^{-1} which, combined with the absence

of the H-bonded C=O stretch at 1715 cm^{-1} indicates that the structure is practically all zwitterionic. The 1616 cm^{-1} peak for the asymmetric CO_2^- stretch is not seen as the NH_3^+ deformation peak overlaps this position. The observation that the Cys SAM is all zwitterionic could be as a result of assembly from ethanol; most other studies used buffered water. The zwitterionic form was found to be less common at lower pH in a study by Ihs *et al* [8], which makes this observation unusual.

RGDC SAMs have the same peaks as the RC SAM spectra [4], this is unsurprising given that the same amino acids are present. It is more surprising that the positioning of the peaks and the relative sizes of the peaks are very similar, as this indicates that the arginyl residue has a similar orientation on the surface in both types of SAM. It is also unexpected that the aspartyl residue of RGDC does not introduce extra COOH related peaks or increase the relative intensity of CO_2^- bands compared to RC SAMs. This suggests that the dipole of the COOH is parallel to the surface and so the band is not seen due to being cancelled out by the surface selection rule.

In both Cys and RGDC SAMs there is only one peak at around 1400 cm^{-1} (Figure 2.7). In previous work [4, 8] two peaks have been identified in this region for Cys. Resolution of the peaks may be possible by averaging more spectra and by studying spectra optimised at a lower frequency.

Overall the peaks of the mixed monolayer are broader and less distinctive than the single component SAM spectra the spectra, this suggests that the mixed monolayers are more disordered. The spectra of RGDC containing SAMS show a more disordered version of the pure RGDC. There is not much variability between the spectra of RGDC75%Cys25%, RGDC50%Cys 50% and RGDC25%Cys75%. The assertion that the mixed SAMs are more disordered is made based on the peak size respective to the background noise level. The differences in peak size are seen in both the 1851 cm^{-1} (Figure 2.7) and 2857 cm^{-1} (Figure 2.8) optimised spectra. The similarity of the mixed monolayers to each other could be due to there being a strong preferential adsorption of the RGDC to the surface over the Cys. When SAMs are formed from a mixed solution the longer thiol usually has a much higher percentage coverage of the surface [9]. In this case it could be nearly complete but a few adsorbed Cys residues create some disorder. This argues against the possibility of different phases in the monolayer.

Efficient ordering of these molecules in SAMs is only likely to be possible when only one type of thiol is present; this is not unusual as only SAMs of similar length have been found to form fully mixed monolayers. In Cys SAMs the zwitterionic form is prevalent, which may mean that inter-molecular H-bonding occurs giving a more stable monolayer [10] though this is not indicated by the lack of a C=O H-bonded peak at 1715 cm^{-1}. In RGDC SAMs the chains should be able to interact with each other to provide stability. This would not be possible between the Cys and

the RGDC as the cystyl residue of the RGDC would be incapable of existing in a zwitterionic form.

While it is probable that the differences between the mixed and single component thiols are due to structural considerations it should be noted that there are a significant number of variables in the spectral analysis procedure. This means that the intensities are by no means absolute and the changes could be a sign of the differences in the behaviour of the instrument between measurements. Instrumental variability is improbable because the noise level remains approximately constant for samples prepared simultaneously with their spectra taken in same week.

2.5.4 Amine and Amine Hydrochloride-terminated Monolayers

The AUT.HCl (C11) and the ADT.HCl (C10) have much the same structure according to the similarity of their spectra, in particular the identical positions of the CH_2 asymmetric peaks. This means that any chain length dependence for these SAMs is unlikely.

The positioning of the CH_2 asymmetric peak indicates that the MEA (C2) is either slightly more disordered than ADT (C10) or has a different structure. One paper was very clear that disorder increases as the chain length of the thiol decreases [5] but there does not seem to be much evidence to support this theory in amine-terminated

thiols. In the same paper it was also hypothesised that ionic H-bonding stabilised the monolayer and increased surface order. The breadth of the bands in particular the NH_3^+ peak, suggests that ionic hydrogen bonds as described by Wallwork *et al* are formed [5]. H-bonding has been found to cause both order and disorder in SAMs so further work would be needed to determine which is the case here. STM and AFM studies will be needed to determine the true degree of structural order on the surface.

The ADT (C10) SAM spectrum is very different from the ADT.HCl (C10) SAM spectrum. This is not due to the association of a chloride ion with the hydrochloride SAM spectra as XPS studies have found that it does not remain [11]. It is therefore either the change between the NH_2 moiety and the NH_3^+ or the NH_2 moiety has been oxidised [12] to an imine or a nitrile by ambient oxygen [13]. Such a large downshift of NH_3^+ area peak from 1657 cm^{-1} to 1601 cm^{-1} and the near disappearance of the C-N/N-H peak indicates that it is probably the oxidation of the NH_2 to the imine that has occurred. The remaining part of the C-N/N-H peak would therefore either be due to incomplete oxidation or some of the C-N stretch remaining. The other differences in the structure such as the CH_2 asymmetric peaks, the methylene scissors vibrations and the lack of wagging bands from 1300-1100 cm^{-1} in the ADT SAM spectra (Table 2.5) could be accounted for by different ordering of the SAM caused by the different monolayer termination.

2.5.5 Carboxylic Acid-terminated Self-assembled Monolayers

There appears to be a chain length effect that occurs for the CH_2 asymmetric peak for short chain mercaptoalkanoic acid SAMs. This finding is supported by the previously mentioned study which found that the degree of liquid-like character decreased with increasing chain length [2]. It is also supported by a study which found that the number of defects in the SAM decreases with the increase of the chain length of the SAM [14]. There may be a chain length around C11 where the most order and the lowest number of defects possible is reached. This would agree with the results from the (MUA (C11) and MHDA (C16)) thiol SAMs, which do not show any chain length or odd-even effect (Table 2.5).

The long chain (MUA (C11) and MHDA (C16)) thiol SAMs have peak positions for the H-bonded C=O which indicate that there are cyclic dimers being formed [15]. As the monolayers have been well washed to dislodge any physisorbed thiols, it must be concluded that these are surface bound (chemisorbed) and as such causing some degree of disruption in the monolayer. This is despite the solution being what Arnold *et al* would have deemed to be low concentration, which is supposed to prevent the formation of cyclic dimers [15]. The CH_2 asymmetric peak indicates these two monolayers (MUA (C11) and MHDA (C16)) are the most ordered in this study while they clearly have linkages that cause disorder. This supports the idea that the position of the CH_2 asymmetric peak cannot be interpreted as direct measure

of disorder unless there is other evidence to support this. Hence it supports the theory that the position of the CH_2 asymmetric peak is more a measure of the packing density of the structure.

The spectrum for the C2 (MAA) thiol SAM shows that there are a significant number of cyclic dimers and that the position of the CH_2 asymmetric peak is at the highest frequency found for the mercaptoalkanoic acid SAMs studied here. This would suggest that the MAA SAM has a fairly high degree of disorder. This conclusion is supported by electrochemical results [14] that found there to be minimal interactions between the chains and maximal repulsion by the negatively charged tail groups of the SAM, which caused disorder.

The conclusion that the SAM is disordered is not supported by the idea that H-bonding stabilises the thiol [16]. The fact that the MPA (C3) monolayer is capable of significant H-bonding with the formation of predominantly acyclic dimers, indicates that there must be something significant occurring with the addition of the further CH_2 unit. It could be that additional flexibility in the chain allows both the Au-S bond and the H-bonding COOH groups to assume preferred conformations. A rather strange structure is found for MPA which indicates either that this structure is still far from ideal or that it takes sometime for the MPA to achieve a conformation that is preferable for both bonds. It is assumed that the amount of van der Waals'

bonding at this chain length will not be particularly significant given the other stronger interactions involved.

The theory that van der Waals' bonding is not particularly significant for short chain carboxylic acid-terminated SAMs is supported by the lack of any significant odd-even effect between the short chain thiol monolayers. It would be interesting to carry out STM studies on the MBA (C4) to see what, if any, differences in structure are actually present between the C3 (MPA) and C4 (MBA). There is a shift of the CH_2 asymmetric peak position to lower frequency and the free C=O peak to higher frequency. The degree of acyclic H-bonding remains constant, which indicates that at this length, the head group is the main driving force for the ordering of the structure.

The results from the 8C (MOA) are inconclusive. A previous study has found that 8C chains are well ordered [16]. This is supported by the high position of the C=O stretching bands at 1746 cm^{-1} as when this band shifts to lower frequency it is considered to be a sign of disorder [8].

2.5.6 Mixed Monolayers

2.5.6.1 Mixed 11-Mercaptoundecanoic Acid and 11-Mercaptoundecylamine Self-assembled Monolayers

The asymmetric CH_2 peaks in figure 2.13 at around 2928 cm^{-1} show that the SAMs in this experiment have a large amount of liquid-like character in their structures and that they have quite similar packing density.

In the mixed monolayers both the CO_2^- and the NH_3^+ degenerate deformation peaks are present, this shows that both MUA and AUT are present in each of the mixed monolayers.

The peak at around 1540 cm^{-1} (Figure 2.14) results from 60% N-H bending and 40% C-N stretch and is strongly affected by H-bonding [5]. This could explain why the peak broadens to such a great extent. In a KBr spectrum of the AUT the 60% N-H bending and 40% C-N stretch peak is at 1607 cm^{-1}, and in another SAM of AUT the peak was at 1549 cm^{-1}. This wide range of peak positions possible due to different levels of H-Bonding could explain the breadth of this peak, particularly when combined with the NH_3^+ degenerate deformation peak which may be present in larger quantities due to the stabilisation provided by H-Bonding. H-bonding of this extent cannot be attributed to bonding between neutral and charged amines [5], and

therefore must be due to H-bonding between the amine and the carboxylic acid which suggests that the molecules are evenly distributed in the monolayer.

There is also some suggestion of H-bonding from the C=O peaks at around 1735 cm^{-1} which indicate by the breadth of the peak (which runs into the free COOH peak at 1720 cm^{-1}) that the H-bonding is fairly extensive.

The peaks at around 1729 cm^{-1} (C=O vibration) and 1540 cm^{-1} (60% N-H bending and 40% C-N stretch) can be used as guides to the composition of the monolayer. The monolayer prepared from AUT75%MUA25% shows the amine peak (1540 cm^{-1}) to be larger than the MUA peak (1729 cm^{-1}). At equimolar solution concentrations the MUA peak appears to be the larger. In the SAM formed from AUT25%MUA75% they appear to be of equal intensity. A possible explanation for this is that in the AUT25%MUA75% monolayer the broadening caused by H-Bonding is so extensive that the peaks overlap to produce no differences between the regions. The huge peak at around 1105 cm^{-1} (Figure 2.13), which is broad enough to cover the CH_2 wagging and the C-C-C stretching peaks supports this theory. There is less of this seen in the AUT50%MUA50% where less AUT character is seen. This is to be expected from the lower stability of the AUT compared to MUA so this result is at least commensurate with expectations. The fact that this trend is not seen again in the AUT75%MUA75% is unusual and even a very broad H-bond created peak is unlikely to account for all of it.

A more realistic possibility is that the Bessel function has been taken out slightly incorrectly. It is difficult to distinguish between the peak and the Bessel function due to the breadth of the peaks. That the spectrum does not rise at around 1500 cm^{-1} (Figure 2.14) is evidence supporting a miscorrected Bessel function. The program currently used for Bessel function correction is incapable of making a more accurate correction so the only improvement that could be made would be to obtain a more precise program. The simplest explanation for the discrepancy however is unfortunately the simple mixing up of samples, therefore the samples should be freshly produced in order to ascertain the source of error and correct it.

A very large new peak appears at around 1445 cm^{-1} in the mixed monolayers. Part of this peak could be attributed to the change in position and the broadening of the methylene scissors peak due to stretching for both MUA and AUT being included. The dramatic change in size compared to the 1263 cm^{-1} wagging peak cannot fully account for such a drastic change in width and in intensity. It is also possible it is attributable to the CO_2^- symmetric band, which could be expected to become greater in magnitude if more of the acids on the surface became CO_2^- instead of CO_2H. The fact that very little is seen of the CO_2^- - asymmetric peak, which is expected around 1400 cm^{-1} could change dramatically due to different hydrogen bonding stabilisation present in the mixed monolayer.

An alternative explanation for the broadening of the peak around 1445 cm^{-1} (Figure 2.13) could be that an amide is formed between the surface bound MUA and AUT giving a C-N stretching peak at 1408 cm^{-1}. The formation of this peak could also be attributable to the formation of SO moieties that have peaks at 1391 cm^{-1} and 1352 cm^{-1} and the molecule is bond to the surface through the NH_2 group. Though if the NH_2 were binding to the gold these peaks would be found in both the AUT and the mixed monolayers. A further possibility is that the peak could have some contribution from both of these phenomena; that the amide bond is not formed between surface bound moieties but is formed as a bilayer and the exposed sulfur forms SO moieties.

The formation of an amide is unlikely due to the magnitude of the CO_2H peaks that would not be seen in an amide; the CO_2^- peaks are all of a significant size, particularly the CO_2H peaks between 1710 cm^{-1} and 1760 cm^{-1}. Formation of an H-bonded amine to the surface is also unlikely due to the thorough washing with purified water. So in conclusion the peak is most likely a mixture of broadened methylene stretch and increased CO_2^- asymmetric stretch in the mixed monolayers. The broadening is probably the effect of the H-bonding.

2.5.6.2 Reacting Mixed Self-assembled Monolayers

2.5.6.2.1 Reaction of 11-Mercaptoundecanoic Acid Self-assembled Monolayers

The peak positions of the MUA SAM as shown in table 2.8 are changed by the introduction of the sterically bulky NHS group. This is probably due to the NHS groups forcing the hydrocarbon chains to perturb in order to give the NHS groups the maximum amount of space.

The peaks of the NHS ester seen in figure 2.15 are much the same as those seen by Frey & Corn [17] from their reaction of a MUA monolayer. This is to be expected as the method and the type of FTIR spectroscopy (PMIRRAS) used was the same. The absence of any change in peak size and shape is not unsurprising given the small changes in intensity of the peaks observed after the initial amine formation [17]. The lack of change in intensity of peaks around 1650 cm^{-1} (the C=O and NH amide stretches), can easily be accounted for by the differences in intensity seen in the spectra due to instrumental instabilities. The fact that there is also no change in the shape of the peak at 1740 cm^{-1} can also be attributed to instrumental problems as the noise level is large enough that such small changes in shape as those observed by Frey & Corn [17] would not be easily discernible.

2.5.6.2.2 Comparing N-Hydroxysuccinimide-terminated SAMs

The CH_2 asymmetric peak is located in the same position in both MUA and Ditbsu SAMs, this indicates that they have the same amount of liquid-like character, which makes it probable they have the same molecular density and the same degree of ordering. The NHS reacted MUA SAM has a higher frequency CH_2 asymmetric peak than the Ditbsu and the MUA SAMs. The positional change of this peak suggests that there is a change in the structure caused by the introduction of the bulky group, which is not necessary if the moiety is present during the self-assembly procedure. The explanation for this is either that the sulfur atoms space themselves at distances better suited to the introduction of the NHS moieties or that the chains are capable of assuming a different conformation, which is equally well ordered, based around the NHS group. The forces involved in the S-Au bond are strong, so changing the position of adsorption is unlikely unless there is a significant amount of force involved. The surface density of a Ditbsu SAM has been found to be only 75% of the surface density of an unsubstituted omega alkanethiol SAM [18], this suggests that there is an entirely different structure present.

Another piece of evidence that the Ditbsu SAM structure is different from the NHS reacted SAM structure is found in the 1851 cm^{-1} optimised spectra; the peak at around 1650 cm^{-1} (assigned to a C=O stretch by Frey & Corn [17]) is not present.

The absence of the peak at around 1650 cm^{-1} is also noted in another FTIR study of Ditbsu [19] so this is unlikely to be an anomaly of this experiment.

No reaction occurs when the Ditbsu monolayer is immersed in the ammonia solution (as evidenced by the fact that the spectra do not change at all (Figure 2.17), this could be attributed to two possible causes: The first is that the monolayer has already hydrolysed to a degree that it is no longer capable of reacting, the second is that the monolayer is so tightly packed that no molecule can gain access to the NHS to react.

The NHS moiety is readily hydrolysable in solution to form the carboxylic acid even at pH 7 [20]. It has been proven that it can be hydrolysed with NaOH on the surface in minutes [19]. However, this does not mean that it reacts easily; it has been found to take 20 mM ethylamine at pH 11 several hours to produce a methyl-terminated monolayer. Since the results show identical spectra it is most probable that it has not been hydrolysed. It could only have hydrolysed during the self-assembly process, in which case it would be expected to form a monolayer with more similarity to MUA than is evidenced here. It is therefore concluded that the monolayer is so well-packed that the NHS is unable to react.

The appearance of the wagging bands in Ditbsu SAM that are absent in the reacted MUA monolayer also suggests an increased degree of order in the Ditbsu SAM.

This suggests that the normal ordered CH_2 asymmetric peak for the Ditbsu may be at 2924 cm^{-1} as lower molecular density is expected for the Ditbsu.

That peak positions for MUA have been found at 2918 cm^{-1} indicate that MUA will probably be disordered when the peak position is at as high a frequency as 2924 cm^{-1}. It is possible that the MUA could have more than one structure and the CH_2 asymmetric peak position could just indicate the lower molecular density of an alternative structure rather than a less ordered one as has been concluded for the methyl-terminated thiols.

2.5.6.2.3 SPDP Reacted Self-assembled Monolayers

The trend of increasing liquid-like character with increasing AUT is to be expected as the degree of reacted RGDC possible increases (Table 2.8) and the extra strain caused in the chain by the attached group leads to increase in disorder observed. The MUA50%AUT50% does not follow this trend probably because an optimal degree of stabilisation due to the H-bonding is possible between the amide and the carboxylic acid.

For the RGDC presenting SAMS the wagging bands are indistinct and the CH_2 asymmetric band is at a relatively high frequency (Figure 2.19), this indicates that the SAM is probably disordered. One explanation is that the RGDC chains could have a

random coil structure on the surface rather than any kind of ordered structure and these become tangled with each other when more RGDC moieties are added to the surface resulting in increasing disorder. This is also evidenced by the increase in disorder with increase in chain number. The surface is unlikely to be completely covered with RGDC due to the steric interactions of peptides which have already reacted. The idea behind presenting low numbers of RGDC molecules on the surface was that they would be more accessible to cells.

The incomplete reaction of the SPDP moieties could mean two things, one that the RGDC groups adsorbed to the surface occlude the group and prevent it from reacting or the concentration/pH/ length of time of reaction was not sufficient to allow full reaction. The peak appears relatively larger for higher concentrations of AUT, which suggests that it is predominantly occlusion that is the problem but there is probably a small amount of incomplete reaction.

The amount of increase in the size of the amide peaks relative to the C=O stretch (Figure 2.19) indicates that the reaction proceeds proportionally to the amount of AUT available. This is a good indicator that the amount of RGDC presented on the surface is roughly proportional to the amount of AUT in the monolayer.

The presence of the anomalous C=O peaks in the amine could actually be NHS asymmetric carbonyl peaks. This would mean that the SPDP is either absorbed or

bound to the surface with the succinimidyl moiety available. As it is unlikely that it is chemisorbed due to intensive washing procedures it is concluded that it is bound. The most likely mechanism for this is that some amine moieties have bound to the surface as previously suggested and the SPDP has reacted with the sulfhydryl tail to form an NHS presenting part. This idea is supported by the presence of peaks at 1380 cm-1 (Figure 2.19) indicating the symmetric C-N-C stretch. This being true would also introduce more disorder and heterogeneity into the monolayer.

2.5.7 C2 Self-assembled Monolayers

The finding of the IR vibrational stretching CH_2 asymmetric peak at 2918cm^{-1} by Kawasaki & Nagayama [21] which matched a spike in the FTIR spectra found in this study gave the idea that possibly there is more than one structure and both are shown in this IR peak. This sort of determination is not possible in molecules with longer carbon chains because they have more than one CH_2 moiety present per molecule.

The consideration that the C2 molecules have 2 bands gives more similarity to the non-methyl terminated SAMs. This is to be expected from the point of view that MEA, MAA and Meth all have structures that allow H-bonding, which gives rigidity and stability to the structure. This is not expected due to the fact that both the MEA and the Meth will have 2 CH_2 moieties. The result, however, may still be valid as there are two different structures present in Meth [12]. It should be borne in mind

that the presence of these peaks is not above the noise level and their similar positioning may be circumstantial. More work would need to be done on reducing the noise level before any concrete assertions could be made.

The Meth SAM has peaks at 1730 cm^{-1} and 1535 cm^{-1} (Figure 2.21) that cannot be identified as belonging to a mercaptoalcohol SAM. The origin of these peaks is though to be from the oxidation of the Meth to MAA, which would explain the similarities between the two spectra. This explanation was suggested by an electrochemical study [22] which found the Meth spontaneously oxidised to MAA, and the data presented here fits that explanation. Whether the oxidation is complete or not, cannot be ascertained without further work. Experiments optimised for higher regions would need to be performed to confirm the presence or absence of the OH peak around 3300 cm^{-1}.

If the oxidation of the OH moiety to COOH is complete in the Meth SAM then perhaps this could be used as a method of forming more ordered MAA SAMs. The acyclic dimers, which are thought to be the main cause of disorder, do not seem to have formed in the Meth SAM. This suggests that the Meth SAM is not the same as the MAA SAM, during the assembly process. This could be due to residual OH groups or due to oxidation having occurred after assembly. The possibility of oxidation after assembly is unlikely due to the fact that the SAMs are stored under vacuum until use. This suggests that there are still some residual OH groups helping

prevent acyclic assembly. To form ordered MAA SAMs it should be possible to self-assemble Meth and then oxidise it.

2.6 Conclusions

The experiments in this chapter are not conclusive enough in themselves to draw very firm conclusions. It is apparent that there are significant differences in the chemistries and structures of the different thiols assembled on Au. Replicates of the experiments need to be performed to determine if any of the effects seen in the spectra presented here are real and not artefacts of the measurement process.

The available literature on the characterisation of SAMs is inconclusive and occasionally contradictory. In order to establish a clear picture of how different SAMs assemble on the surface, and what structures they form, a study with a wider scope would need to be performed. The ideal study would use many more thiols and would also study the same surfaces by STM and AFM as well as PMIRRAS to find correlations between the actual structures seen and the spectral peaks produced.

This study has made some suggestions regarding the structure of the thiol SAMs, which may be used in the cell adhesion and growth experiments to partially explain differences, however further work on clarifying which structures exactly are present

in which proportions of the surfaces would be needed before these theories could become more than speculation.

2.7 References

1. Schreiber, F., *Structure and growth of self-assembling monolayers*. Progress in Surface Science, 2000. **65**(5-8): p. 151-256.
2. Porter, M.D., T.B. Bright, D.L. Allara, and C.E.D. Chidsey, *Spontaneously organized molecular assemblies .4. Structural characterization of normal-alkyl thiol monolayers on gold by optical ellipsometry, infrared-spectroscopy, and electrochemistry*. Journal of the American Chemical Society, 1987. **109**(12): p. 3559-3568.
3. Kluth, G.J., C. Carraro, and R. Maboudian, *Direct observation of sulfur dimers in alkanethiol self-assembled monolayers on Au (111)*. PHYSICAL REVIEW B, 1999. **59**(16): p. 10449-10452.
4. Choi, J.H., S.W. Han, S.J. Lee, and K. Kim, *Temperature-dependentFT-IR spectroscopy study of silver 1,9-nonanedithiolate*. Applied Spectroscopy, 2001. **55**(8): p. 1085-1091.
5. Uvdal, K. and T.P. Vikinge, *Chemisorption of the dipeptide Arg-Cys on a gold surface and the selectivity of g-protein adsorption*. Langmuir, 2001. **17**(6): p. 2008-2012.

6. Arnold, R., W. Azzam, A. Terfort, and C. Woll, *Preparation, modification, and crystallinity of aliphatic and aromatic carboxylic acid terminated self-assembled monolayers*. Langmuir, 2002. **18**(10): p. 3980-3992.

7. Wallwork, M.L., D.A. Smith, J. Zhang, J. Kirkham, and C. Robinson, *Complex chemical force titration behavior of amine-terminated self-assembled monolayers*. Langmuir, 2001. **17**(4): p. 1126-1131.

8. Joo, S.W., S.W. Han, and K. Kim, *Adsorption characteristics of aliphatic dithiols on silver and gold revealed by ellipsometry and FT-IR spectroscopy*. Molecular Crystals and Liquid Crystals, 2001. **371**: p. 355-358.

9. Duwez, A.S., L.M. Yu, J. Riga, J. Delhalle, and J.J. Pireaux, *Vibrational structure and organization of various self- assembled alkanethiol monolayers: A HREELS study*. Langmuir, 2000. **16**(16): p. 6569-6576.

10. Ihs, A. and B. Liedberg, *Chemisorption of L-cysteine and 3-mercaptopropionic acid on gold and copper surfaces: An infrared reflection - absorption study*. Journal of Colloid and Interface Science, 1991. **144**(1): p. 283-292.

11. Laibinis, P.E., M.A. Fox, J.P. Folkers, and G.M. Whitesides, *Comparisons of self-assembled monolayers on silver and gold - mixed monolayers derived from $HS(CH_2)21x$ and $HS(CH_2)10y$ (x, y = CH_3, CH_2OH) have similar properties*. Langmuir, 1991. **7**(12): p. 3167-3173.

12. Shin, T., K.N. Kim, C.W. Lee, S.K. Shin, and H. Kang, *Self-assembled monolayer of L-cysteine on Au(111): Hydrogen exchange between*

zwitterionic L-cysteine and physisorbed water. Journal of Physical Chemistry B, 2003. **107**(42): p. 11674-11681.

13. Kawasaki, M., T. Sato, and T. Yoshimoto, *Controlled layering of two-dimensional j-aggregate of anionic cyanine dye on self-assembled cysteamine monolayer on Au(111)*. Langmuir, 2000. **16**(12): p. 5409 -5417.

14. Esplandiu, M.J., H. Hagenstrom, and D.M. Kolb, *Functionalized self-assembled alkanethiol monolayers on Au(111) electrodes: 1. Surface structure and electrochemistry*. Langmuir, 2001. **17**(3): p. 828-838.

15. Xiao, S.J., M. Textor, and N.D. Spencer, *Covalent attachment of cell-adhesive, (Arg-Gly-Asp)-containing peptides to titanium surfaces*. Langmuir, 1998. **14**: p. 5507-5516.

16. Xia, J., W. Wei, Y. Hu, H. Tao, and L. Wu, *A novel voltammetric method for the direct determination of copper in complex environmental samples*. Analytical Sciences, 2004. **20**: p. 1037-1041.

17. Schmitt, H., A. Badia, L. Dickinson, L. Reven, and R.B. Lennox, *The effect of terminal hydrogen bonding on the structure and dynamics of nanoparticle self-assembled monolayers (SAMs): An NMR dynamics study*. Advanced Materials, 1998. **10**(6): p. 475-480.

18. Frey, B.L. and R.M. Corn, *Covalent attachment and derivatization of poly(L-lysine) monolayers on gold surfaces as characterized by polarization-modulation FT-IR spectroscopy*. Analytical Chemistry, 1996. **68**(18): p. 3187-3193.

19. Wagner, P., M. Hegner, P. Kernen, F. Zaugg, and G. Semenza, *Covalent immobilization of native biomolecules onto Au(111) via n-hydroxysuccinimide ester functionalized self-assembled monolayers for scanning probe microscopy*. Biophysical Journal, 1996. **70**(5): p. 2052-2066.

20. Schonherr, H., C.L. Feng, and A. Shovsky, *Interfacial reactions in confinement: Kinetics and temperature dependence of reactions in self-assembled monolayers compared to ultrathin polymer films*. Langmuir, 2003. **19**(26): p. 10843-10851.

21. Pierce, *Determine reactivity of NHS ester biotinylation and cross-linking reagents*. 2003, Pierce Biotechnology Inc.

22. Kawasaki, M. and H. Nagayama, *Observation of highly ordered 3 x 4 phase of ethanethiol self- assembled monolayer on Au(111)*. Chemistry Letters, 2001(9): p. 942-943.

23. Weisshaar, D.E., M.M. Walczak, and M.D. Porter, *Electrochemically induced transformations of monolayers formed by self-assembly of mercaptoethanol at gold*. Langmuir, 1993. **9**(1): p. 323-329.

Chapter 3

Cell Adhesion and Growth on Self-Assembled Monolayers of Alkanethiols

3.1 Introduction

The aim of this work is to determine if angstrom scale structure and chemistry of cell growth substrates have an effect on cellular adherence and growth. The cell growth substrates chosen for this investigation were self-assembled monolayers (SAMs) of thiols formed on gold (Au), as it is possible to control the chemistry while introducing variability of molecular scale structure.

In this study biologically active thiols and alkanethiols with different carbon chain lengths and functionalities were structurally well characterized (Chapter 2). In this chapter work on the cellular adherence and growth of baby hamster kidney (BHK) fibroblast and SF268 cell lines on these surfaces is presented.

The adherence of the cells to the surfaces can be assessed by measuring the number of cells on the surface before and after washing. One way of measuring the number of cells on the surface is to fluorescently label them and measure the fluorescence. A fluorescent compound that is relatively easy to introduce into cells is 2',7'-bis-(2-

carboxyethyl)-5-(and-6)-carboxyfluorescein acetoxymethyl ester (BCECF AM-ester). This compound is non-toxic, easy to use and can be used to produce quantitative results. For these reasons this reagent has been used to label cells in the experiments presented in this chapter.

For measuring cell proliferation alamarBlue was thought to be a suitable indicator compound; firstly it is a fluorescent indicator, this means that the opaque surfaces present no problem to a plate reader. Secondly this indicator is non-cytotoxic and therefore cell growth over time can be measured.

It should be noted that the alamarBlue could not have been used in place of the BCECF, as it does not localize in the cell.

3.2 Materials

All chemicals were obtained from Sigma (Poole, Dorset, UK) unless otherwise stated. The alamarBlue was obtained from Biosource (Nivelles, Belgium) and the 2', 7'-bis-(2-carboxyethyl)-5-(and-6)-carboxyfluorescein acetoxymethyl ester (BCECF AM-ester) was obtained from Insight Biotechnology Ltd. (Wembley, Middlesex, U.K.)

The BHK and SF268 cells were cell lines obtained from Integrin Advanced Biosystems Ltd. These cell lines were stored in liquid nitrogen.

3.3 Methods

3.3.1 Initial Culture of Cell Lines

The cell lines BHK and SF268 were grown from frozen stock. Two vials of cells were thawed in a water bath at 37°C and the cells were immediately added to 25 cm^2 (surface area) tissue culture flasks (Corning), one vial per flask. To each flask 9 ml of RPMI-1640 medium with L-glutamine and sodium bicarbonate and 1 ml of Foetal Bovine Serum (FBS) were added. The cell lines were maintained at 37°C in a humidified 95% air / 5% CO_2 incubator. The cells were transferred to 75 cm^2 tissue culture flasks (Corning) when the cell monolayers were confluent. This was done by adding a solution of 0.05% Trypsin / EDTA to each flask and incubating the flask at 37°C for 5 minutes. After this time the flask was tapped until all cells were observed to be free from the flask. This cell suspension was centrifuged at 250 g for 5 minutes. The pellet was resuspended in 1 ml of RPMI-1640 and transferred to the new flask, which subsequently had 18 ml of RPMI-1640 and 2ml of FBS added.

3.3.2 Sterilization of Surfaces

The alkanethiol presenting surfaces were prepared as described previously and were sterilized by dousing with absolute ethanol (Bamford Laboratories, Rochdale U.K.) from a wash bottle in a class 2 cabinet. After the surface and the plastic tweezers used to hold it had been thoroughly washed, the surface was placed on an ethanol sterilized piece of tin foil in the class 2 cabinet. After the placing of all the surfaces, a class 2 cabinet was closed and the surfaces left to dry overnight. The next morning the surfaces were placed in well-labelled, sterile 6 well plates (Greiner Bio-One) with one slide per well. The lidded plates were then removed from the class 2 cabinet and were stored for a maximum of 2 weeks before use.

3.3.3 BCECF Experiment

Unless otherwise detailed the BCECF experiment was performed as specified here. The cells were pelleted as described above and resuspended in ~2.5 ml of Hanks' buffered salt solution per confluent 75 cm^2 flask of cells. Unless otherwise mentioned the cells used were BHK cells. The cells were counted using a Neubauer haemocytometer and the concentration of cells was diluted to 10^7 cells / ml with Hanks' buffered salt solution.

The BCECF-AM ester was dissolved in 1 ml of dry, sterile DMSO per mg of compound. The DMSO was warmed to 37°C prior to dissolution to ensure full solubilization of the compound. The stock solution was stored at -20°C. The stock solution was added to an equal amount of solubilizing agent, Pluronic F-127. This additive was also dissolved in dry, sterile DMSO (warmed to 37°C) at 20% (w/v). This solution was then diluted with Hanks' buffered salt solution to produce a working solution that was a 500-fold dilution of the BCECF stock solution.

The working solution and the diluted cell suspension were mixed together, and left to incubate for 30 minutes at 37°C. The cell suspension was then centrifuged at 250 g for 5 minutes. The pellet was resuspended in 25 ml of RPMI-1640 and centrifuged again as before. This pellet was then resuspended in RPMI-1640 medium with 10% FBS to give an approximate cell concentration of $8.3 * 10^3$ cells / ml.

Labelled 6-well plates containing the alkanethiol presenting surfaces as described earlier (Chapter 2) were prepared by the addition of 1.5 ml RPMI-1640, and 200 μl of FBS to each well. The fluorescence of the plates was measured with excitation and emission wavelengths of 485 nm and 530 nm respectively. 300 μl of the BCECF labelled cell suspension (concentration $8.3 * 10^3$ cells / ml) was then added to each of the wells except the negative control wells. After the addition the plates were measured for fluorescence again at the same excitation and emission wavelengths as before. The plates were then placed in an incubator set at 37 °C with humidified

atmosphere of 95% air / 5% CO_2. The cells were left to incubate for 2 hours before the plates were measured for fluorescence once again at the same excitation and emission wavelengths. After measurement, the surfaces were removed from the plates with plastic tweezers and immersed in RPMI-1640 medium to wash off any non-adherent cells. Once washed, the surfaces were placed in wells containing 1.5 ml of RPMI 1640 and 200 μl of FBS. The fluorescence was measured in the same manner as previously.

3.3.4 Modified Alkanethiols

SAMs of 11-Mercaptoundecanoic acid (MUA) or 11-Mercaptoundecylamine hydrochloride (AUT) were prepared as described previously (Chapter 2). Monolayers were also prepared from solutions composed of a mixture of MUA or AUT. The surfaces produced from these mixed solutions are referred to by the % molar composition of each constituent in the solution, which is not identical to the actual composition of the surface. The difference is discussed in Chapter 2.

3.3.4.1 NHS Modified Alkanethiol SAMs

The slides were modified with NHS and reacted with RGDC in the same manner as in Chapter 2. They were subsequently sterilised by the method mentioned above.

3.3.4.2 SPDP Modified Alkanethiol SAMs

The slides were modified with SPDP and reacted with RGDC in the same manner as in Chapter 2. They were subsequently sterilised by the method mentioned above.

3.3.5 Other Thiols

In this experiment biological compounds containing thiol groups were used to form SAMs. These were prepared as previously described.

3.3.6 AlamarBlue Experiment

Directly after completion of the BCECF experiment the surfaces with adhered cells were washed in RPMI-1640 medium and were transferred to 6 well plates containing 1.5 ml RPMI-1640 and 200 μl FBS. 150 μl of alamarBlue solution was then added to the plates and the fluorescence at time 0 was measured by plate reader set at 530 nm excitation and 590 nm emission. The plates were then read at least four times within the first 24 hours.

3.4 Results

3.4.1 BCECF

The results for the BCECF experiments are presented in numerical terms as % adhesion. This value is the mean of the fluorescence value of each surface after washing presented as a percentage of the fluorescence value found for the same surface directly before washing.

$$\%\ \text{Adhesion} = \text{Mean}\left(\left(\frac{\text{Fluorescence After Washing}}{\text{Fluorescence After Incubation Before Washing}}\right)*100\right)$$

3.4.1.1 Methyl-terminated Thiol SAMs

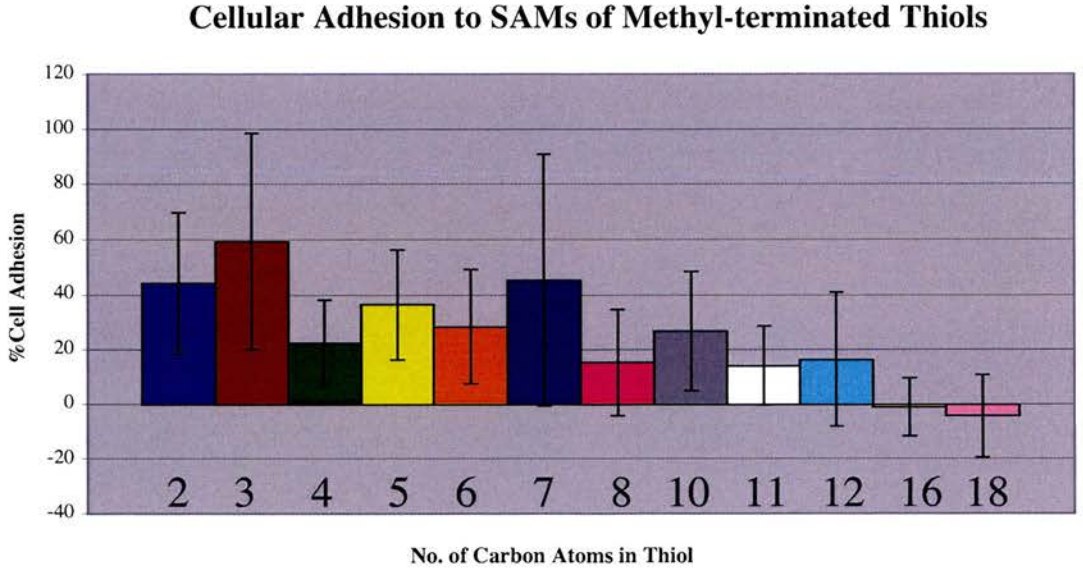

Figure 3.1 The percentage of BHK cells adhering to each type of methyl-presenting surface using BCECF as a fluorescent indicator of cell number.

3.4.1.1.1 Odd-Even Effect

The first trend that can be seen in the BCECF results (Figure 3.1) is that there is a difference in the level of cellular adhesion to short chain thiol SAMs (C2-C8) with an odd number of carbons and those with an even number of carbons. This means that the surfaces presenting short, methyl-terminated alkanethiol SAMs with an even number of carbons had fewer cells adhering to them through the washing process than surfaces presenting short, methyl-terminated alkanethiol SAMs with an odd number of carbons. Each odd carbon chain length SAM is only compared to those even carbon chain length SAMs on either side of it so that the effect of chain length is not confused with the odd-even effect. This effect is noticeable for methyl-terminated alkanethiol SAMs up to a chain length of 8 (Figure 3.1). Although this effect is seen from the values for % cell adhesion, the result is not statistically significant.

3.4.1.1.2 Length Effect

There is a generally downward trend with increasing chain length seen in Figure 3.1, though this can only be seen clearly when comparing the shortest thiol SAMs (C2-C5) to the longest thiol SAMs (C16 and C18). The SAMs in between these two regions show no clear results. The only statistically significant results that can be

seen from the data are that the C16 and C18 thiol SAMs have a lower degree of cellular adhesion than the C2, C3 and C5 thiol SAMs.

3.4.1.2 Dithiol SAMs

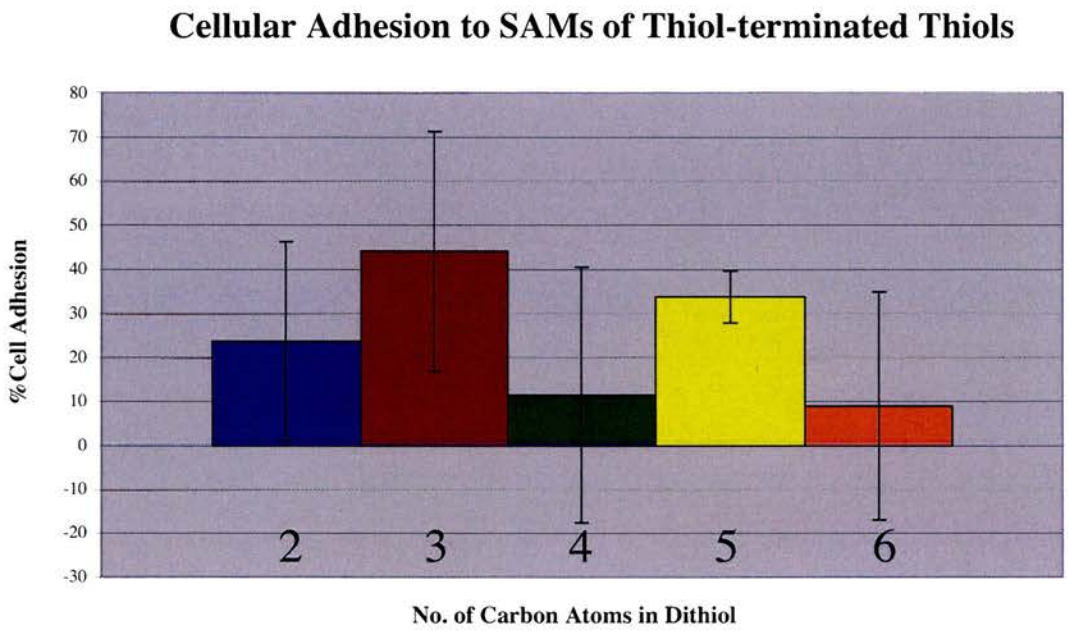

Figure 3.2 The percentage of BHK cells adhering to each type of thiol-presenting SAM surface using BCECF as a fluorescent indicator of cell number

There is a pronounced difference between the mean cellular adhesion to dithiol SAMs with odd carbon chain lengths and those with even carbon chain lengths (Figure 3.2). This suggests a possible odd-even effect for the thiols although this result is not statistically significant. There is a minor decline in the cellular adhesion when comparing odd chain length SAMs to each other and when comparing even chain length SAMs to each other. This is unlikely to be a real effect due to the magnitude of the errors involved.

3.4.1.3 Amine- and Carboxylic Acid-terminated SAMs

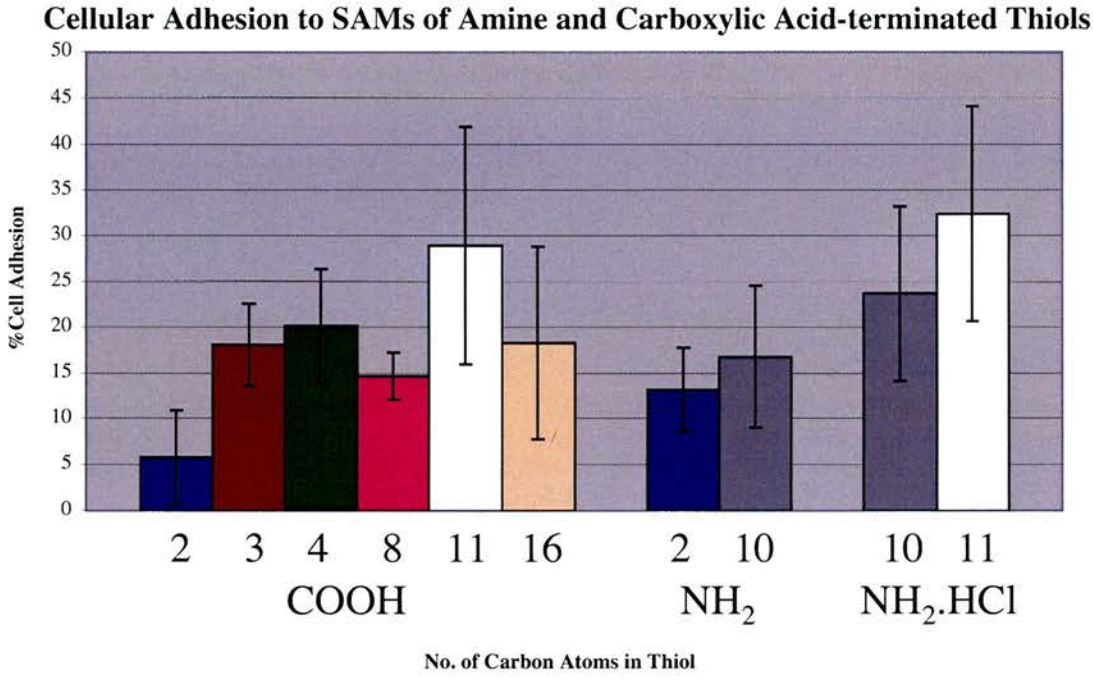

Figure 3.3 The percentage of BHK cells adhering to each type of amine- and carboxylic acid-presenting surface using BCECF as a fluorescent indicator of cell number.

No overall trend can be seen for the amount of adhesion to the carboxylic acid-terminated thiol SAMs (Figure 3.3). This is partly because so many were unavailable for experimentation that it would require a lot of extrapolation to fill in the blanks. One trend that can be observed in Figure 3.3 is the increase in the cellular adhesion between the SAMs of the 2C and the 4C mercaptoalkanoic acid SAMs. This is only statistically significant for the difference between the 2C and the other carboxylic acid-terminated SAMs. The only carboxylic acid-terminated SAM that has a reasonable statistical probability of having the same or less cellular

adhesion than the 2C is the 16C SAM 16-Mercaptohexadecanoic acid (MHDA). The carboxylic acid-terminated surface that has the highest mean cellular adhesion is the 11C SAM MUA.

In the amine presenting surfaces, there is more cellular adhesion to SAMs of the 10C hydrochloride salt of the amine, than the amine and the longer surfaces have more adherent cells than the shorter. Neither of these observations are statistically significant.

3.4.1.4 Comparison of Different Functionalities

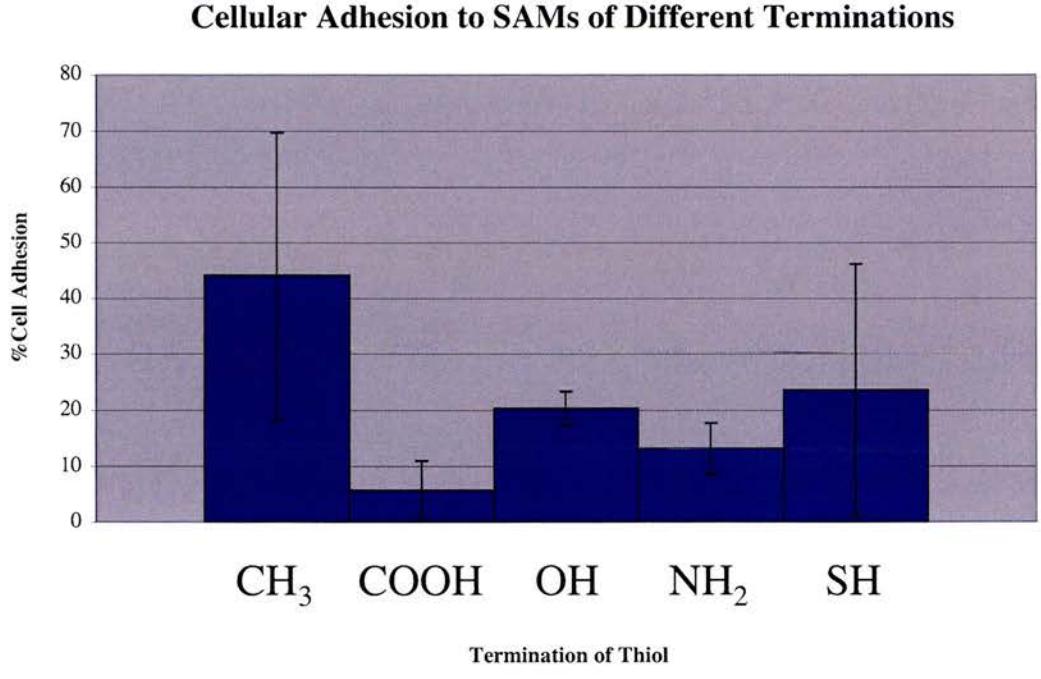

Figure 3.4 The percentage of BHK cells adhering to each type of 2 carbon SAM surface using BCECF as a fluorescent indicator of cell number.

For this comparison a 2C chain alkanethiol SAMs were used, as the most diverse range of functionalities are available commercially with this length of carbon chain. The greatest amount of cellular adhesion occurs using the methyl-terminated thiol (Figure 3.4). Although this is not statistically significant for all 2C SAMs, more cells adhere to the methyl-terminated SAM than the amine or carboxylic acid-terminated SAMs. The thiol-presenting surface has the next highest value of cellular adhesion, however, there is a high degree of uncertainty regarding this value. The hydroxyl-terminated surface has the next highest cellular adhesion value followed by the amine- terminated surface. The carboxylic acid-terminated surface has the lowest level of cellular adhesion for the 2C SAMs.

3.4.1.5 Alkanethiol SAMs Modified by Reaction

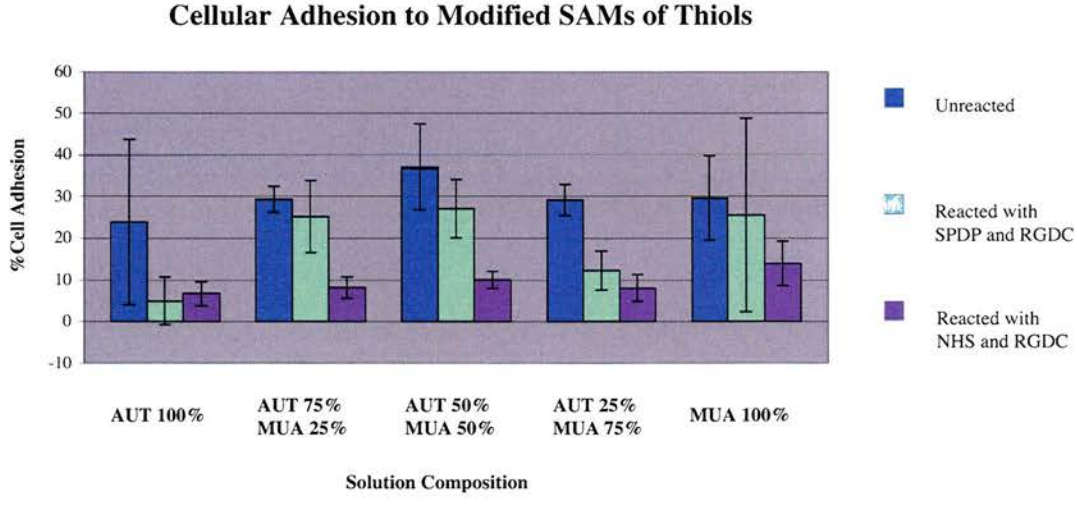

Figure 3.5 The percentage of BHK cells adhering to each type of modified SAM surface using BCECF as a fluorescent indicator of cell number. The composition indicated is the % molar composition of each constituent in the thiol solution use to form the SAMs.

As highlighted previously, the amounts in solution do not directly correspond to proportion of thiols on the surface. The general trend seen in Figure 3.5 is that amount of cellular adhesion is greatest to the unreacted SAMs, followed by the SPDP reacted SAMs then the NHS reacted SAMs. There is one exception; that there is more cellular adhesion to the NHS reacted AUT SAM is higher than that for the SPDP reacted SAM.

For all series the AUT reacted SAM surface has the lowest rate of cell adhesion. The SAM with the most adherent cells is the unreacted AUT50%MUA50% SAM. All the series (unreacted, SPDP reacted and NHS reacted) show a similar pattern with increasing adhesion to AUT50%MUA50% then a fall in adhesion at AUT25%MUA75% and a rise at MUA 100%. The SPDP and RGDC reacted AUT50%MUA50% surface is the most cell adherent SPDP reacted surface and as such it is the RGDC presenting surface with the most cellular adhesion. The most cell adherent NHS reacted surface is the MUA 100% surface reacted with NHS and RGDC.

The differences between the series are statistically significant between the unreacted and NHS reacted surfaces. Only some SPDP reacted surfaces are significantly different from the unreacted surfaces. The differences between different surfaces in the same series are generally not statistically significant.

3.4.1.6 Biological Thiol SAMs

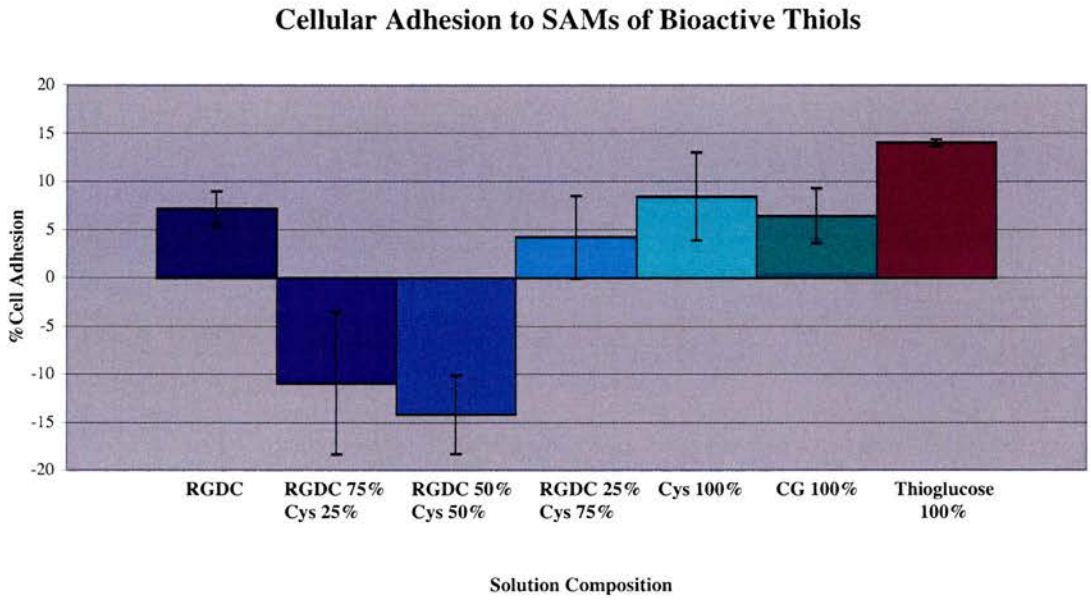

Figure 3.6 The percentage of BHK cells adhering to each type of bioactive-terminated SAM surface using BCECF as a fluorescent indicator of cell number.

It has been shown in several papers that amino acids, peptides and even thiol containing sugars can be attached to Au as SAMs [1]. How ordered these monolayers are is debatable, however, their attachment to Au has been confirmed by IR spectroscopy. They are presented here to show the difference between the bioactive thiols self-assembled on the surface and the reacted with alkanethiol SAMs.

The differences between the cellular adhesion to the RGDC, CG and the cysteine (Cys) SAMs are fairly minor as can be seen in Figure 3.6. The amount of cellular adhesion is greatest on the thioglucose SAMs. Mixed RGDC and Cys SAM

combinations have very low values of cellular adherence. The mixed RGDC75%Cys25% and RGDC50%Cys50% monolayers have significantly less cell adhesion and growth than the RGDC or the Cys alone (Figure 3.6). There is no significant difference between the single molecule SAMs and the RGDC25%Cys75% SAM.

3.4.1.7 Comparison of Two Cell Types

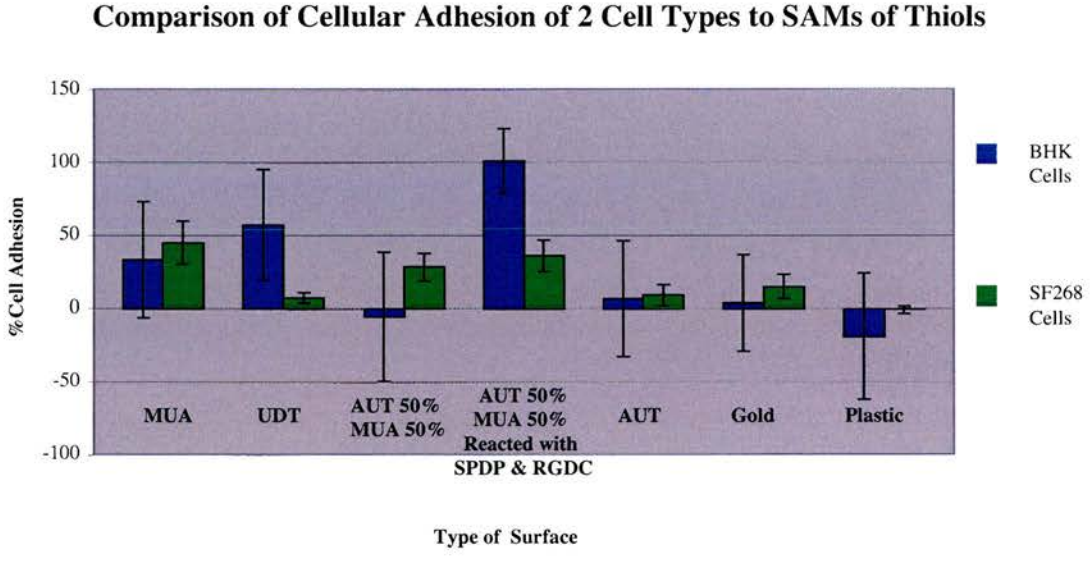

Figure 3.7 The percentage of BHK cells adhering to each type of surface using BCECF as a fluorescent indicator of cell number.

From the SAMs modified by reaction with RGDC it was determined that the RGDC attached to AUT50%MUA50% via SPDP was the most adherent RGDC presenting surface. It was therefore used as the most promising RGDC presenting cell growth substrate in this experiment. The amount of cellular adhesion is greatest to this surface for the BHK cells. The SF268 cells appear to exhibit less variability in the

amount of adhesion to the available surfaces than the BHK cells. There is not much correlation between the adhesion of the BHK and SF268 cells to the surfaces. They both adhere very little to the Au and AUT surfaces and have comparable amounts of adhesion to MUA SAMs.

The SF268 cells are most adherent to MUA SAMs. In general all the MUA containing SAM surfaces appear to be favourable for cellular adhesion of SF268 cells. These results are statistically significant when compared to most other surfaces. The surfaces with the least adhesion by SF268 cells are the plastic and the UDT (1-undecanethiol) surfaces; this is significant when compared to all other surfaces except the AUT SAMs.

3.4.2 alamarBlue

The results from this assay were not as consistent as possible due to differing cell numbers. This means that the results are no directly comparable between experiments. The initial cell numbers are more a measure of the adhesion of cells to the surface as at this point the surface has been washed twice in RPMI-1640 media. The data are presented in the form of rate of cell growth from the linear part of the growth curve; the gradient of relative fluorescence against time (minutes). The gradient is taken from the linear part of the growth curve by the least-squares method from at least 5 data points by Microsoft Excel.

3.4.2.1 Methyl-terminated Thiol SAMs

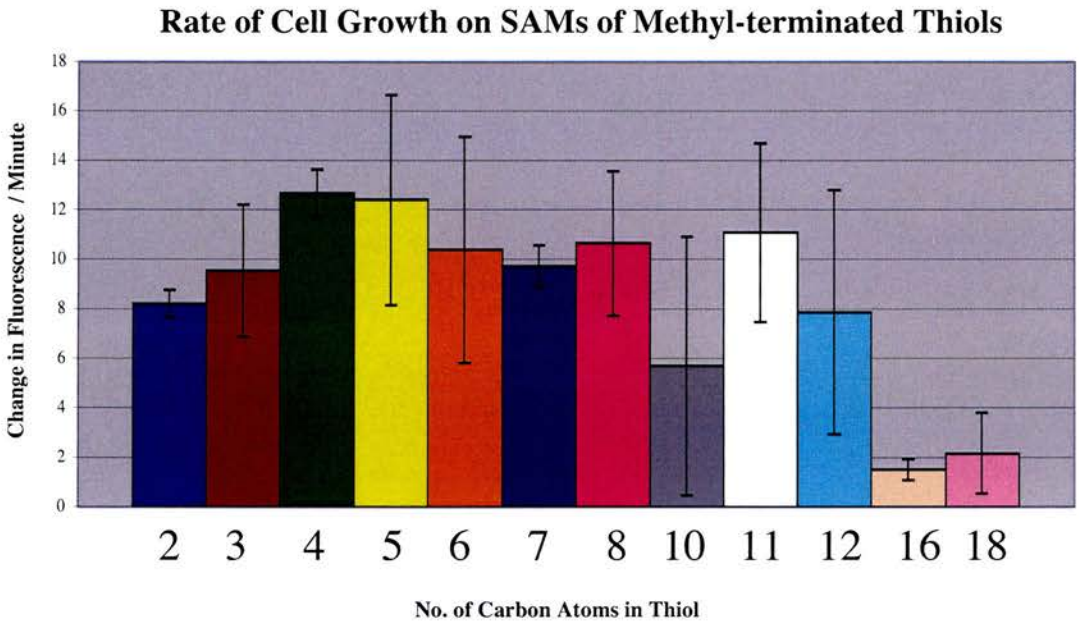

Figure 3.8 The rate of cell growth on SAMs of methyl-terminated alkanethiols measured by the change in fluorescence using alamarBlue as an indicator.

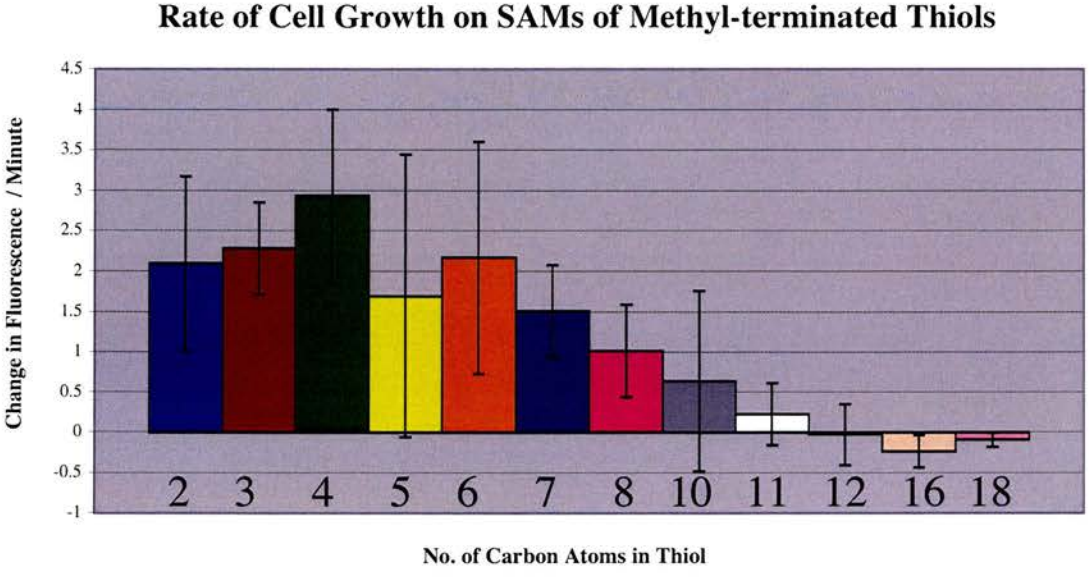

Figure 3.9 The rate of cell growth on SAMs of methyl-terminated alkanethiols measured by the change in fluorescence using alamarBlue as an indicator.

The results shown in Figures 3.8 and 3.9 are duplicates of the same experiment investigating cell growth on methyl-terminated thiols. There is a downward trend in cell growth with increasing thiol chain length to C16 (1-Hexadecanethiol (HDT) and C18 (1-Octadecanethiol (ODT)). This trend has a reasonable level of statistical significance and matches that seen in the BCECF experiment (Figure 3.1). There is no odd-even effect seen for the rate of cell growth. The two experiments (Figures 3.8 & 3.9) do not exhibit any other correlations with each other and the errors are often large compared to the magnitude of the rates of cell growth.

3.4.2.2 Dithiol SAMs

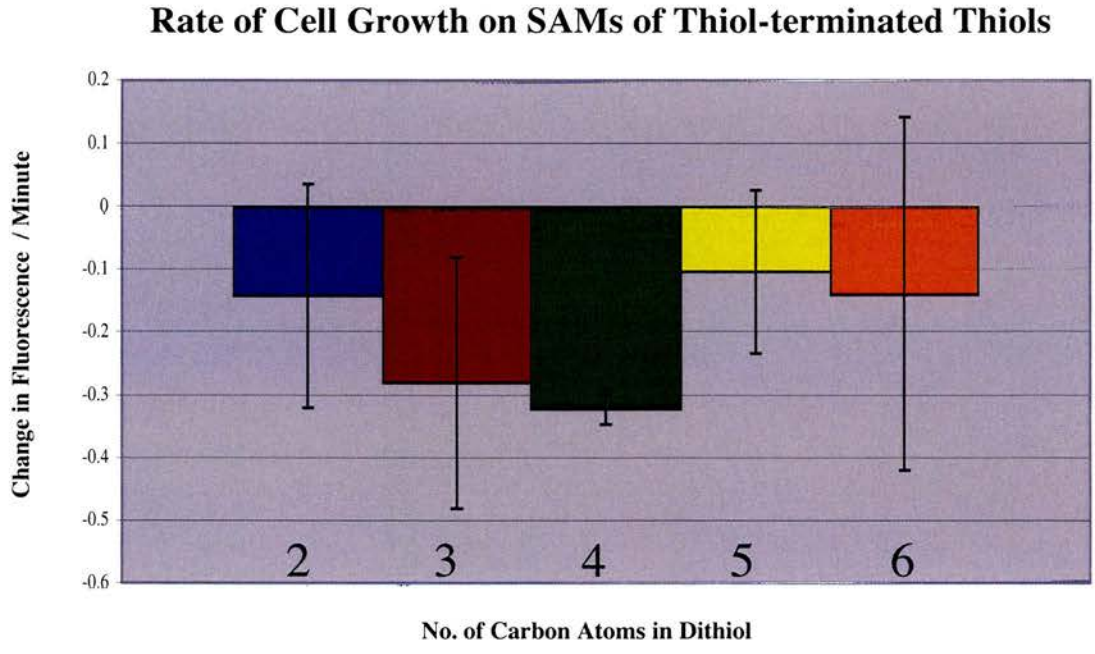

Figure 3.10 The rate of cell growth on SAMs of thiol-terminated alkanethiols measured by the change in fluorescence using alamarBlue as an indicator.

The first experiment on cell growth on dithiols indicated that there was negative cell growth that means that the medium with no cells added developed more fluorescence than the thiol surfaces with cells attached. Cell growth was seen in the second experiment using dithiols. It shows a non-statistically significant odd-even effect up to C5 (1,5-Pentanedithiol). This is the only obvious theme found in the results cell growth on the dithiol SAMs, statistically significant or otherwise.

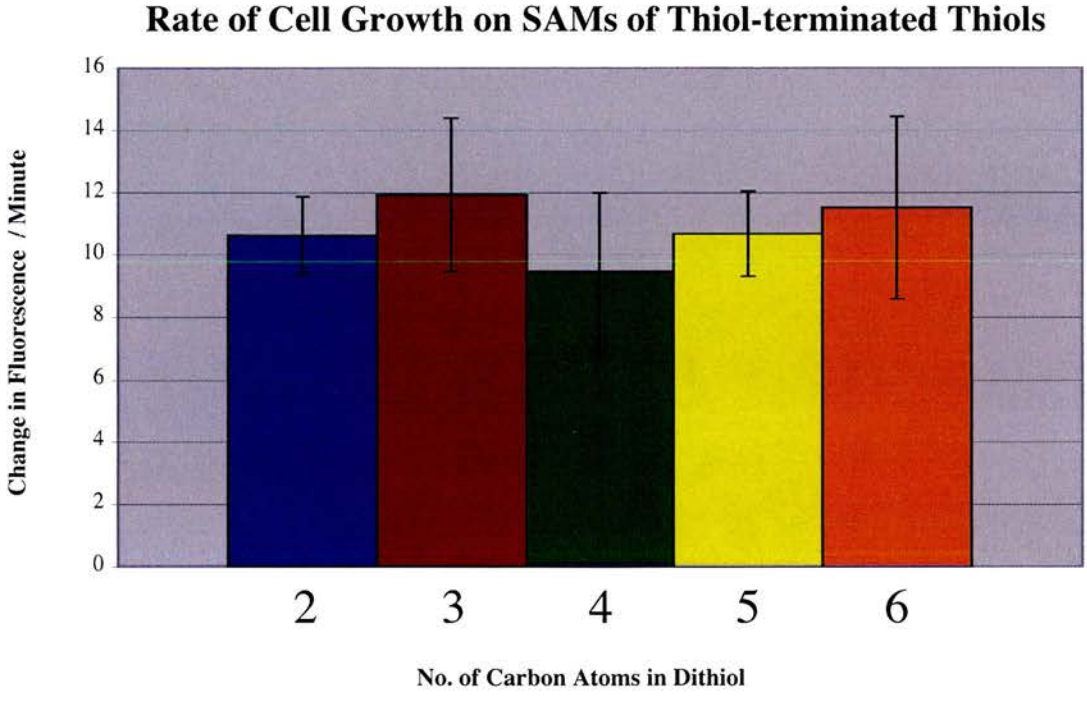

Figure 3.11 The rate of cell growth on SAMs of thiol-terminated alkanethiols measured by the change in fluorescence using alamarBlue as an indicator.

3.4.2.3 Hydroxy-, Carboxylic Acid- and Amine-terminated SAMs

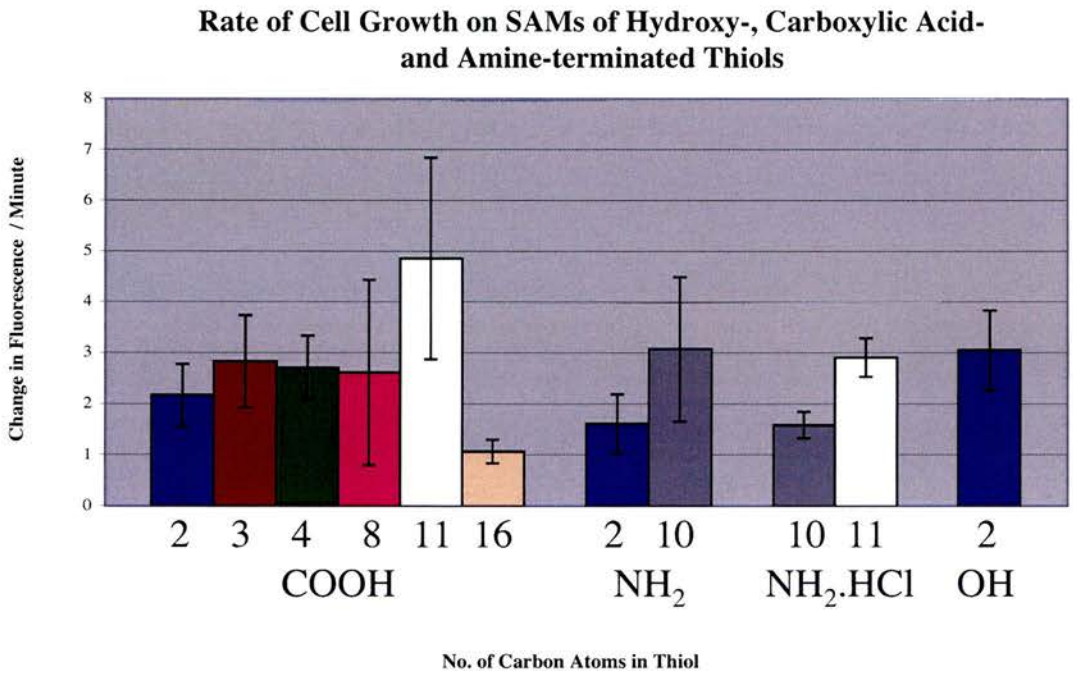

Figure 3.12 The rate of cell growth on SAMs of hydroxy-, carboxylic acid-, and amine-terminated alkanethiols measured by the change in fluorescence using alamarBlue as an indicator.

There is not much difference in the rates of cell growth on Mercaptoalkanoic acids with a chain length of 8 and below (Figure 3.12); the 2C thiol (2-Mercaptoethanoic acid (MAA)) does exhibit a lower rate of cell growth but this is not statistically significant. The highest rate of cell growth is seen on the 11C mercaptoalkanoic acid SAM (MUA) and the lowest rate of cell growth is seen on the 16C SAM (MHDA). The SAM with the highest rate of cell growth (MUA) is also the SAM with the largest amount of cell adhesion. When comparing the 10C amines it can be seen that the hydrochloride amine SAMs support a lower rate of growth than the amine surface

(Figure 3.12). The 11C mercaptoalkylamine hydrochloride (AUT.HCl) has a higher rate of cell growth than the 10C mercaptoalkylamine hydrochloride (ADT.HCl). The hydroxyl-terminated surface (2-Mercaptoethanol (Meth)) is the 2C surface with the highest rate cell growth (Figure 3.12), the amine-terminated SAM (MEA) is the 2C surface that has the lowest rate of cell growth.

3.4.2.4 Alkanethiol SAMs Modified by Reaction

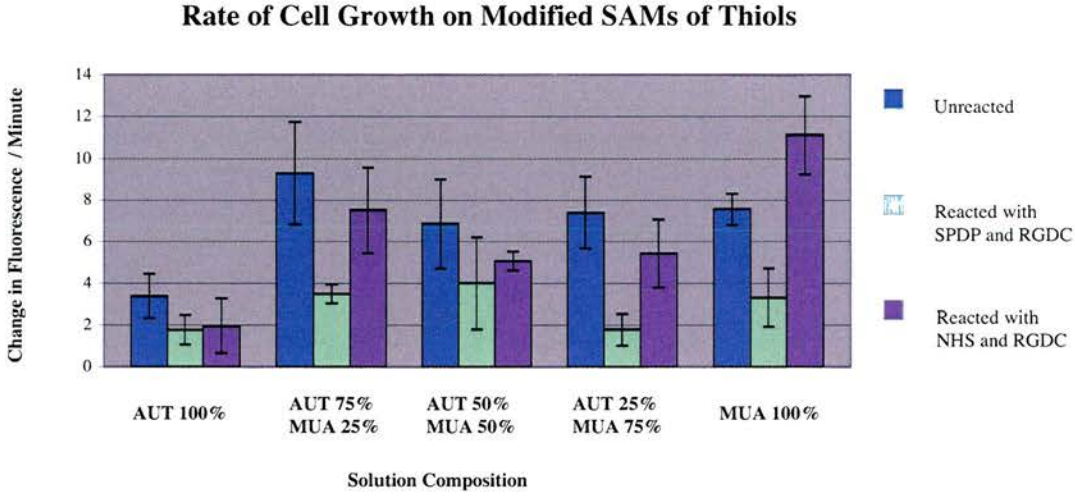

Figure 3.13 The rate of cell growth on modified SAMs of alkanethiols measured by the change in fluorescence using alamarBlue as an indicator. The composition indicated is the % molar composition of each constituent in the thiol solution use to form the SAMs.

BHK cells have the highest rate of growth on unreacted thiols (Figure 3.13). The overall highest growth rate is by the MUA 100% NHS reacted SAMs with RGDC attached. For all series the AUT reacted SAM surface has the lowest rate of cell growth. This is statistically significant for all but the SPDP reacted SAM. The NHS and unreacted SAMs are not significantly different from each other, however they

are statistically different from the SPDP reacted series for most surfaces. The SAMs show different trends for cell growth than for their adhesion. The NHS reacted SAMs have a higher rate of cell growth than the SPDP reacted SAMs, whereas the SPDP reacted SAMs have a higher rate of cellular adhesion than the NHS-reacted SAMs.

3.4.2.5 Biological Thiol SAMs

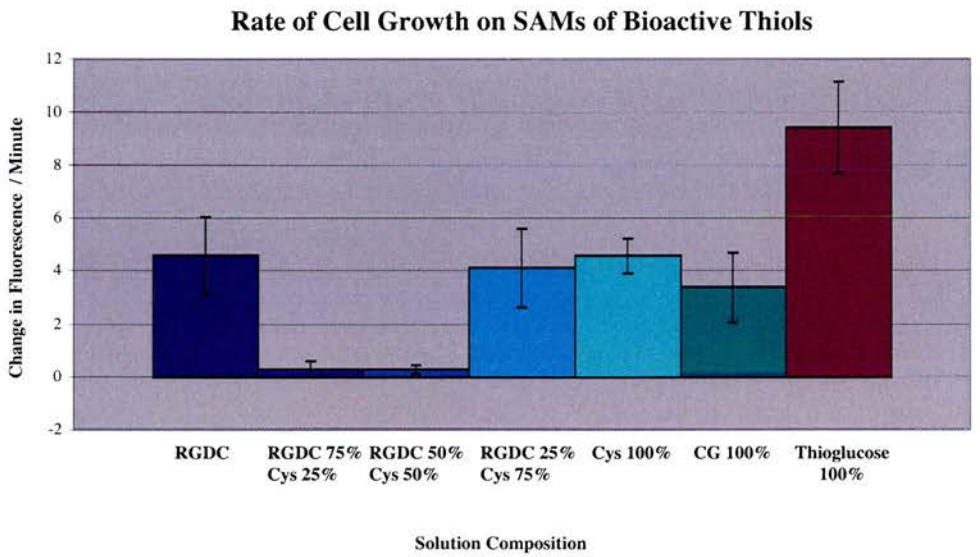

Figure 3.14 The rate of cell growth on SAMs of bioactive thiols measured by the change in fluorescence using alamarBlue as an indicator.

The alamarBlue growth data (Figure 3.14) shows much the same trends as the adhesion data. The RGDC, RGDC25%Cys50%, CG and Cys SAMs are roughly equivalent to each other with RGDC50%Cys50% and RGDC50%Cys50% showing virtually no cellular growth. The thioglucose is the bioactive SAM which has the highest level of cell growth.

3.4.2.6 SF268 cells

The results (Figure 3.15) show that the SF268 cells have only slightly different preferences for surfaces for adhesion and growth. The UDT and Plastic surfaces are those with the least cellular adhesion and the least growth. The MUA surface has the most cell growth though this is not significantly different from the RGDC and SPDP reacted AUT50%MUA50% SAM and the AUT SAM. Apart from the AUT having very little cellular adhesion and one of the highest rates of cell growth there is little change between the cell adhesion data and the cell growth data.

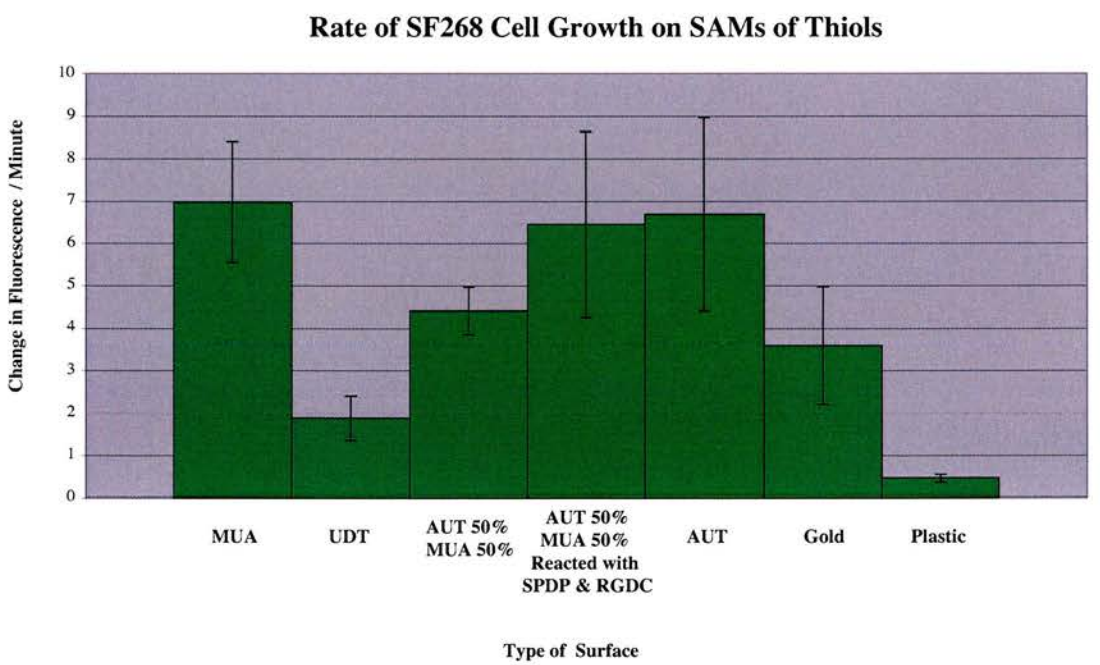

Figure 3.15 The rate of cell growth of SF268 cells on surfaces measured by the change in fluorescence using alamarBlue as an indicator.

3.5 Discussion

3.5.1 General

From the variety of results produced there appears to be a relationship between the type of alkanethiol SAM used and the level of cell adhesion and growth on the surfaces. Unfortunately these results are often not statistically significant and therefore no solid conclusions can be drawn (Figures 3.1-3.15).

Previous studies have explored the use of different thiols on the surfaces but this study also systematically explores the effect of chain length on cell growth. BHK cells were used because they were known to be particularly sensitive to the topography of the surface on a nanometre scale and therefore it was conjectured that they may be able to respond to very small changes in topography such as the packing of the alkanethiol molecules on the surface. Explanations are presented elucidating the way that differences in the chain length of the alkanethiol SAMs translate to differences in chemistry and structure.

In some of the samples the values of fluorescence reported were negative, this effect was found in both BCECF and alamarBlue experiments. This phenomenon could be an artefact of the fluorescence measurement process. For the BCECF experiment

there is time between the reading of the first and second fluorescence values during which there is a decay of fluorescence. Also the sample will not be in an identical position in its new well as the samples were moved to new plates after washing. This means that there may be local change in the number of cells that could affect the fluorescence reading. The solution to this problem would be to take an average of several readings of fluorescence but this also would cause significant fluorescence decay and as such introduce new inconsistencies.

For the alamarBlue experiment this could be due to the reduction of resorufin to dihydroresorufin causing in a decrease in fluorescence. This may occur if the cells stopped proliferating and died.

One vagary of the alamarBlue procedure that should be noted in the interpretation of the data, is that it is possible for the procedure to reach a level past which its accuracy declines, and this level can be reached before the experiment reaches a steady-state where the fluorescence value no longer increases. This occurs when the amount of reduction by the cells is such that they are also reversibly converting the resorufin to dihydroresorufin at a significant rate and this means that although it is possible to achieve higher fluorescence values, they are not reproducible.

The results of the BCECF experiment are comparable between experiments as they are expressed as percentages of cells adhered so any non-homogeneity in the solution

of cells will not affect the results. Theoretically the same proportion of cells should attach up to a point where the entire surface is covered (visual inspection confirmed this was not the case), though in practice this may not be true and this may account for the very large statistical errors between duplicate experiments using methyl and thiol-terminated SAMs.

3.5.2 Methyl-terminated Thiol SAMs

Of previous studies only one provides information on differences in cellular adherence and growth on different lengths of methyl-terminated SAMs. It was found that for fibroblasts grown on methyl-terminated SAMs, the number of adherent cells decreased with an increase in chain length [2]. In the same study it was found that the number of osteoblast cells attached to the surface was larger for propanethiol (PPT (C3)) than for octanethiol (OTT (C8)) or dodecanethiol (DDT (C12)), which were roughly equivalent. This illustrated two different growth profiles, and demonstrated that different cell types react to the same growth substrate in different ways.

3.5.2.1 Odd-Even Effect

The graph in Figure 3.1 shows a difference between the alkanethiol SAMs with carbon chains of odd length and those of even length that is not statistically significant. This effect appears only in the cell adhesion data for the short chain thiol SAMs (C2-C8) (Figure 3.1) and not the cell growth data (Figures 3.8 and 3.9).

Even chain length alkanethiol SAMs present a slightly different structure and a slightly different chemical surface from odd chain length alkanethiol SAMs [3] and this would be expected to have an effect on the cellular adherence. These differences would be small, if present, compared to the inter-experiment errors seen for the cell adhesion data on methyl-terminated thiols. As a result of the large errors no firm assertions can be made about the existence of this effect without further experimentation. This is the first time that such observations have been made from cell adhesion data though further investigation is needed to confirm them.

3.5.2.2 Length Effect

The results from both the cell adhesion (Figure 3.1) experiment and the cell growth experiment (Figures 3.8 & 3.9) show downward trends with increasing chain length for long chain alkanethiol SAMs. While not all the results are statistically

significant, both the cell adhesion data (Figure 3.1) and some cell growth data (Figure 3.8) show this trend. The second cell growth experiment (Figure 3.9) does not provide much useful information on this trend as the errors in the area concerned are very large. The graph (Figure 3.9) does show that the C16 and C18 SAMs have a statistically significant lower rate of cell growth than all other methyl-terminated SAMs except C10 where the errors are especially big. This trend agrees with the results obtained by Cooper *et al* [2] who found that the amount of cell growth of fibroblasts decreased with increasing chain length. They found that it decreased from PPT (C3) to OTT (C8) to DDT (C12). The result was also found in the experiments presented here for cellular adhesion (Figures 3.1) and cell growth (Figures 3.8 & 3.9). Although the trend involving PPT (C3) and OTT (C8) may still appear here for the cell adhesion data and part of the cell growth data it is difficult to make any assertions about the relationship between chain length and cell growth for alkanethiols SAMs due to the lack of statistically significant differences, especially between C5 (1-pentanethiol (PTT)) and C12 (DDT). The apparently random results in this area could be due to error or it could be due to the many different structures that methyl-terminated thiols of these lengths can form.

The rationale for the chain length effect is that structural changes in the alkanethiol SAMs that occur over chain length, cause slightly different topographical and chemical surfaces that cells have different affinities for. Porter *et al* [4] performed an IR study on SAMs of even chain length, methyl functionalized alkanethiols and

concluded that the short chain thiols were more disordered than those with a longer chain length. The region that has the biggest change is between 1-hexanethiol (HXT (C6)) and DDT (C12). Another study [5], which included the odd chains, found that the shorter chains (in this case C14 and below) packed with a slightly lower coverage. These studies concluded that the lower packing meant that the short chain alkanethiols were disordered. However subsequent studies have refuted this [3, 6], and it has been found that the films are actually in an all *trans* conformation from BTT (C4), and that changes are due to a phase transition of the alkanethiol [3], where the type of structure the alkanethiol SAM forms on the surface changes. Phase transitions have been proposed at C12 [7] and C10 [8]. A different structure for C10 has also been suggested [9]. Differing adsorption site positions have been proposed for short chain alkanethiols [10] and this concurs with evidence of well ordered structures in short chain thiols, such as in BTT (C4) [11] and ethanethiol (ETT) (C2) [6]. It is therefore possible that there are many different structures, which give different packing densities, and that these subtle phase changes between the structures lead to changes in the amount of cell adherence and growth.

3.5.3 Dithiol SAMs

The amount of cellular adhesion on thiol-terminated SAMs is significantly lower than that on methyl-terminated SAMs (Figures 3.1 and 3.2). These values are directly comparable as they come from the same experiments. The odd-even effect

that appears to be present in the cellular adhesion results of methyl-terminated SAMs (Figure 3.1), also appears to be present in the cellular adhesion results of the thiol-terminated SAMs (Figure 3.2). The BCECF cellular adhesion experiment (Figure 3.2) shows no obvious chain length effect for adhesion in the short chain length thiol-terminated SAMs, though this could be due to the apparent intensity of the odd-even effect. There is a very slight decrease in the amount of cellular adhesion when comparing all odd chain length and all even chain length dithiol SAMs that is not statistically significant and is unlikely to be a real effect due to the small size of the difference compared to the statistically calculated errors. The experiments investigating the rate of cellular growth show no conclusive evidence (Figures 3.10 & 3.11) for any trend as the values are very similar. For Figure 3.11 there is a slight odd-even effect visible for cell growth rates up to C5 (PTDT) but this is very unlikely to be significant and for Figure 3.10 all the rates of cell growth are negative. The reasons for the negative growth rates could be that the dithiol SAM surface has a minor effect which inhibits the reduction of resazurin or the cells could be dying and lysing to produce an oxidative environment. It could also be due to experimental error as the majority of the values have a statistical error that goes into positive amounts.

There has been some disagreement as to whether the thiol terminated SAMs, particularly those of short chain length, are upstanding or lying flat. These data could be interpreted to mean that the odd-even effect is caused by the differing

orientations of the upstanding chains, the difference in the sulfur orientation causing the same effect as difference in methyl termination. Alternatively, the thiols lying flat on the surface, could explain why no difference in chain length effects could be seen, if this is the case the odd-even effect could be caused by different packing on the surface by odd and even chain length SAMs.

3.5.4 Carboxylic Acid- and Amine-terminated SAMs

From a previous experiment [2] it was found that neither fibroblasts nor osteoblasts had any change in cell growth with chain length for carboxylic acid SAMs [2]. This is from the limited data of MPA (C3) and MUA (C11). This is neither confirmed nor excluded as a possibility by the data for the BHK cells presented in Figures 3.3 and 3.12.

The data on cellular adherence (Figure 3.3) suggests that there may be a chain length dependant difference between the first three mercaptoalkanoic acids (C2-C4) investigated. This is not entirely supported by the data, as the C2 (MAA) is the only significantly different SAM, however it could indicate that there is some chain length dependent adhesion effect for very short carboxylic acid-terminated SAMs where the head group and the carboxylic acid group would be the major determinants of structure.

The carboxylic acid group is thought to have a large effect on the structure of the SAM. The head group (sulfur)-substrate (Au) interaction is also known to have a big effect on the orientation of the alkanethiol molecules in the SAM, which is less significant with increasing chain length as van-der waals interactions become more important.

The preferred positioning of the head group could adversely affect the preferred positioning of the carboxylic acid group. This could be detrimental to the hydrophilicity of the SAM and this would affect protein deposition from the media and the cells and hence affect cellular adherence. It should be made clear that even this limited effect only appears to affect adhesion and not cell growth.

The cell growth data agrees with the assertion by Cooper *et al* [2], that there is no chain length effect at least up to Mercaptooctanoic acid (MOA) (C8). Looking at differences between C8, C11 and C16 (MHDA), it is clear that the C11 has better adhesion and proliferation than the others for both cell growth (Figure 3.12) and cell adhesion (Figure 3.3) experiments but this is not statistically significant. There is no obvious reason for the increased cell adhesion and growth on MUA SAMs though there could be structures on the C11 SAM surface that could account for this preference. The C8 and C16 could have different structures with different potentials for cell adhesion and growth.

Between chain lengths of C6 (HXT) and C12 (DDT) in the methyl-terminated SAM there are many different structures found. The same could be true for carboxylic acid-terminated thiols, presumably at slightly different chain lengths as the carboxylic acid moiety is likely to have an effect. To confirm that for carboxylic acid-terminated SAMs C8-C16 was an area of structural flux, STM or AFM experiments would need to be performed to visualise the surface. If this theory is correct it would account for the differences seen in cellular adherence and growth for these lengths of carboxylic acid terminated SAMs.

To properly assess whether or not the chain length effect exists, work should be done on different lengths of carboxylic acid SAMs, in particular the relation between the C11 SAM and the SAMs of the surrounding chain lengths should be determined.

In the amine presenting surfaces, the hydrochloride salt of the amine induces more cell adhesion than the amine. A possible reason for this effect is that cells that generally prefer hydrophilic environments are more attracted to the charged, amine hydrochloride surfaces. For both the amine and the amine hydrochloride the longer carbon chain length SAMs have more adherent cells than the shorter chain SAMs (Figure 3.3). The explanation for this effect is the same as for previously discussed SAMs; the structure and chemistry of the surface change and this has an affect on cellular adherence and growth. This assertion is based on very little data, two results cannot make a trend. While the same effects are seen for the cell growth experiment

(Figure 3.12) they have less statistical significance. More experimentation on different lengths of both amine and amine hydrochloride SAMs would be needed to draw any firm conclusions.

3.5.5 Comparison of Different Functionalities

The experimental results shown in Figure 3.4 were taken from 2 different experiments and as such their compatibility is not absolute. The results from the cell growth experiments have not been displayed together in this manner as they are not directly comparable.

The 2C methyl-terminated SAM (ETT) has the highest adhesion, though this is not statistically significant (Figure 3.4). This is an unusual result from the point of view that cells prefer hydrophilic environments. An explanation for this is that cells do not adhere directly to the surface, as soon as the surface is placed in medium with FBS, proteins begin to deposit themselves on the surface; it is the composition and conformation of these proteins that is directly affected by the surface structure, and this in turn has an effect on the amount of cellular adhesion and growth. Therefore it is possible that this is an accurate result and short chain methyl-terminated alkanethiol SAMs cause proteins to deposit onto the surface in preferred conformations.

The thiol-presenting surface (1,2-Ethanedithiol (ETDT)) has the next highest amount of cell adhesion shown by the BCECF experiment (Figure 3.4). This is followed by the hydroxyl SAM surface (Meth) then the amine SAM (2-Mercaptoethylamine (MEA)). The carboxylic acid surface (MAA) has the least cell adhesion.
The methyl- and thiol -terminated SAMs are not available for direct comparison and a further experiment to clarify their rate of cell growth on these surfaces relative to the others would be useful for future work. For the data available for comparative cell growth, the hydroxyl-terminated SAM has a higher rate than the carboxylic acid SAM (Figure 3.12). The amine SAM has the lowest rate of cell growth (Figure 3.12). In general these experiments suggest that the cells prefer the more hydrophobic environments which is unexpected but possible as explained previously due to the layer of proteins that deposit between the cell surface and the cell growth substrate.

3.5.6 Alkanethiol SAMs Modified by Reaction

A result that was surprising was that the unreacted monolayers had more cell adhesion than the reacted monolayers (Figure 3.5). This is unexpected for two reasons: Firstly, the surfaces presenting RGDC are usually more cell adherent than those without, and secondly, the surfaces became slightly scratched due to the liquid drying out from under the cover slip and sticking to the sample. This, while non-optimal, would have been expected to produce an effect of more cell growth rather

than less. One possible explanation for this is that some of the RGDC presenting groups became knocked off by the removal of the partially adhered cover slips. Alternatively the RGD groups could be in unfavourable conformations for promotion of cellular adhesion.

The amount of cellular adhesion to SPDP reacted SAMs is higher than that to NHS reacted SAMs for all but the AUT SAM (Figure 3.5). This difference is only significant for some surfaces. The SPDP having more cell adherence than NHS is likely to be due to the NHS linking the amine (N terminal) end and the SPDP linking the carboxy (C terminal) end of the RGDC peptide to the surface. Carboxy linked peptides have been found to induce more cell adhesion and proliferation than amino-linked peptides [12]. The SPDP does not link through the carboxyl but instead though the SH on the Cys, so this may give a slightly different structure, but nonetheless it appears to be the preferred way of adhering RGDC to the SAM surface. It was unexpected that the SPDP reacted SAMs would have the lowest cell growth. This could possibly be an artefact from the relative amount of scratching that occurred on each slide however it would have been unusual for it to occur identically across all five slides. A more interesting explanation is that different orientations of the RGD peptide have a different effect on adhesion and growth, and this could explain why the same peptide is present in different proteins; it could have different functions depending on its conformation.

The result that the optimal concentration of presented groups for cell adhesion was at 50% coverage for SPDP and RGDC reacted SAMs (Figure 3.5) was expected as the number of reacted alkanethiols has to be less than 100% in order for the RGDC sequence to have any effect. This is because the sequence is inaccessible to cells at too high an RGDC concentration. A concentration of around 50% coverage is most likely to allow the cells accessibility to the presented groups without having too few groups to induce preferential adhesion. This number is approximate because the concentration of groups on the surface does not necessarily reflect the concentration of groups in the solution from which the monolayer was assembled.

For the NHS reacted series the preferred SAM for cellular adherence was 100% MUA, this was expected as a higher concentration of reactable groups was necessary to produce the same concentration of RGDC peptides on this surface. This is due to steric factors that mean the NHS only reacts with a fraction of the presented COOH groups. The NHS is a very bulky molecule that is removed entirely in the reaction to add the peptide. This means that the peptide will take up less space than NHS on the monolayer so that even when reacted with a 100% MUA SAM there will still be plenty of space around the peptide for interactions with cells.

The adhesions of all the NHS-reacted SAMs are not significantly different from each other and only the MUA has a much higher value, this is likely to be due to the concentration of RGDC groups being too low.

The NHS reacted SAMs do not follow the same pattern for cell growth (Figure 3.13) as cell adhesion (Figure 3.5). The MUA 100% SAM NHS reacted surface is the surface preferred for cell growth preferred surface although this is not statistically significant, except when compared to the AUT SAM surface in the cell growth experiment. This is to be expected as there should be no reaction of the NHS with the AUT SAM surface.

The SPDP reacted SAMs also do not have much intra-series differences for either cell adhesion or cell growth experiments. The only really significant effect is that there is the lowest cell preference for the 100% AUT SAM surface. This could be due to too high a packing density of the RGDC molecules.

3.5.7 Biological Thiol SAMs

The mixed RGDC75%Cys25% and RGDC50%Cys50% monolayers have significantly less cell adhesion and growth than the RGDC or the Cys alone (Figures 3.6 and 3.14). There is no significant difference between the single molecule SAMs and the RGDC25%Cys75% SAM. This is probably due to the conformation of the RGDC being disordered as the chains will not be able to assume an upright

conformation if the RGDC and Cys are mixed with too much RGDC present. If the two thiols do not form a homogeneous monolayer then perhaps it is the size of the phase domains that are unfavourable for cell growth.

One previous study has investigated cell adhesion and growth of an RGD peptide adhered on the surface via a Cys residue [1]. In that study it was found that there was virtually no cellular adsorption to the surface. This means that these results are surprising. The difference between that study [1] and this one is that the Cys is at the C-terminal (Carboxy) end as opposed to the N-terminal (Amine) end. This was suggested to be the preferred orientation of the RGD peptide for cellular adhesion and growth by Pakalns *et al* [12]. It is most probable that it is the differing orientation of the peptide that has the different effect but it may also be due to a different cell line being used.

The thioglucose is the preferred biologically active SAM for both cellular adhesion and growth in this experiment (Figures 3.6 and 3.14), however the cellular adhesion is much lower than for some of the RGDC presenting surfaces studied so overall the SPDP and RGDC reacted AUT50%MUA50% SAM (Figure 3.5) is the most cellular adherent surface. The cell growth experiments were not comparable so no conclusions could be drawn about the differences between the cell growth data.

The CG SAM has a similar amount of cell adhesion (Figure 3.6) and growth (Figure 3.14) to the RGDC and the Cys this seems to indicate that length and functionality of the amino acids have no effect, but mixing the peptides does. This is an interesting result that will require further investigation to ascertain whether there is a small effect that cannot be seen without a reduction in error, or whether there is some way of the peptides ordering themselves on the surface that produces a surface with roughly the same cellular adherence and growth each time. It is unlikely that the chains are completely disordered as it is the disorder that is attributed as the cause of the low cell adhesions of two of the mixed SAMs. The alternative is that the mixed SAMs are actually ordered causing less cellular adhesion and growth and vice versa. More experimentation would be needed to determine which is the case.

3.5.8 SF268 Cells

The two cell types showed different preferences for the RGDC presenting surface (SPDP and RGDC reacted AUT50%MUA50% SAM) in cell adhesion (Figure 3.7). The differences in levels of cell adhesion in this experiment can be accounted for by the different rates of BCECF uptake possible for each cell type or by the SF268 cells being less adherent to the available surfaces. If different conformations of the RGD peptide support adhesion or growth better, it is also possible that the preferred conformation signalling adhesion or growth idea is dependant on the cell type exposed to it.

The UDT SAMs and the plastic surfaces support the least cellular adhesion (Figure 3.7), and this is statistically significant when compared to all the other surfaces except the AUT SAMs. There is no particular trend identifiable other than the MUA containing surfaces seem to be preferred by the SF268 cells. There is no particular correlation between the adhesion of BHK cells and adhesion of SF268 cells to the surfaces other than the low adherence to AUT and plastic, and a similar amount of adhesion on MUA these values are not statistically significant, so they are likely to be coincidence.

The UDT SAMs and the plastic surfaces also have the statistically significant lowest rate of cell growth and the MUA containing surfaces are favourable for cell growth. The main difference from the cell adhesion data is that the rate of cell growth on AUT is similar to the MUA containing surfaces. This perhaps indicates that the rate of cell growth is related to the hydrophilicity of the SAM.

3.6 Conclusion

There are no solid conclusions that can be made from this work. In order to obtain results that have smaller errors the experiments need to be repeated with more replicates. In addition controls that contain slides of alkanethiol SAMs should be used as opposed to medium controls and a positive control surface should be found

that has a reproducible amount of cell growth. A positive control would allow some means of comparison for the cell growth experiments as the values could be expressed as percentages of the positive control value.

Having addressed these general considerations, alkanethiols with chain lengths C2-C18 should be obtained for each different functionality so that a true study of the effect of chemistry and molecular structure can be performed. To obtain a better understanding of bioactive thiol SAMs surfaces of dipeptides CX and XC where X is substituted by each type of amino acid should be obtained. In addition glucose sugars should be obtained with thiols substituted at each different position in order to determine if it is possible to control the exact shape of the bioactive surface constituents.

3.7 References

1. McMillan, R., B. Meeks, F. Bensebaa, Y. Deslandes, and H. Sheardown, *Cell adhesion peptide modification of gold-coated polyurethanes for vascular endothelial cell adhesion*. Journal of Biomedical Materials Research, 2001. **54**(2): p. 272-283.

2. Cooper, E., L. Parker, C.A. Scotchford, S. Downes, G.J. Leggett, and T.L. Parker, *The effect of alkyl chain length and terminal group chemistry on the*

attachment and growth of murine 3T3 fibroblasts and primary human osteoblasts on self-assembled monolayers of alkanethiols on gold. Journal of Materials Chemistry, 2000. **10**(1): p. 133-139.

3. Nishi, N., D. Hobara, M. Yamamoto, and T. Kakiuchi, *Chain-length-dependent change in the structure of self- assembled monolayers of n-alkanethiols on Au(111) probed by broad-bandwidth sum frequency generation spectroscopy*. Journal of Chemical Physics, 2003. **118**(4): p. 1904-1911.

4. Porter, M.D., T.B. Bright, D.L. Allara, and C.E.D. Chidsey, *Spontaneously organized molecular assemblies .4. Structural characterization of normal-alkyl thiol monolayers on gold by optical ellipsometry, infrared-spectroscopy, and electrochemistry*. Journal of the American Chemical Society, 1987. **109**(12): p. 3559-3568.

5. Wolf, K.V., D.A. Cole, and S.L. Bernasek, *High-resolution TOF-SIMS study of varying chain length self- assembled monolayer surfaces*. Analytical Chemistry, 2002. **74**(19): p. 5009-5016.

6. Kawasaki, M. and H. Nagayama, *Observation of highly ordered 3 x 4 phase of ethanethiol self- assembled monolayer on Au(111)*. Chemistry Letters, 2001(9): p. 942-943.

7. Fenter, P., P. Eisenberger, and K.S. Liang, *Chain-length dependence of the structures and phases of ch3(ch2)n-1sh self-assembled on Au(111)*. Physical Review Letters, 1993. **70**(16): p. 2447-2450.

8. Kakiuchi, T., H. Usui, D. Hobara, and M. Yamamoto, *Voltammetric properties of the reductive desorption of alkanethiol self-assembled monolayers from a metal surface*. Langmuir, 2002. **18**(13): p. 5231-5238.

9. Rosenbaum, A.W., M.A. Freedman, S.B. Darling, I. Popova, and S.J. Sibener, *Surface vibrations in alkanethiol self-assembled monolayers of varying chain length*. Journal of Chemical Physics, 2004. **120**(8): p. 3880-3886.

10. Roper, M.G., M.P. Skegg, C.J. Fisher, J.J. Lee, V.R. Dhanak, D.P. Woodruff, and R.G. Jones, *Atop adsorption site of sulphur head groups in gold-thiolate self-assembled monolayers*. Chemical Physics Letters, 2004. **389**(1-3): p. 87-91.

11. Truong, K.D. and P.A. Rowntree, *Formation of self-assembled butanethiol monolayers on Au substrates: Spectroscopic evidence for highly ordered island formation in sub-monolayer films*. Journal of Physical Chemistry, 1996. **100**(51): p. 19917-19926.

12. Pakalns, T., K.L. Haverstick, G.B. Fields, J.B. McCarthy, D.L. Mooradian, and M. Tirrell, *Cellular recognition of synthetic peptide amphiphiles in self-assembled monolayer films*. Biomaterials, 1999. **20**(23-24): p. 2265-2279.

Chapter 4

General Conclusion

The structure of an omega terminated alkanethiol SAMs depends on many factors. This has led to a great variety of structures. Some structural features of the SAM can be elucidated by FTIR spectroscopy. In particular it has been considered that the degree of order is closely linked to the asymmetric CH_2 position. This assertion is dependent on the density of the SAM remaining constant. This is unlikely to be true especially for short chain thiol SAMs that have been found previously to have decreased electrochemical barrier properties.

Different structures with a variety of different packing densities have been imaged by other studies. This leads to the conclusion that the position of the asymmetric CH_2 spectral peaks are not just a measure of disorder in the SAM, but also give information about what type of structure is present. This does not preclude the peak positioning being affected by the amount of disorder. It is therefore necessary to examine other peaks such as the wagging bands, the presence of which has been said to indicate a high degree of structural order to ascertain the degree of ordering in the SAM. The presence of the odd-even effect should also be a good indicator of ordering.

The determination of the degree of ordering in SAMs from the position of a few peaks, would be very useful for all types of experimentation involving SAMs, as it would simplify detailed analysis of the structure, and perhaps allow for automated analysis. If a correlation could be found between which surface structures are present for which peaks, at which intensities, then detailed examination of surfaces could be carried out much more quickly than is currently possible with STM. FTIR spectroscopy also does not have the risk of molecular rearrangements occurring that STM does, so the surfaces could be used for experimentation after analysis. This would make possible experiments that could correlate the cell growth on the surface with surface structure. It has not been possible to find any correlations between peak position and structure and how this varies with the type of alkanethiol used in this study due to time constraints. However, data have been provided that suggests that short chain thiols are not as disordered as was once thought, only structurally different. More experiments would need to be carried out on which exact structures are present in which proportions of the alkanethiol SAM surfaces and how these correlate to the FTIR spectra, before any firm assertions could be made.

A minimum width of topographical feature that cells can react to has not been identified and very shallow changes in topography can produce a reaction from cells. This suggests that it is possible that even at a molecular level the cells are reacting to the topography as well as to the chemistry. It has been shown that the structures of alkanethiol SAMs are different at a nanometre level dependant on chain length and

tailgroup functionality, it is possible that the cells are reacting to this as well as to the hydrophilicity of the monolayer influencing protein deposition. This idea is supported by the fact that there is a chain length effect for the methyl-terminated SAMs. The extent of the difference between short chain SAMs and long chain SAMs is an indication that the length of the SAM is important for cell adhesion and growth, and this implies that the cells must be able to sense the difference between different structures. That there also appears to be an odd-even effect is interesting because it implies that the cells can sense very small changes in the topography at the angstrom level and possibly below.

Very few of the cell growth experiments produced significant results. This means that not many conclusions can be drawn about cell growth on the alkanethiol SAMs studied. In order to produce statistically significant results the experiments would need to be repeated with more replicates.

This study has shown that there do appear to be differences in cell growth characteristics on different surfaces of the same functionality. This suggests that very small changes in the structure can have an effect on cell growth, though more work would have to be done to ascertain the precise relationship between each structure and the amount of cell adhesion or growth possible on it.